RDR 1554-6

APPLICATION OF INTEGRAL DAMPING FOR DUCT ASSEMBLY VIBRATION SUPPRESSION

by

G. E. Bowie and W. A. Compton

Final Report

Contract NAS8-21128

April 1969

Prepared For

George C. Marshall Space Flight Center
Huntsville, Alabama 35812

Solar Division of International Harvester Company
San Diego, California 92112

NOTICE

RDR 1554-6

APPLICATION OF INTEGRAL DAMPING FOR DUCT ASSEMBLY VIBRATION SUPPRESSION

by

G. E. Bowie and W. A. Compton

Final Report

Contract NAS8-21128

April 1969

Prepared For

George C. Marshall Space Flight Center
Huntsville, Alabama 35812

This report was prepared by Solar Division of International Harvester Company under Contract No. NAS8-21128 for the George C. Marshall Space Flight Center of the National Aeronautics and Space Administration. The work was administered under the technical direction of the Propulsion and Vehicle Engineering Laboratory.

Solar Division of International Harvester Company
San Diego, California 92112

FOREWORD

This is the final report on NASA Contract No. NAS8-21128 and covers the work performed during the period 1 July 1967 through 30 November 1968. The Solar Research project number is 6-2697-7 and the internal number of the report is RDR 1554-6.

The contract was initiated by the National Aeronautics and Space Administration, Marshall Space Flight Center with the Solar Division of International Harvester Company for the application of integral damping to suppression of duct assembly vibratory response. The technical Contracting Officer's Representative (COR) for the program was Mr. R. H. Veitch (with Mr. H. J. Bandgren as alternate COR) of NASA, MSFC Propulsion and Engineering Laboratory, Huntsville, Alabama.

Mr. W. A. Compton, Assistant Director Research, was the program manager during the program and acted as the principal investigator for several months following the resignation of Mr. A. W. Coutris, Staff Research Engineer, the initial principal investigator. Dr. Glenn E. Bowie, Senior Staff Research Engineer, was the principal investigator for the program and the principal author of the final report. Major contributions were made by Mr. John V. Long, Director of Research, who originally conceived and demonstrated the idea of applying inelastic damping to suppress vibratory response in duct assemblies; Mr. A. N. Hammer, Research Engineer, was responsible for the application of braze-bond methods for attaching damping sleeves to test duct assemblies; Mr. J. A. Davies, Research Engineer, established experimental methods and conducted response and fatigue testing; and Mr. M. I. Seegall, Research Engineer, contributed to the dynamic response analysis and data reduction.

PUBLICATION REVIEW

W. A. Compton
Assistant Director - Research

John V. Long
Director of Research

CONTENTS

PRECEDING PAGE BLANK NOT FILMED

ILLUSTRATIONS

ILLUSTRATIONS (Cont)

ILLUSTRATIONS (Cont)

PRECEDING PAGE BLANK NOT FILMED.

TABLES

SECTION I

INTRODUCTION

The objective of this study was to compare the fundamental bending mode vibratory response of simply supported uniform ducts with the response of ducts modified by the addition of midspan damping sleeves. An experimental approach was followed which included the measurement of midspan response of uniform ducts (Test Series I), development of metallurgical bonding procedures for attaching damping sleeves to ducts, and determination of response and fatigue lives of damped ducts (Test Series II). The scope of the program encompassed experiments on uniform ducts made of four structural alloys and of three geometries, and on ducts of three materials and three geometries modified by the addition of uniform midspan damping sleeves made of one high damping structural alloy.

Major space booster ducting systems now built, use AISI 321 stainless steel as the material for the duct, gimbal, flanges, gimbal rings, and bellows; however, higher pressure and high angulation ducting systems require higher strength materials such as Inconel 718, to contain the pressures and angulations. Although Inconel 718 has higher strength to contain pressure than AISI 321 stainless steel, efforts to use Inconel 718 have been unsuccessful in many cases because of severe vibratory inputs which cause excessive stresses. The reasons why the AISI 321 stainless steel proved to be so effective were learned during extensive dynamic response studies at Solar. This discovery was attributed to the high damping properties of AISI 321 stainless steel at stresses in the inelastic range. When AISI 321 stainless steel ducts are severely vibrated, inelastic strains occur which provide a high damping capacity, limiting assembly response to a level which the assembly components can withstand. This is not the case with aluminum, titanium, or Inconel 718 (heat treated) ducts, which have relatively low damping properties throughout most of their useful strain range.

In certain cases, the problem of excessive vibratory response has been surmounted with Inconel 718 by introducing intermediate supports to reduce the free length of the ducting runs. Some of these supports have incorporated special damping devices and materials to aid in suppressing the vibratory response; however, this approach does not represent a fundamental solution to the problem since large space boosters have wide cavities which must be bridged by free lengths of ducting. Therefore, installing intermediate supports is a difficult task to accomplish, considering the thin walls of the main booster tanks and the lack of extensive inner framework.

It has been discovered as an alternate solution, that the superior inelastic stress damping properties of the AISI 321 stainless steel may be applied to an Inconel 718 duct; for example, in the high strain range, thereby causing substantial reduction of the vibratory response. Thus, the high performance material such as Inconel 718 operates in the elastic range to contain the pressures in the duct, while the superior damping of the AISI 321 stainless steel may operate in the inelastic region to suppress the vibratory response.

A variety of methods for bonding AISI 321 stainless steel to aluminum, Inconel 718, and titanium have been developed at Solar to allow quantitative evaluation of the inelastic damping concept on full-scale duct sizes ranging up to 20 centimeters in diameter. Since the program was oriented to study the parameters which govern the application of inelastic damping sleeves to the reduction of vibratory responses in ducts, it was reasoned that the most expedient method of bonding the sleeves should be chosen. The simple method of induction heating localized sections of the duct for bonding the sleeve, tended to degrade the fatigue life of the duct material; however, it did not affect the response characteristics of the test duct-sleeve combinations. Thus, a large number of duct materials and sleeve combinations could be response tested. This testing allowed the evolution of the somewhat generalized theory governing the application of the integral damping function to suppressing vibratory response of long unsupported ducts. Joining methods for the materials combinations, which do not degrade the duct material strength, have been developed and can be applied when other conditions permit.

The body of the report is divided into five sections and three appendices. Section II describes test duct materials and geometries and includes a discussion on the unit material damping properties of AISI 321 stainless steel. Test apparatus and procedures are described in Section III. All experimental results on uniform ducts (Test Series I) and damped ducts (Test Series II) are presented in Section IV. A discussion of the results is given in Section V and conclusions are contained in Section VI. Appendix A discusses a method of predicting integral damping of uniform AISI 321 stainless steel ducts based on a unit material damping law hypothesized in Section II. A derivation of a unit impulse response function for a mathematical model of a duct in which damping is introduced in a complex stiffness term is presented in Appendix B. A description of a new high friction gimbal design is given in Appendix C. Four prototypes of the new design were fabricated during the study period, but were not evaluated.

SECTION II

MATERIALS TESTED

Specimens tested in this program consisted of straight beams of hollow, circular cross-sections and were designated as either duct sections or ducts, to distinguish them from duct systems. Diameters, wall thicknesses, and duct lengths were representative of those used in space vehicle production practice and were compatible with available test apparatus. Emphasis was placed on obtaining comparative dynamic response data for duct sections of four materials. AISI 321 stainless steel was selected as a baseline material for the following reasons:

- It is widely used by the NASA on such structures as the Saturn V S-1C stage booster
- It exhibits strongly inelastic stress-strain properties.

Dynamic response of duct sections in the fundamental bending mode can be inhibited by selecting a duct material that has high unit material damping properties. B. J. Lazan (Ref. 1) has shown that the unit material damping of many structural alloys can be described adequately by an equation of the form

$$D = J\sigma^{n}, \tag{1.}$$

where D = unit material damping, m-newtons/m^3-cycle

σ = steady state stress amplitude, newtons/m^2

and J and n are material parameters

The uniaxial tensile test curve in Figure 1 shows the inelastic stress-strain behavior of AISI 321 stainless steel. The solid curve represents the empirical Ramberg-Osgood law

$$\epsilon = \frac{\sigma}{E} + 0.002 \left(\frac{\sigma}{\sigma_Y}\right)^{m}, \tag{2.}$$

where ϵ = uniaxial strain (m/m)

σ = uniaxial stress (newtons/m^2)

σ_Y = 0.2 percent offset yield stress (newtons/m^2)

E = tangent Young's modulus of elasticity (newtons/m^2)

and m is a parameter.

For the curve shown in Figure 1,

σ_Y = 30.0×10^7 newtons/m^2

E = 20.5×10^{10} newtons/m^2

and m = 5.7.

The manner in which inelastic stress-strain behavior and unit material damping properties of a structural alloy are related can be described as follows. After a certain number of reversed loading cycles, at either constant stress or constant strain amplitude, it is often found that the stress-strain behavior can be characterized by a stable hysteresis loop that is subsequently independent of the number of loading cycles. An exception occurs when the stress amplitude is allowed to increase to a limit defined as the cyclic stress sensitivity limit. Below this limit, the area of hysteresis loops can often be represented either by a single curve computed according to Equation 1, or by a series of curve segments with different values of J and n. It is often found that the hysteresis loop portions for tensile and compressive stresses have the same shape and area (i.e., the material does not exhibit a Bauschinger effect). Segments of the loop for which the magnitude of the stress is decreasing with time often have nearly constant slope. The cusps of the loops may fall on a locus of the form of the Ramberg-Osgood equation, although the values of E and σ_Y for the locus may be distinctly different than those for the onset of loading. Materials of this type are described in Reference 1 as ones with rate independent symmetric hysteresis loops. When σ is greater than the cyclic stress sensitivity limit, the area of hysteresis loops undergo a noticeable increase and the parameters J and n depend on the history of loading.

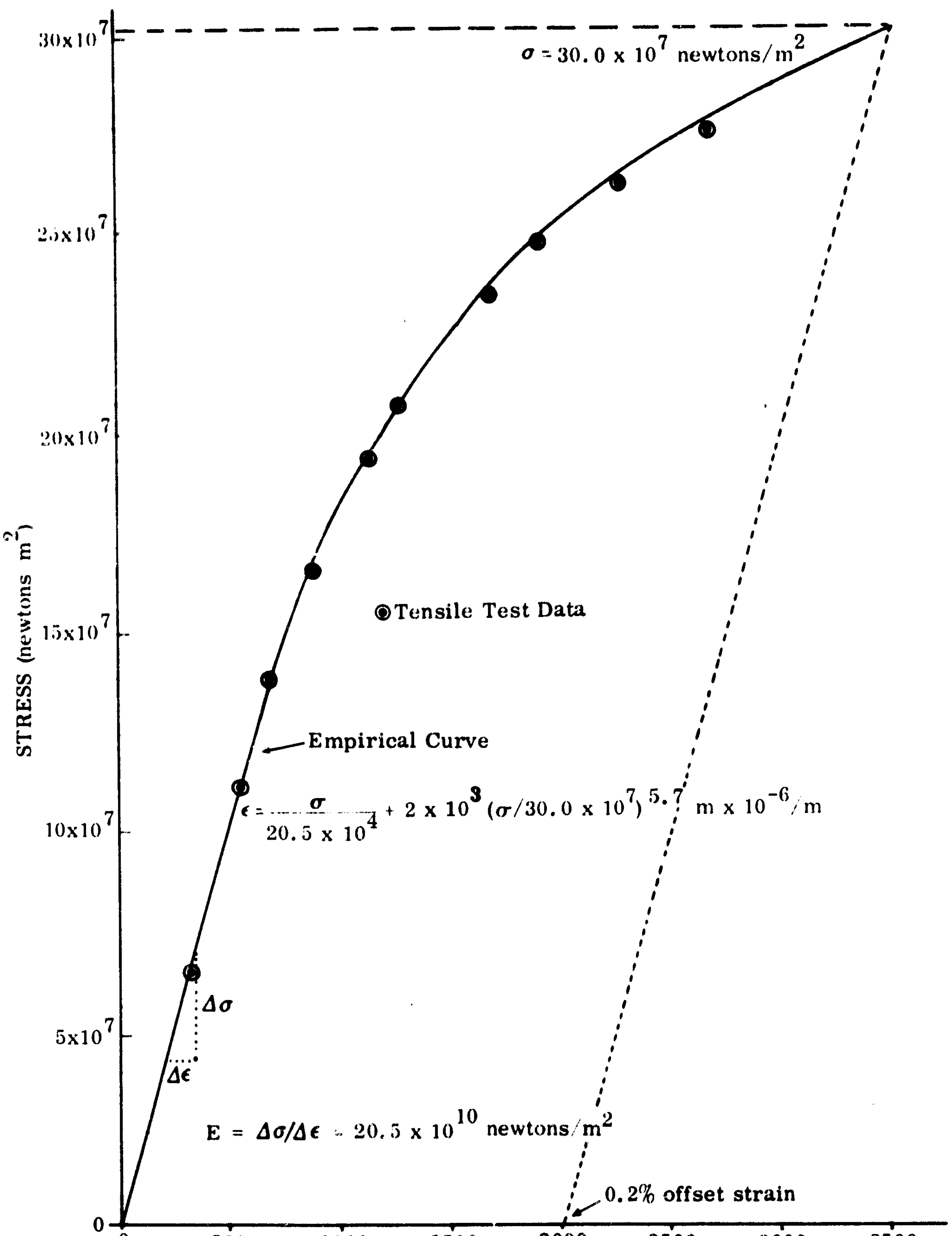

FIGURE 1. STRESS VERSUS STRAIN FOR AISI 321 STAINLESS STEEL; Annealed

A hypothetical hysteresis curve for AISI 321 stainless steel (Fig. 2) has been prepared for analysis purposes. It is presumed that

- The hysteresis loop is symmetric and rate independent
- The locus of the cusps is given by the form of the static stress-strain curve
- The slope of segments cd and ab shown in Figure 2 is equal to E.

The particular loop in Figure 2 was computed for a stress amplitude $\sigma = 0.8\,\sigma_Y$. The area of the loop was found by counting squares and has a unit damping value $D = 45.5 \times 10^4$ m-newtons/m^3-cycle.

A closed form expression has been derived for the area of a hysteresis loop of the type shown in Figure 2, as follows:

$$D = \frac{0.008m}{m+1}\,\frac{\sigma^{m+1}}{\sigma_Y{}^m}$$

$$= \frac{0.008\,(n-1)}{n}\,\frac{\sigma^n}{\sigma_Y{}^{n-1}},$$

where $$n = m + 1 .$$

For example, when $\sigma/\sigma_Y = 0.8$, $\sigma_Y = 30.0 \times 10^7$ newtons/m^2 and $n = 6.7$, it is found that $D = 45.5 \times 10^4$ m-newtons/m^3-cycle.

Let $$J = \frac{0.008\,(n-1)}{n} \cdot \frac{1}{\sigma_Y{}^{n-1}}$$

and write $D = J\,\sigma^n$. In the following paragraph, the values of J and n that are hypothesized for 321 stainless steel are 3.25×10^{-51} and 6.7, respectively.

The value of the damping exponent for this material has been shown to be in the order of $n = 6.7$. This value is in contrast to values for most structural alloys, normally in the range $2 < n < 3$. Therefore, it is apparent that the unit material damping of AISI 321 stainless steel increases significantly with increases in stress amplitude

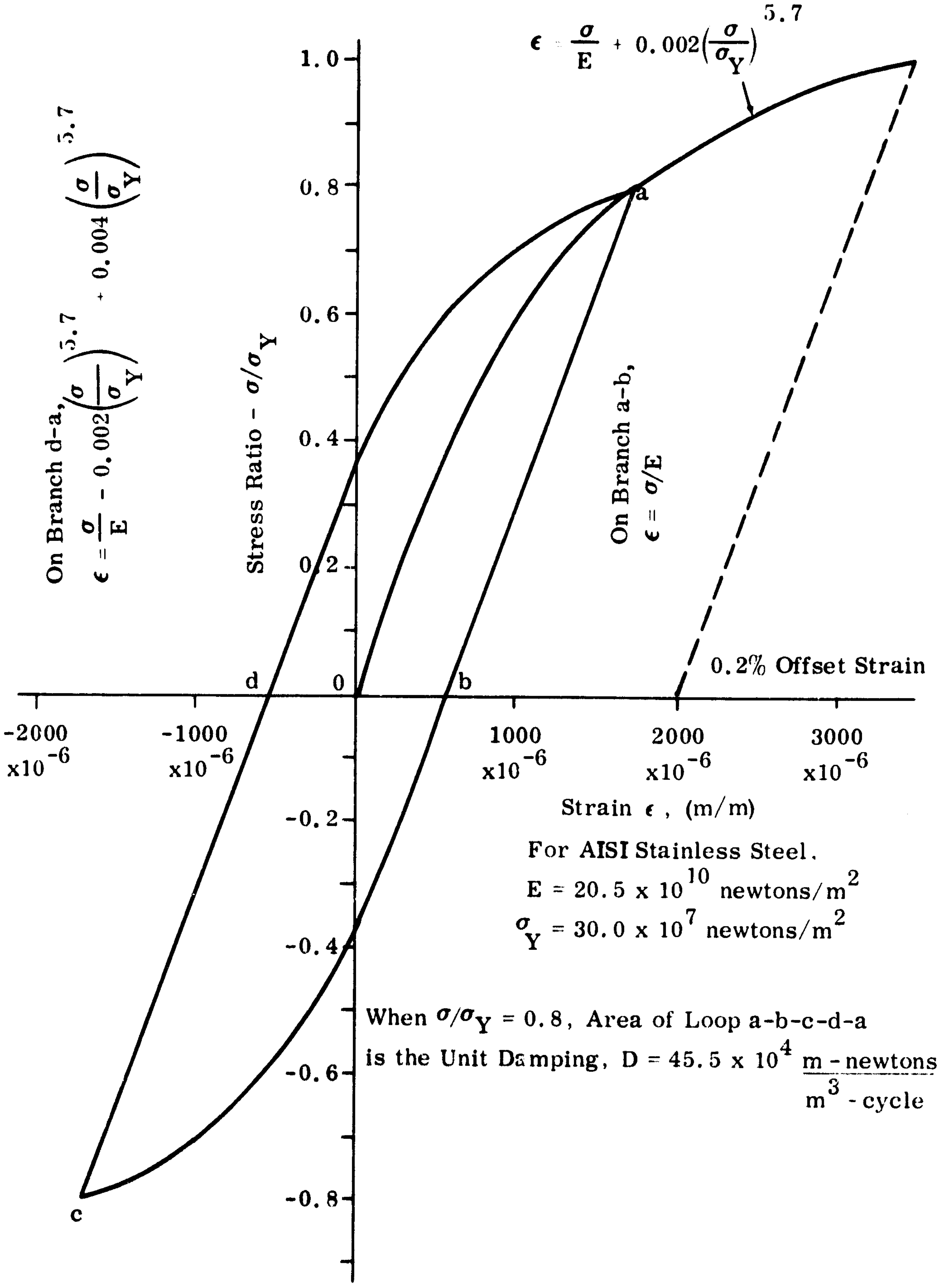

FIGURE 2. HYPOTHETICAL HYSTERESIS LOOP FOR AISI 321 STAINLESS STEEL

Three additional duct materials were selected for comparison with AISI 321 stainless steel.

- Inconel 718
- 6Al-4V titanium alloy
- 6061-T6 aluminum alloy

Two series of tests were conducted. In Test Series I, dynamic response data were obtained using ducts of each of the four materials with diameters of 5.1, 7.6, and 10.2 centimeters. In Test Series II, AISI 321 stainless steel sleeves were metallurgically bonded to central portions of duct sections constructed of Inconel 718, 6061-T6 aluminum, and 6Al-4V titanium.

2.1 TEST SERIES I AND II DUCT SECTIONS

The mounting fixtures for the duct sections are shown in Figures 3 and 4. One end of a duct section was shaker mounted and the opposite end wall was mounted in a pinned/sliding joint. Clearances of 0.13 millimeter were maintained on the pins. Alignment was accomplished at the shaker mounted end. In some instances, shims were placed in the pin joints after strain gage signals measured on the duct indicated that clearances were excessive. Lateral alignment was checked by manually twisting the duct to ensure that no binding would occur at the joints. The joint surfaces were repeatedly lubricated with SAE 30 weight oil during set up and test operation.

During the early stages of the program, the flanged ends of the ducts were welded to the ends of the ducts prior to precision boring of the pinholes. This practice was discontinued in favor of removing the flanges from a previously tested duct of the same diameter and material, aligning the pins with respect to the duct on a tooling plate, and then welding the flanges. This change in procedure represented a time and cost saving measure without sacrifice in quality of the experiments.

The geometries of duct sections tested are summarized in Table I. In the program test plan, Task letters A, E, and B were used to distinguish duct sections with outer diameters of 5.1, 7.6, and 10.2 centimeters, respectively. The Test Numbers in Column 3 of Table I identify the chronological order of the tests. The wall thickness of each duct section was equal to 1.24 millimeters. All duct sections 5.1 centimeters in diameter were 152 centimeters long. The sections 7.6 and 10.2 centimeters in diameter were 198 centimeters long.

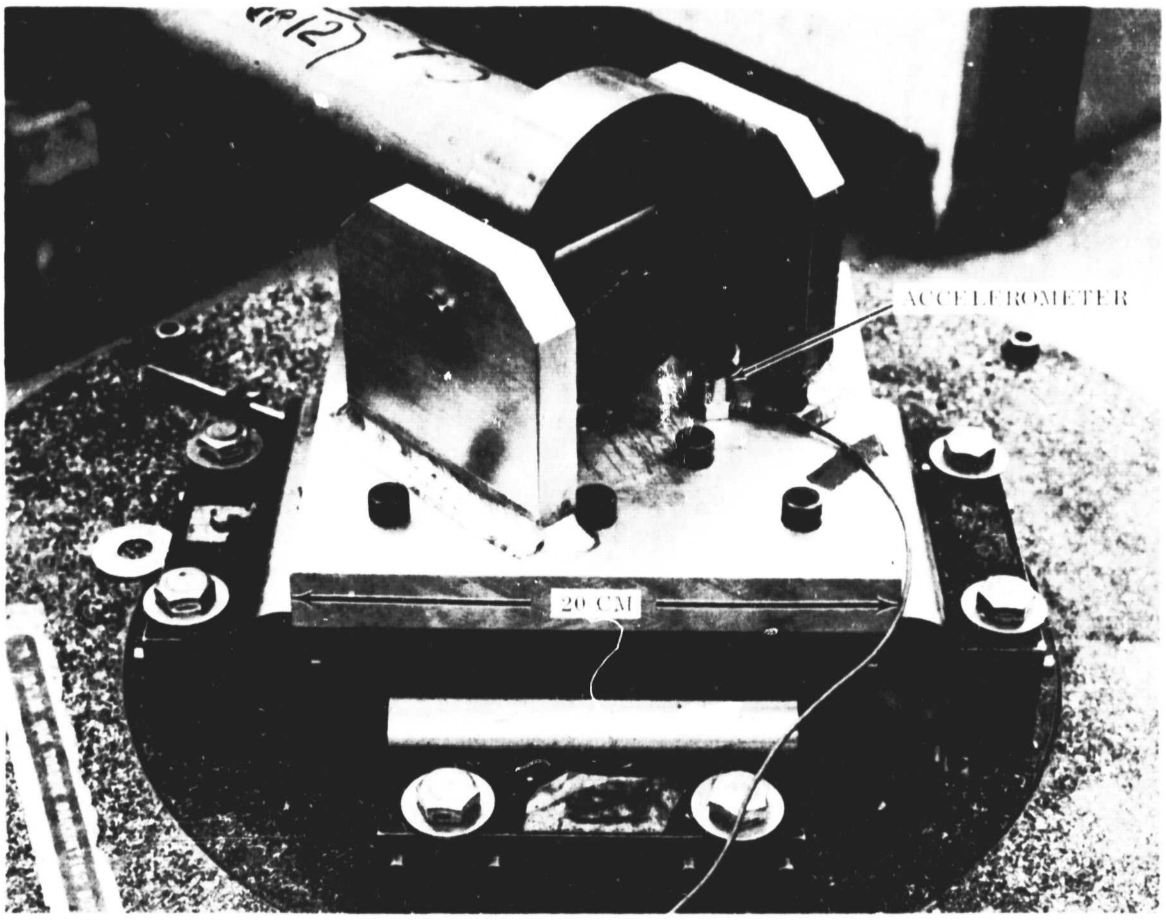

FIGURE 3. SHAKER FIXTURE SHOWING PINNED DUCT END AND ACCELEROMETER LOCATION

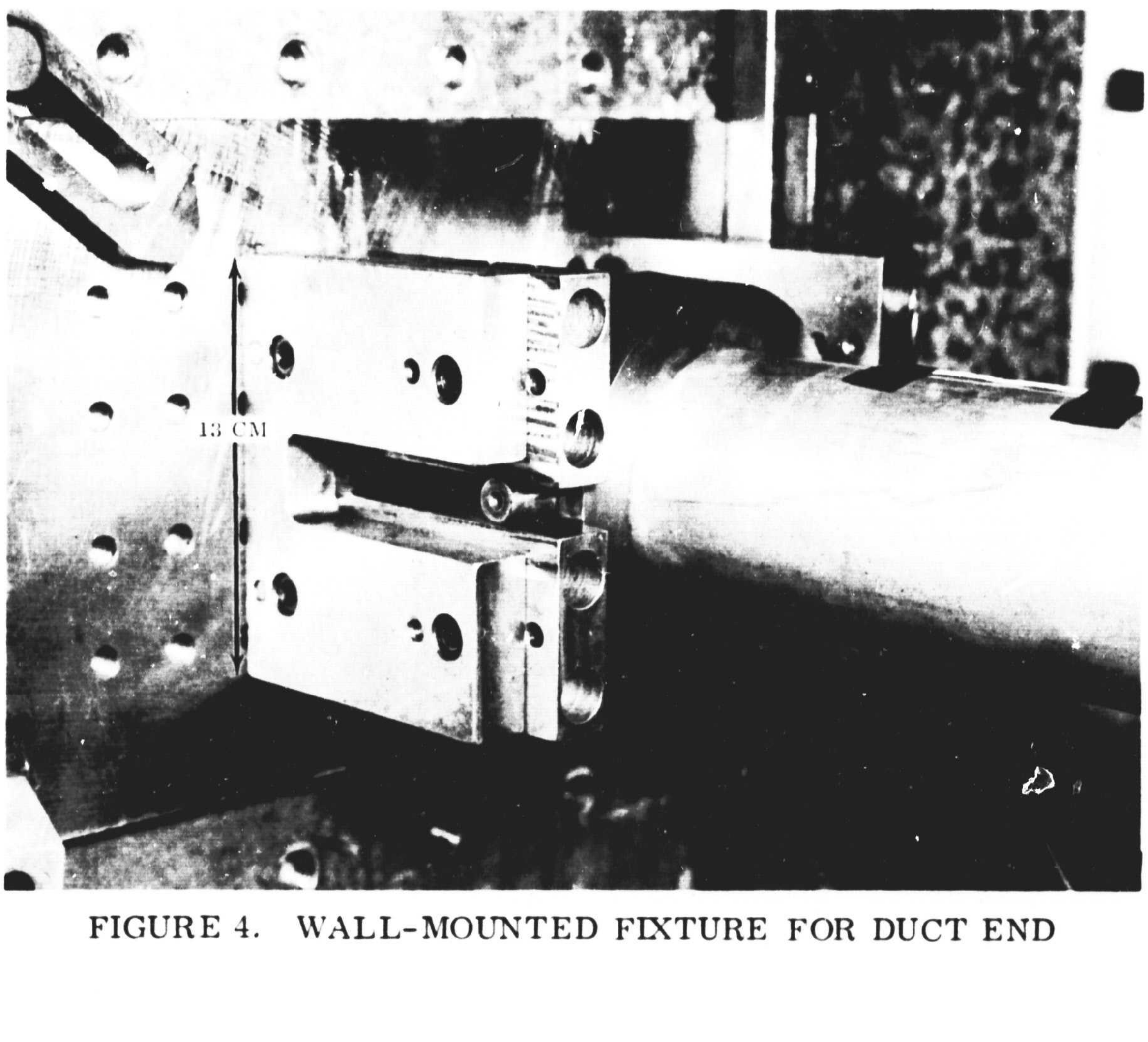

FIGURE 4. WALL-MOUNTED FIXTURE FOR DUCT END

TABLE I

DESCRIPTION OF DUCT GEOMETRIES

Test Series	Task	Test No.	Duct Material	Duct Geometry: Diameter (cm)	Duct Geometry: Length (m)	Duct Geometry: Wall Thickness (mm)	321 Stainless Steel Sleeve Geometry: Thickness (mm)	321 Stainless Steel Sleeve Geometry: Lengths in Response Tests (cm)			Sleeve End Description in Fatigue Tests
I	A	1	321 Stainless Steel	5.08	1.52	1.24					
		2	Inconel 718	5.08	1.52	1.24					
		3	6061-T6 Aluminum	5.08	1.52	1.24					
		4	6Al-4V Titanium	5.08	1.52	1.24					
I	E	29	321 Stainless Steel	7.62	1.98	1.24					
		30	Inconel 718	7.62	1.98	1.24					
		31	6061-T6 Aluminum	7.62	1.98	1.24					
		32	6Al-4V Titanium	7.62	1.98	1.24					
I	B	8	321 Stainless Steel	10.16	1.98	1.24					
		9	Inconel 718	10.16	1.98	1.24					
		10	6061-T6 Aluminum	10.16	1.98	1.24					
		11	6Al-4V Titanium	10.16	1.98	1.24					
II	A	5	Inconel 718	5.08	1.52	1.24	0.127	30.5			Plain
		6	6061-T6 Aluminum	5.08	1.52	1.24	0.127	28.4			Plain
		7	6Al-4V Titanium	5.08	1.52	1.24	0.127	30.5			Plain
II Addendum	A	38	Inconel 718	5.08	1.52	1.24	0.254	35.6	30.5	25.4	Plain
		39	Inconel 718	5.08	1.52	1.24	0.254	35.6			Chevrons
		40	6061-T6 Aluminum	5.08	1.52	1.24	0.254	35.6	30.5	25.4	Plain
Rerun		40	6061-T6 Aluminum	5.08	1.52	1.24	0.254	35.6	30.5	25.4	Plain
		41	6061-T6 Aluminum	5.08	1.52	1.24	0.254	35.6			Chevrons
II	E	33	Inconel 718	7.62	1.98	1.24	0.127	40.6	38.1	35.6	Plain
		34	6061-T6 Aluminum	7.62	1.98	1.24	0.127	40.6	35.6		Plain
		35	6Al-4V Titanium	7.62	1.98	1.24	0.127	40.6	35.6	30.5	Plain
II Addendum	E	42	Inconel 718	7.62	1.98	1.24	0.254	40.6	35.6	30.5	Plain
		43	Inconel 718	7.62	1.98	1.24	0.254	40.6			Chevrons
		44	6061-T6 Aluminum	7.62	1.98	1.24	0.254	35.6	30.5	25.4	Plain
		45	6061-T6 Aluminum	7.62	1.98	1.24	0.254	40.6			Chevrons
		46	6Al-4V Titanium	7.62	1.98	1.24	0.254	40.6	35.6	30.5	Plain
		47	6Al-4V Titanium	7.62	1.98	1.24	0.254	40.6			Chevrons
II	B	12	Inconel 718	10.16	1.98	1.24	0.127	38.1			Plain
		13	6061-T6 Aluminum	10.16	1.98	1.24	0.127	38.1			Plain
		14	6Al-4V Titanium	10.16	1.98	1.24	0.127	35.6			Chevrons

In Test Series II, AISI 321 stainless steel damping sleeves were metallurgically bonded in the central portions of duct sections constructed of Inconel 718, 6Al-4V titanium and 6061-T6 aluminum alloys (Fig. 5). Response tests were performed on ducts with plain-ended damping sleeves of various lengths (Table I), and with sleeve thicknesses of 0. 13 and 0. 25 millimeters. Fatigue tests were performed on duct sections with both plain- and chevron-ended damping sleeves. The chevrons were 2. 54 centimeters deep and shaped as shown in Figure 6.

2.2 PREPARATION OF TEST SERIES II DUCT SECTIONS

Specimens in Test Series II were prepared by bonding AISI 321 stainless steel damping sleeves to duct sections using the facility shown in Figure 7. The facility consists of a controlled atmosphere pyrex tube and an induction heater. Each bimetallic combination required different bonding materials and processes. The fabrication history of each duct section in Test Series II is summarized in Table II.

2.2.1 Stainless Steel to Inconel 718

This is the simplest of the joining problems and was accomplished in a relatively straightforward manner. Each damping sleeve was prepared in two halves to minimize differential thermal expansion. The two halves were form-rolled to perfectly fit the contour of the tube prior to assembly. A foil of Sta-Flo 761 was wrapped around the Inconel tube where the 321 stainless steel sleeve was to be applied. The 321 stainless steel damping sleeve was placed over the Sta-Flo foil and held in position by an outer band of AISI Type 1010 steel. This outer 1010 steel foil was tightened using stepless banding clamps and tack welding. The entire assembly was then placed in a pyrex tube muffle and purged with gettered argon prior to induction brazing. An induction heating coil was traversed along the damping sleeve to raise the area to a temperature of 900°C for braze bonding. At the end of the cycle, the outer 1010 foil was removed and the entire assembly placed in an argon muffle for completion of the heat treat. The heat treatment was a duplex-age type which exposed the entire duct assembly (already in the solution heat treated condition) to 730°C and to 600°C for periods of four hours each. Good quality bonds were achieved. Two ducts each of 5. 1 and 7. 6 centimeters diameter were prepared in this manner for Tasks A and E.

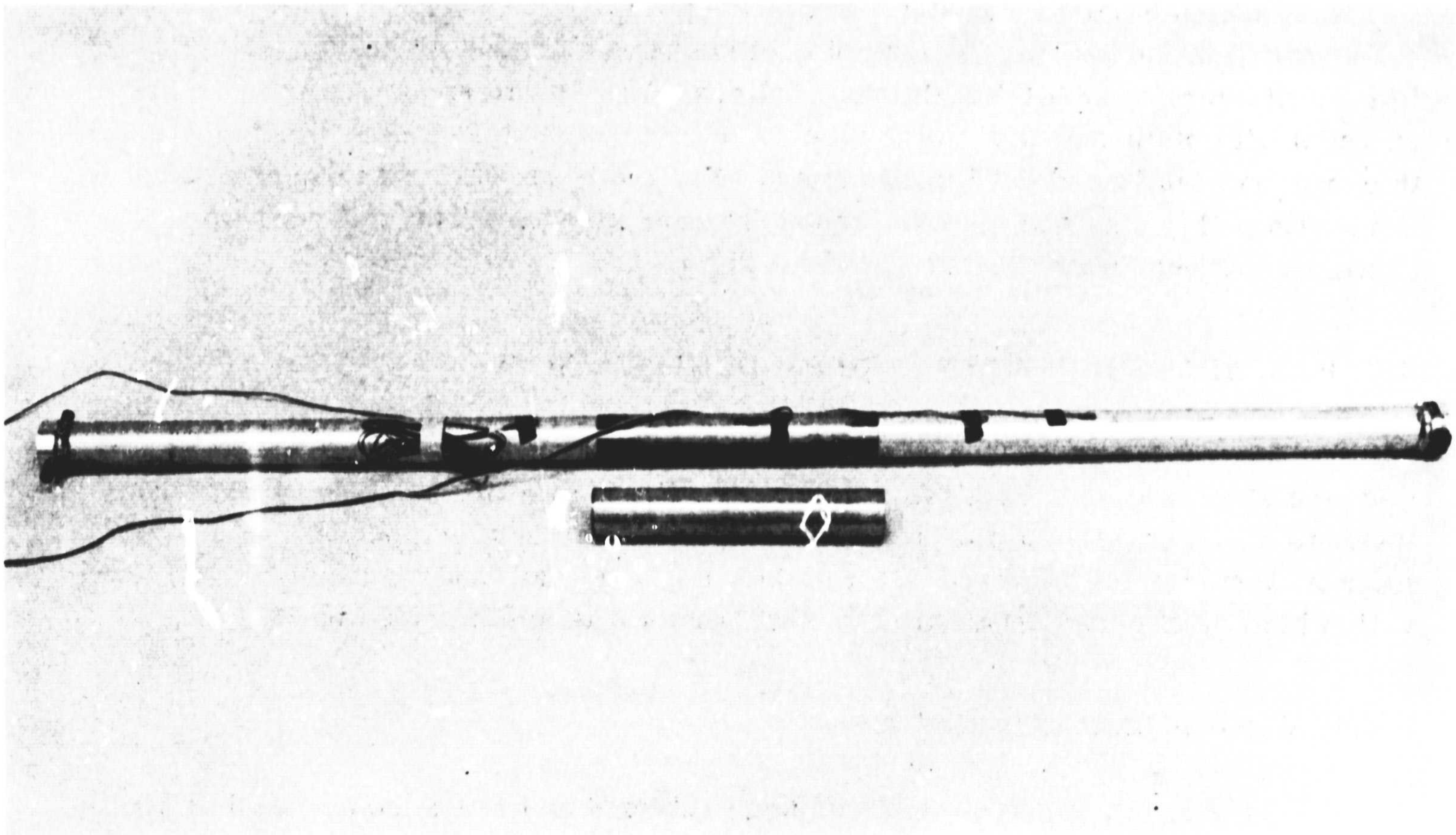

FIGURE 5. TYPICAL DUCT SECTION SHOWING LOCATION ON PLAIN-ENDED AISI 321 STAINLESS STEEL DAMPING SLEEVE

FIGURE 6. DUCT SECTION II-B-14 AFTER FATIGUE TEST FAILURE

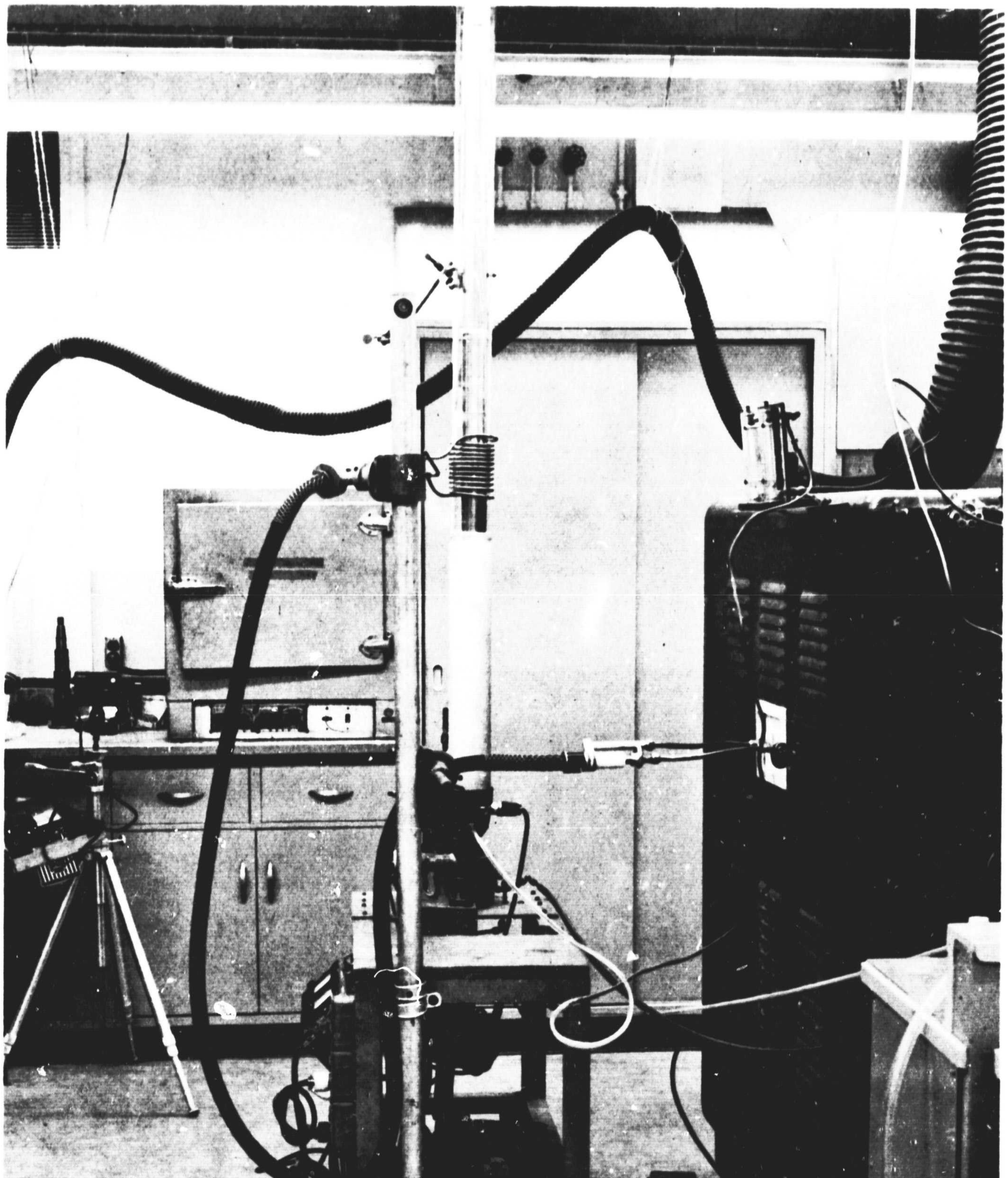

FIGURE 7. BRAZE BONDING FACILITY

TABLE II

TEST SERIES II DUCT FABRICATION HISTORY AND FAILURE LOCATION DATA

Test No.	Duct Material	Duct OD (cm)	Sleeve Thickness (mm)	Braze Alloy(1)	Atmosphere	Banding Material	Prebraze Composite Sleeve: Alloy	Prebraze Composite Sleeve: Atmosphere	Prebraze Composite Sleeve: Diffusion Barrier	Inner Support	Heat Treat	Failure Location
5	Inconel 718	5.08	0.127	Sta-Flo	Vacuum	1010 Steel				None	Duplex age(7)	Failed 15.6 cm from center of duct, near end of 30.5-cm sleeve
33	Inconel 718	7.6	0.127	Sta-Flo	Argon	1010 Steel				None	Duplex age (7)	Failed 20.3 cm from center at end of original 40.6-cm sleeve after peel back by 2.54 cm on each end.
12	Inconel 718	10.2	0.127	Lithobraze	Argon	1010 Steel				None	Duplex age	Did not fail. Sleeve cracked in several places.
38	Inconel 718	5.08	0.254	Sta-Flo	Vacuum	1010 Steel				None	Duplex age(7)	Crack occurred 2.54 cm. from center, coincident with two cracks in the sleeve.
39	Inconel 718	5.08	0.254	Sta-Flo	Vacuum	1010 Steel				None	Duplex age (7)	Duct cracked at end of sleeve, 17.2 cm. from center of duct.
42	Inconel 718	7.62	0.254	Sta-Flo	Vacuum	1010 Steel				None	Duplex age(7)	No duct failure but sleeve cracked.
43	Inconel 718	7.62	0.254	Sta-Flo	Vacuum	1010 Steel				None	Duplex age(7)	Failed 26.3 cm. from center, 5.71 cm beyond chevron tips at location of an arc burn.
6	Aluminum	5.08	0.127	Alcoa 718	Argon	321 SS(3)	Salt bath titanium plated			None	HT & age(6)	Failed at edge of sleeve bond, with sleeve remaining intact.
34	Aluminum	7.62	0.127	Alcoa 718	Argon	321 SS	Sta-Flo	Vacuum	Yes	None	HT & age(6)	Failed 20.3 cm from center at end of original 40.6-cm. sleeve, after being peeled back once.
13	Aluminum	10.16	0.127	Epoxy	Air	321 SS				None	As received Condition T-6	Failure occurred as a crack in the sleeve 7 cm from center of duct.
40	Aluminum	5.08	0.254	Alcoa 718	Argon	321 SS	Sta-Flo	Vacuum	Yes	321 SS Tube(8)	HT & age(6)	Not suitable for fatigue test due to inadequate braze
40 (Rerun)	Aluminum	5.08	0.254	Alcoa 718(5)	Argon	1010 Steel	Sta-Flo	Vacuum		321 SS Tube(9)	HT & age(6)	Failed 14.7 cm from center of duct at sleeve termination.

TABLE II (Cont)

TEST SERIES II DUCT FABRICATION HISTORY AND FAILURE LOCATION DATA

Test No.	Duct Material	Duct OD (cm)	Sleeve Thickness (mm)	Braze Alloy(1)	Atmos-phere	Banding Material	Prebraze Composite Sleeve Alloy	Prebraze Composite Sleeve Atmos-phere	Prebraze Composite Sleeve Diffusion Barrier	Inner Support	Heat Treat	Failure Location
41	Aluminum	5.08	0.254	Alcoa 718	Argon	1010 Steel	Sta-Flo	Vacuum	Yes	321 SS Tube(8)	HT & age(6)	Failed 16.1 cm from center of duct at the root of the sleeve chevrons.
44	Aluminum	7.62	0.254	Alcoa 718	Argon	321 SS	Sta-Flo	Vacuum	Yes	321 SS Tube(9)	HT & age(6)	Failed 20.3 cm from center at chevron tips of original 40.6-cm. sleeve after being peeled back twice.(10)
45	Aluminum	7.62	0.254	Alcoa 718	Argon	321 SS	Sta-Flo	Vacuum	Yes	321 SS Tube(9)	HT & age(6)	Failure occurred as a broad crack 20.3 cm from center at tips of sleeve chevron.
7	Titanium	5.08	0.127	Sta-Flo	Vacuum	Cb66	Sta-Flo	Vacuum	Yes	None	None	Failure occurred as a crack 15.2 cm from center at end of 30.4-cm sleeve.
35	Titanium	7.62	0.127	Sta-Flo	Vacuum	Cb66	Sta-Flo	Vacuum	Yes	None	None	Failure occurred as a crack near sleeve end 16.4 cm. from center of duct.
14(4)	Titanium	10.16	0.127	Sta-Flo	Argon	Cb66	Sta-Flo	Vacuum	Yes	None	None	Failure occurred as a crack 18.1 cm from center through duct and chevrons 0.9 cm from chevron tips.
46	Titanium	7.62	0.254	Sta-Flo	Vacuum	Cb66	Sta-Flo	Vacuum	Yes	None	None	Failure occurred as a crack at end of shortened sleeve 15.2 cm from center of duct
47	Titanium	7.62	0.254	Sta-Flo	Vacuum	Cb66	Sta-Flo	Vacuum	Yes	None	None	Failure occurred as a crack 18.7 cm from center through duct and chevrons 0.9 cm from chevron tips.

Thickness of Braze Alloys:
Sta-Flo 0.038 mm.
Lithobraze 0.05 mm.
Alcoa 718 0.076 mm.
Diffusion Barrier 0.025 mm.
Spiral wrap
Rebrazed to bond chevrons
No brazing flux applied

6. Solution heat treat at 537°C for 30 minutes; water quench, age at 182°C for four hours.
7. 720°C for four hours: 560°C for four hours in argon.
8. Spring Fit.
9. Press Fit.
10. Duct originally designed for life test only; chevron tips were removed and duct was used for response test instead.

2.2.2 Stainless Steel to Titanium

The brazing method initially used for the 5.1- and the 10.2-centimeter OD ducts caused degradation of the duct material in each case. Originally, Lithobraze BT was applied on both sides of a diffusion barrier and brazed on the tube. However, the copper content in the BT braze alloy reduced the base metal strength of the titanium tube, which contributed to premature failure during vibration testing. This condition was not expected because of the minimum quantities of bond alloy used in the process. In fabricating the second 5.1-centimeter titanium duct, a substitute bond alloy containing much less copper, Sta-Flo 761, was used. A considerable improvement was obtained; however, the weak point in the duct shifted to the transition areas at the sleeve ends.

The procedure for the first 7.6-centimeter duct (OD), and subsequent ducts, was to pre-braze a diffusion barrier foil to the 321 stainless steel sleeve with BT alloy. These composites were then shaped and brazed in two halves to the duct with Sta-Flo 761. Restraint was applied in the same manner as when joining stainless steel to Inconel 718, except that the outer band consisted of a columbium alloy foil. Brazing was by induction heating in a vacuum. Temperature control was carefully maintained to avoid overheating, which could cause erosion or degradation of the base material.

The two 7.6-centimeter OD titanium ducts (Task E) were processed with the foregoing procedure and braze quality was seen to be adequate for determination of response.

2.2.3 Stainless Steel to Aluminum

The four stainless steel sleeve/aluminum test duct systems presented the greatest fabrication problems. One of the 5.1-centimeter ducts (OD) and one 7.6-centimeter duct (OD) with the chevron damping sleeve ends were processed with acceptable quality. The plain-end 0.25 millimeter thick damping sleeves had noticeable unbonded areas. The problem arose from the difficulty in optimizing the pressure loading on the damping sleeve during the bonding cycle. The process used for the bonding of the damping sleeves for these test series was similar to that described for the 7.6-centimeter titanium duct (OD), in that pre-brazed composites were prepared with a diffusion barrier foil, 321 stainless steel sleeve end Lithobraze BT braze alloy. These composite sleeves were then shaped to a net fit and brazed in two half sections to the aluminum duct with Alcoa 718 aluminum-silicon alloy. Brazing was conducted in an argon muffle resting horizontally on the hearth of a large steel tempering oven.

The 7.6-centimeter ducts (OD) were banded externally with AISI 321 stainless steel foil to provide compressive forces (by differential thermal expansion) on the sleeves. Considerable distortion resulted in the first of these with plain sleeve ends, but the problem was relieved in the chevron-cut end specimen by placing a diagonally split length of stainless steel tubing inside the aluminum tube to stiffen the braze area.

The first of the 5.1-centimeter ducts (OD), with plain sleeve ends, was similarly banded with AISI 321 stainless steel which, perhaps because of the smaller diameter, did not provide sufficient differential thermal expansion strain to compress the sleeve tightly against the aluminum tube. The resultant braze was of poor quality. The procedure was revised for the second 5.1-centimeter duct (OD), with chevron ends, by substituting a banding material with a lower thermal expansion coefficient, Type 1010 steel. A second 5.1 centimeter OD aluminum duct with a plain ended damping sleeve, designated Test No. 40 Rerun in Table II, was also fabricated using a 1010 steel band rather than a 321 stainless steel band. Much better quality brazing resulted in each case.

All aluminum ducts with brazed damping sleeves were solution heat treated and aged to return them to the T6 condition. In brazing the aluminum ducts, the basic problem is the proximity of the minimum brazing temperature of Alcoa 718, 590°C, to the melting range of 6061 Aluminum, 595 to 650°C. Even without the distortion problem, resulting from loss of strength at the braze temperature, there is a serious possibility that irreparable metallurgical damage can occur by incipient grain boundary melting at the elevated braze temperature.

SECTION III

TEST APPARATUS AND PROCEDURES

A schematic of the test apparatus is shown in Figure 8. Vertical steady state sinusoidal motion was imparted to one end of a duct section by a 6.7×10^3-newton capacity electrodynamic shaker. Input acceleration load factors, N, were measured with a piezoelectric accelerometer and vibration meter.

Duct and sleeve strains were measured with Budd Metalfoil, C-121 temperature compensated gages (gage length = 3.2 mm). They were bonded with an equal parts mixture of Shell Epon Resin No. 828 and Versamid No. 125 Polyamide Resin. Curing time was 1.5 hours at 66°C. If gages failed during a test, they were replaced with either a [illegible]ld gage from the original lot or with Baldwin A5-1 gage. In either case, the replacement for the failed gage was bonded with Eastman 910 contact cement. Drift problems with the strain gages were minimal since no static strain was

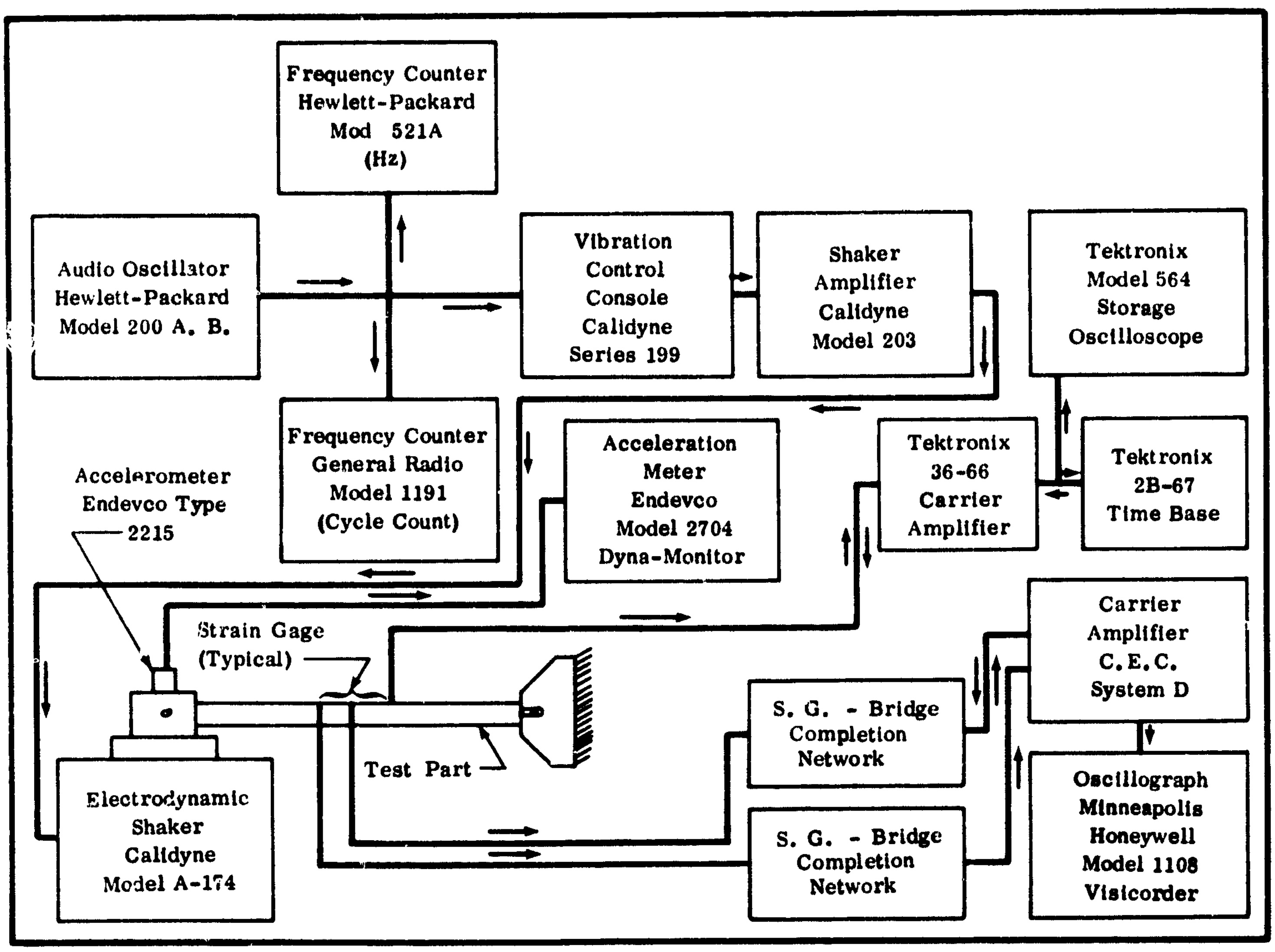

FIGURE 8. CONTROL AND MONITORING SYSTEM FOR VIBRATION OF DUCT ASSEMBLIES

involved. Strain gage bonding was satisfactory in all cases. A sample of each discrete strain value was recorded on a Honeywell, Model 1108 Recording Oscillograph using a C. E. C. System D amplifier unit with three Model 113-B carrier amplifiers as gage conditioning units. The gages were resistance calibrated in the conventional manner for strain gage bridge circuits. Typical calibration oscillograph traces are shown in Figure 9.

A strain gage located at one quarter of the duct length from one duct end was continuously monitored on a Tektronix Model 564 Storage Oscilloscope using a Type 3C-66, twenty-five K-Hz carrier plug-in amplifier. This provided a visual means of fine-tuning the frequency to assure maximum strain at each discrete value of force-input and assurance that good strain waveform quality would be obtained on oscillograph traces for gages at other duct locations. Shaker oscillator gain was increased at discrete intervals with the frequency swept manually from slightly below resonance through the resonance peak, and then carefully returned to the frequency of peak strain response for given load input, N.

Test frequencies were monitored on a Hewlitt-Packard, Model 521A electronic counter. A continuous cycle count was recorded on a General Radio, Model 1191, eight-digit counter to determine numbers of stress cycles at each load level during response and fatigue tests. The output from the shaker oscillator supplied the input for both counters.

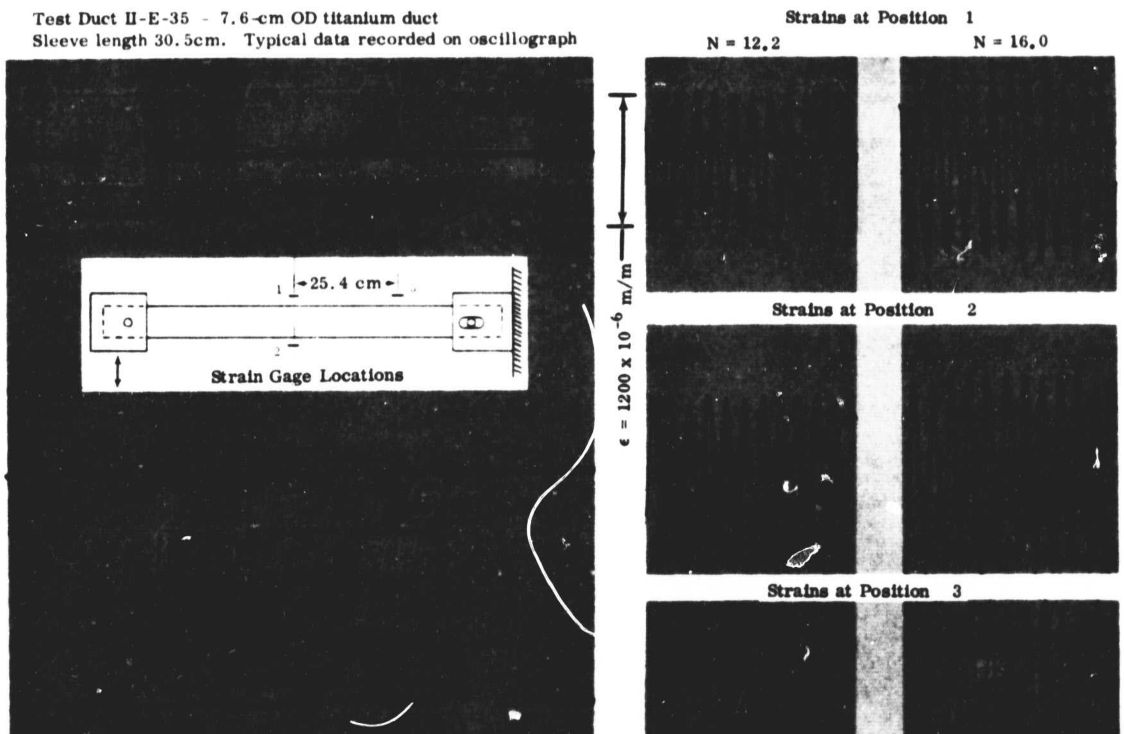

FIGURE 9. TYPICAL STRAIN GAGE CALIBRATION AND STRAIN RESPONSE DATA

SECTION IV

TEST RESULTS

To develop a rational design procedure for predicting vibration response and fatigue life of structural components in a duct system, it is advisable to define a simple duct section test configuration that is amenable to both analysis and experimental testing. The design procedure must be validated on a simple physical model before it can be applied with confidence to more complicated duct systems. The duct section test configuration selected for this program was one in which a straight duct was mounted with one end free to rotate about a single axis and the opposite end free to rotate about the same axis and slide in the axial direction. The latter pinned and sliding joint was mounted in a wall fixture and the former pinned end was attached to an electrodynamic shaker head. The shaker was used to drive the pinned end of the duct at the fundamental frequency of bending vibration in the duct section.

The duct sections used in Test Series I had uniform geometric and elastic properties with length, while those used in Test Series II were made to be nonuniform by the application of AISI 321 stainless steel damping sleeves. The uniform duct sections were amenable to the simple, single degree of freedom analysis given below. A theoretical model that would provide a consistent basis for direct comparison of nonuniform with uniform duct section vibration response was not evolved in the performance of the program.

4.1 THEORETICAL MODELS FOR TEST SERIES I DUCT SECTIONS

The theoretical methods that were applied to the analysis of a uniform duct section vibrating in the fundamental mode are as follows. In the first, the deflection at midspan relative to the displacement of the driven end of a duct was treated as the response parameter of a single degree of freedom model. Damping was introduced in a complex modulus stiffness term in the model. The approach is considered to be useful for engineering design purposes, but is not sufficiently refined to reveal the detailed influence of material damping and geometric parameters on the response. The second theoretical method was based on the definition of a logarithmic decrement for vibration decay in the fundamental bending mode as the ratio of two-volume integrals. The numerator represents the total internal damping in the duct section and the denominator is two times the maximum elastic energy stored in the duct per vibration cycle.

The first theoretical method requires measurement of strain amplitude at midspan as a function of input acceleration. The second method requires an hypothesis concerning the unit damping as a function of stress amplitude at midspan. The hypothesis was tested by performing vibration decay and swept-sine response experiments on a 7.6-centimeter diameter AISI 321 stainless steel duct section. The latter two types of experiments yield direct measurements of either logarithmic decrement or damping ratio for comparison with theoretical predictions. An outline of the second theoretical method is given in Appendix I.

4.1.1 Single Degree of Freedom Models

When a duct section is to be vibrated in the fundamental mode (Fig. 10), it is usual to compare the deflections of the vibrating duct with those that would occur when the driven end is subjected to a uniform acceleration. The procedure adopted here follows the technique described in Reference 2. The vibrating duct is first considered to be undamped to simplify the determination of the vibrating mode shape. Damping is then considered to affect only the amplitude of vibration and not the mode shape or resonant frequency.

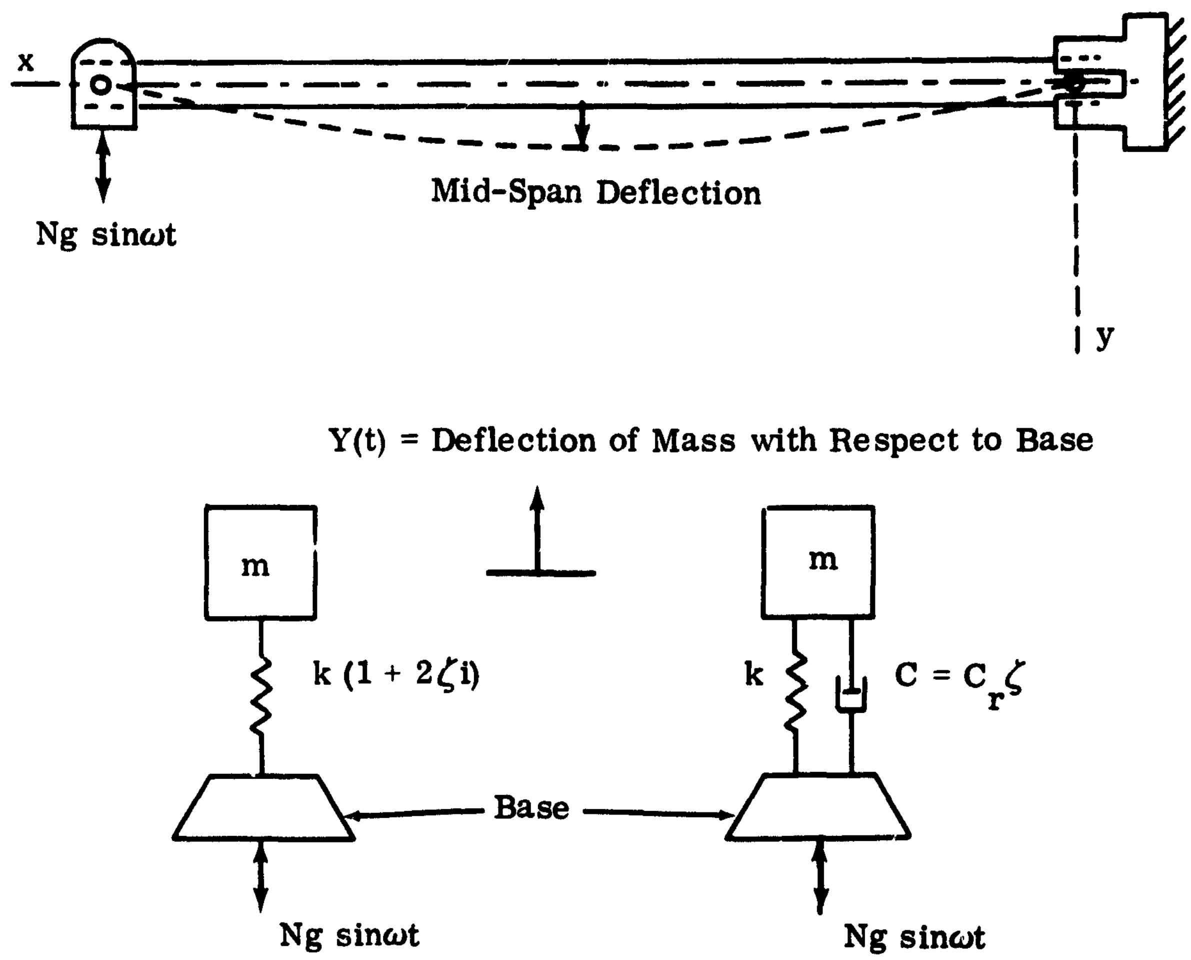

FIGURE 10. SINGLE DEGREE OF FREEDOM MODELS FOR DUCT SECTION VIBRATING IN THE FUNDAMENTAL BENDING MODE

Uniform Acceleration of One End of a Duct Section

When one end of a simply supported duct section is subjected to a uniform acceleration, Ng, the deflection of the duct in the direction of the acceleration, Y(x), is given by the solution of the equation

$$EI \frac{d^4 Y(x)}{dx^4} = Ng\rho A,$$

where ρ = mass density of the duct material and A = duct cross sectional area.

The natural mode shapes of the undamped duct are known to be of the form

$$\sin \frac{n\pi x}{\ell}, \quad n = 1, 2, 3, ----.$$

The deflection Y(x) can be expressed as a superposition of the form

$$Y(x) = \sum_n B_n \sin \frac{n\pi x}{\ell}.$$

To a first approximation,

$$Y(x) = B_1 \sin \frac{\pi x}{\ell}$$

$$= \frac{4}{\pi} \frac{Ng}{\omega_1^2} \sin \frac{\pi x}{\ell}$$

where ω_1 = circular frequency of fundamental vibration mode.

A condensed nomograph consisting of three parallel straight scales is presented in Figure 11 for estimating fundamental bending mode resonant frequencies of simply supported thin-walled ducts. The nomograph is based on the equation

$$f_1 = \frac{\omega_1}{2\pi} = \frac{1}{2\pi}\left(\frac{\pi}{\ell}\right)^2 \left(\frac{EI}{\rho A}\right)^{1/2}, \qquad 3.$$

where f_1 = fundamental bending mode frequency (Hz)

ℓ = duct length (m)

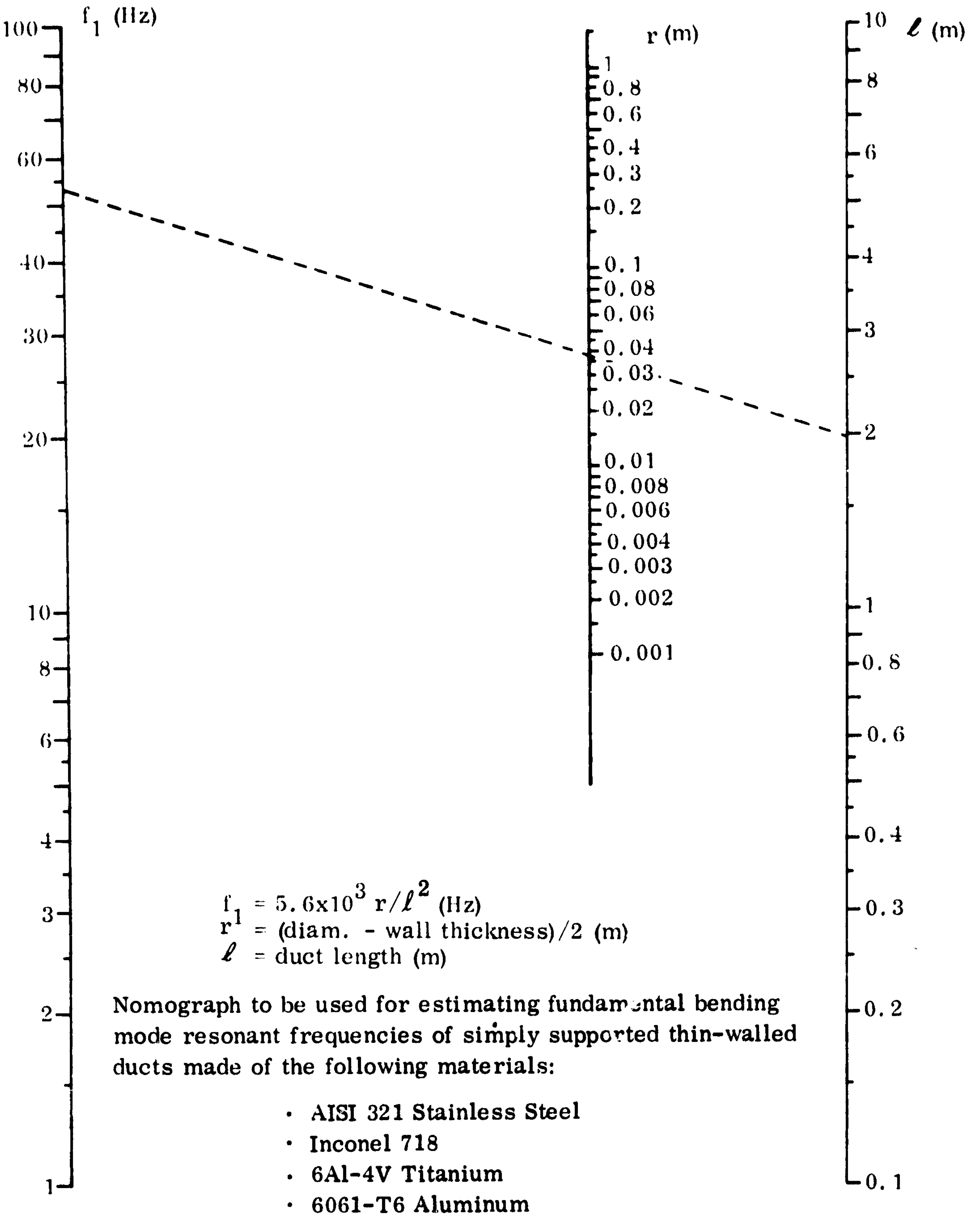

$f_1 = 5.6 \times 10^3 \, r/\ell^2$ (Hz)
$r = $ (diam. - wall thickness)/2 (m)
$\ell = $ duct length (m)

Nomograph to be used for estimating fundamental bending mode resonant frequencies of simply supported thin-walled ducts made of the following materials:

- AISI 321 Stainless Steel
- Inconel 718
- 6Al-4V Titanium
- 6061-T6 Aluminum

FIGURE 11. NOMOGRAPH FOR ESTIMATING FUNDAMENTAL BENDING MODE FREQUENCIES OF THIN WALLED DUCTS

E = Young's modulus of elasticity (newtons/m^2)

I = duct cross section second moment of area (m^4)

ρ = mass density of duct material (kgm/m^3)

A = duct cross sectional area (m^2)

The equation was simplified by using the thin-walled duct relations

$I = \pi r^3 t$

$A = 2\pi rt$,

and $r = (d - t)/2$

where t = duct wall thickness (m),

and d = duct outer diameter (m).

The simplified equation is

$$f_1 = \frac{\pi}{2\sqrt{2}} \left(\frac{E}{\rho}\right)^{1/2} \frac{r}{\ell^2}$$

The derivation of an average value of $(E/\rho)^{1/2}$ for four duct materials is summarized in Table III.

It can readily be shown that fundamental bending mode frequencies for ducts made of the four materials listed in Table III may be estimated by using the expression

$$f_1 = 5.6 \times 10^3 \frac{r}{\ell^2} . \qquad 4.$$

For example, the AISI 321 stainless steel duct used in Test I-E-29 had a length of 198 centimeters, an outer diameter of 7.6 centimeters, and a wall thickness of 1.24 millimeters. The mks values of ℓ and r for this duct are 1.98 meters and 0.0373 meters, respectively. When the dashed line in Figure 11 is used to estimate the fundamental bending mode frequency of this duct, the value f_1 = 53 Hz is obtained, in close agreement with results of a direct calculation based on material properties of the test duct.

TABLE III

DERIVATION OF AN AVERAGE VALUE FOR $(E/\rho)^{1/2}$

Material	E (newtons/m^2)	ρ (kgm/m^3)	E/ρ	$(E/\rho)^{1/2}$
AISI 321 Stainless Steel	19.3×10^{10}	7.83×10^{3}	24.6×10^{6}	4.96×10^{3}
Inconel 718	20.7×10^{10}	8.25×10^{3}	25.2×10^{6}	5.02×10^{3}
6A1-4V Titanium	11.7×10^{10}	4.44×10^{3}	26.4×10^{6}	5.14×10^{3}
6061-T6 Aluminum	6.9×10^{10}	2.27×10^{3}	25.4×10^{6}	5.04×10^{3}
		Average $(E/\rho)^{1/2}$	=	5.04×10^{3}

Response of the Single Degree of Freedom Model at Arbitrary Frequencies

Figure 10 shows two alternate single degree of freedom models for the deflection at midspan with respect to the deflection of a driven end of the duct. In the model on the left, the deflection of a mass with respect to a base is given by the solution of the equation

$$\frac{d^2 Y(t)}{dt^2} + \omega_1^2 (1 + 2\xi i)\, Y(t) = Ng \sin \omega t \ ,$$

where the term $(1 + 2\xi i)$ is a complex stiffness factor. The amplitude of motion at resonance is found by substituting

$$Y(t) = B_1' \sin \omega t$$

in the above equation. The result can readily be seen to be

$$B_1' = \frac{Ng}{2 \omega_1^2 \xi i}$$

A uniform acceleration of the base of the model, Ng, would produce a deflection of the mass given by

$$B_1 = \frac{Ng}{\omega_1^2} .$$

The resonance amplification factor of the model is defined as the ratio

$$Q = \frac{|B'_1|}{B_1} = \frac{1}{2\xi} .$$

In the single degree of freedom model on the right in Figure 10, damping is contributed by a dashpot with viscous damping factor, C. The relative deflection of the mass with respect to the base is the solution of the equation

$$\frac{d^2Y(t)}{dt^2} + \frac{C}{M}\frac{dY(t)}{dt} + \omega_1^2 Y(t) = Ng \sin \omega t .$$

In this case, the resonance amplification factor for a lightly damped model is given by

$$Q = \frac{1}{2\xi}, \text{ where } \xi = \frac{C}{C_r} \text{ is the damping ratio for}$$

and $\qquad C_r = 2M\omega_1$ is the critical damping factor.

Although the equations governing the two models yield the same expression for the resonance amplification factor, the first model has been selected here on the grounds of physical arguments.

A function, $H(i\omega)$, called the transfer function of the model can be derived which characterizes the response of a single degree of freedom model at arbitrary frequencies. If the particular solution

$$Y(t) = H(i\omega)\, e^{i\omega t}$$

is substituted in the equation

$$\frac{d^2Y(t)}{dt^2} + \omega_1^2 (1 + 2\xi i) = e^{i\omega t}$$

it is found that

$$H(i\omega) = \frac{1}{\omega_1^2 - \omega^2 + 2\zeta\omega_1^2 i} \cdot$$

If $H(i\omega)$ is expressed in the polar form

$$H(i\omega) = |H(i\omega)| e^{-i\theta} ,$$

it can be shown that the amplitude characteristic is

$$H(i\omega) = \frac{1}{\left(\left(\omega_1^2 - \omega^2\right)^2 + 4\zeta^2 \omega_1^4\right)^{1/2}}$$

$$= \frac{1}{(2\pi)^2\left(\left(f_1^2 - f^2\right)^2 + 4\zeta^2 f_1^4\right)^{1/2}}$$

and the phase angle is

$$\theta = \tan^{-1} \frac{2\zeta\omega_1^2}{\omega_1^2 - \omega^2} \cdot$$

It is shown in Appendix II that the transfer function, $H(i\omega)$, can be used to derive an impulse response function, $h(t)$, given by

$$h(t) = \frac{e^{-\omega_1 \frac{\zeta}{2} t} (\sin \omega_1 t)}{\omega_1} .$$

The impulse response is seen to be a damped sine wave with period $\tau = 2\pi/\omega_1$. Positive peaks occur at time intervals

$$t = \frac{\left(\frac{\pi}{2} + 2n\pi\right)}{\omega_1}, \qquad n = 0, 1, 2, 3, \text{------} .$$

The ratio of successive peaks h_n and h_{n+1} is given by

$$\frac{h_n}{h_{n+1}} = \frac{e^{-\frac{\zeta}{2}\left(\frac{\pi}{2} + 2n\pi\right)}}{e^{-\frac{\Delta}{2}\left(\frac{\pi}{2} + 2(n+1)\pi\right)}} = e^{2\zeta\pi} = e^{\delta}$$

where $\delta = 2\zeta\pi$ is called the logarithmic decrement.

Thus, the damping ratio, ζ, for an equivalent single degree of freedom model with light viscous damping can be obtained from measurements of the logarithmic decrement by using the relation

$$\delta = 2\pi\zeta .$$

<u>Sinusoidal Acceleration of One End of a Duct Section at Resonance</u>

When one end of a simply supported duct section is subjected to a sinusoidal acceleration, Ng $\sin\omega t$, at the frequency of the fundamental vibration mode, the duct deflection can be represented in the form

$$Y(x,t) = B'_1 \sin\frac{\pi x}{\ell} \sin\omega_1 t .$$

The bending strains are given by

$$\epsilon_x(x,y,t) = -y \frac{\partial^2 Y}{\partial x^2}(x,t)$$

and have a maximum value, at the section $x = \ell/2$, and at a distance $y = \pm r_2$ from the duct axis, of magnitude

$$\epsilon = \left|\epsilon_x\left(\frac{\ell}{2}, \pm r_2\right)\right| = r_2\left(\frac{\pi}{\ell}\right)^2 B'_1 .$$

If N and ϵ are measured in an experiment and the duct damping coefficient is defined as

$$2\zeta = \frac{B_1}{B'_1} ,$$

it can be seen that for a thin-walled duct

$$\zeta = \frac{4}{\pi^3} \frac{\gamma}{E} \frac{N}{\epsilon} \frac{\ell^2}{r}$$

where $r = d_2 - t/2 = r_1 + r_2/2$ is an effective duct ratio, $\gamma = \rho g$ is the weight density of the duct material, d_2 and r_2 are the outer diameter and radius of the duct cross-section, r_1 is the internal radius, t is the duct wall thickness, and the second moment of area has been assigned the approximate value

$$I \approx \pi r^3 t .$$

The present equation for ζ is greater by a factor of $4/\pi$ than the result reported earlier on NASA Contract NAS8-21128. The difference arises because the duct section subjected to a uniform acceleration in the above analysis was considered to be elastic. If it had been considered to be rigid, the previous result would have been obtained.

The prediction equation has been expressed therefore in the alternate forms

$$\zeta = \frac{1}{\pi^2} \frac{\gamma}{E} \frac{N}{\epsilon} \frac{\ell^2}{r} , \qquad 5.$$

and

$$\zeta = \frac{4}{\pi^3} \frac{\gamma}{E} \frac{N}{\epsilon} \frac{\ell^2}{r} . \qquad 6.$$

The latter equation is to be used when deflections of the vibrating duct are compared with those of an elastic duct that is subjected to a uniform acceleration on one end. The former equation is one in which deflections of the vibrating duct are compared with those of a rigid duct subjected to a uniform acceleration on one end.

Tabular and graphical data, presented below for Test Series I duct sections, have been computed on the basis of Equation 5, using the average value of γ/E given in Table IV.

TABLE IV

DERIVATION OF AN AVERAGE VALUE FOR γ/E

Material	E (newtons/m^2)	γ (newtons/m^3)	γ/E
AISI 321 Stainless Steel	19.3×10^{10}	76.9×10^{3}	39.8×10^{-8}
Inconel 718	20.7×10^{10}	80.8×10^{3}	39.0×10^{-8}
6A1-4V Titanium	11.7×10^{10}	43.5×10^{3}	37.2×10^{-8}
6061-T6 Aluminum	6.9×10^{10}	26.6×10^{3}	40.3×10^{-8}
		Average γ/E =	39.1×10^{-8}

When the average value, $\gamma/E = 39.1 \times 10^{-8}$, is substituted in Equation 5, the damping ratio prediction equation can be written in the simplified form

$$\zeta = 4.0 \times 10^{-8} \frac{N}{\epsilon} \frac{\ell^2}{r} . \qquad 7.$$

Equations 4 and 7 may be used to obtain the alternate expression

$$\zeta = 2.2 \times 10^{-4} \frac{1}{f_1} \frac{N}{\epsilon} . \qquad 8.$$

Equations 7 and 8 have been used to construct a condensed nomograph consisting of three parallel straight scales (Fig. 12). Conversion of damping ratio values to other damping quantities, according to the following relations, is shown in Figure 13.

$$\delta \simeq 2\pi\zeta \simeq \pi\eta \simeq \frac{\pi}{Q} ,$$

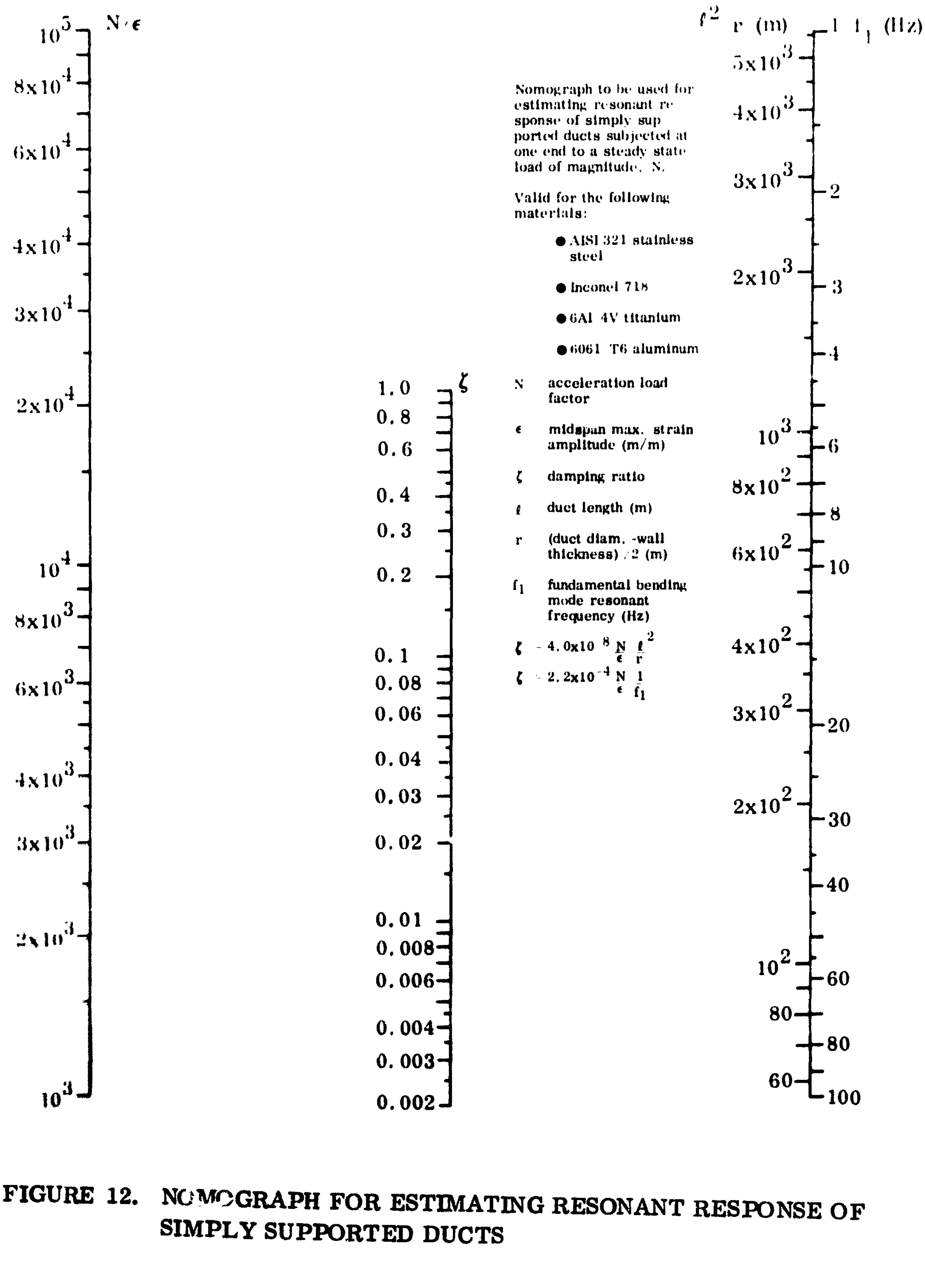

FIGURE 12. NOMOGRAPH FOR ESTIMATING RESONANT RESPONSE OF SIMPLY SUPPORTED DUCTS

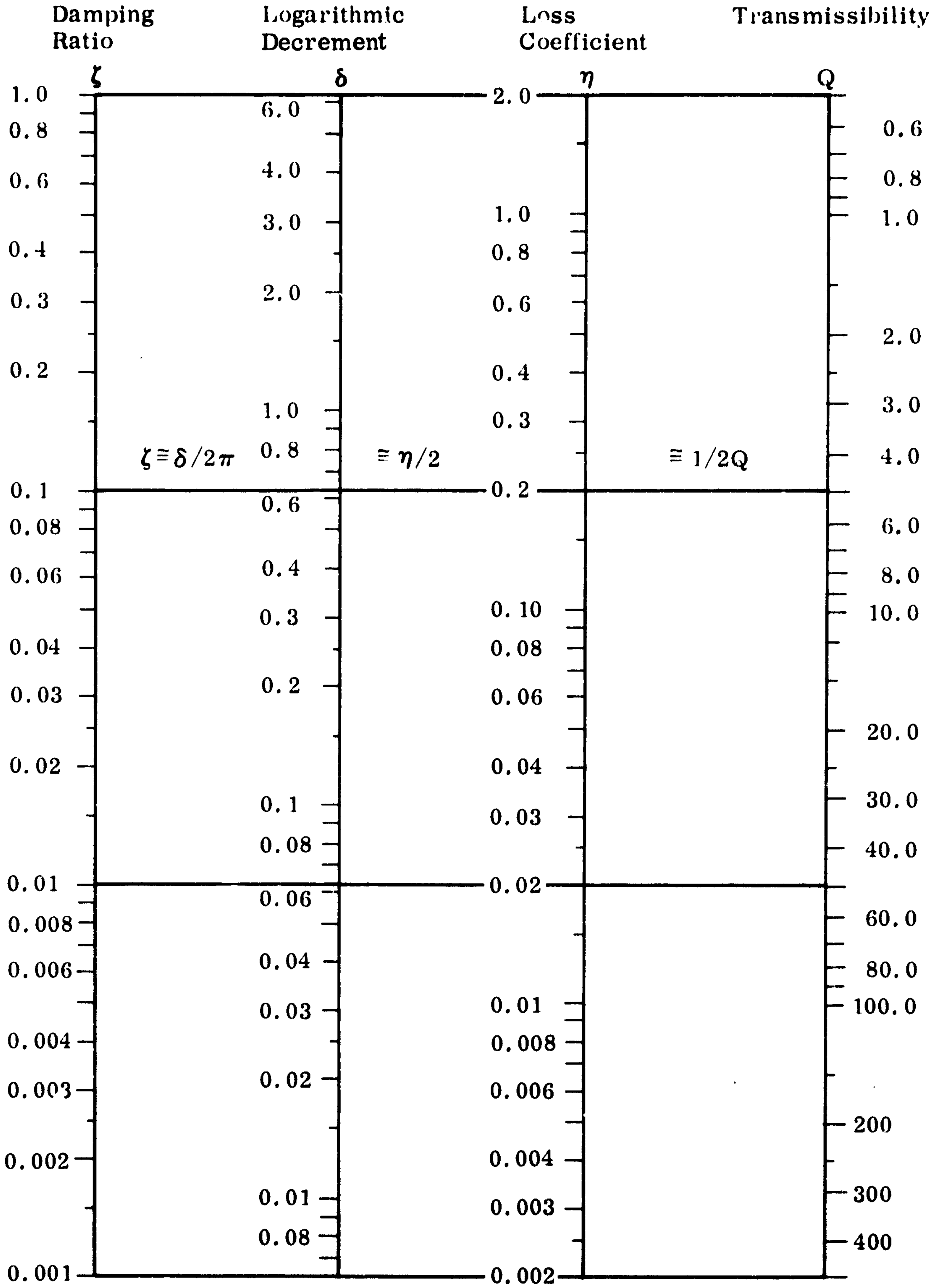

FIGURE 13. CONVERSION OF DAMPING QUANTITIES

where δ = logarithmic decrement

ζ = damping ratio

η = loss coefficient

and Q = transmissibility

4.2 TEST SERIES I RESULTS

Test Series I results are presented in Tables V through VIII. Test numbers and duct materials and geometries are identified. If the electrodynamic shaker input force at a fundamental bending mode resonant frequency is defined as

$$F_1 = |F_1| \sin \omega_1 t \ ,$$

the amplitude of the driving force $|F_1|$ may be expressed as

$$|F_1| = NMg \text{ (newtons)},$$

where N = acceleration load factor, dimensionless

and g = local acceleration due to gravity (m/sec^2)

M = effective mass (kgm)

Additional symbols used in the tables are as follows:

ℓ = duct length (m)

d = duct diameter (m)

t = wall thickness (m)

ϵ = midspan maximum strain amplitude (m/m)

ζ = damping ratio, dimensionless

Q = amplitude amplification factor, or transmissibility, dimensionless

σ = midspan maximum stress amplitude (newtons/m^2 or lb/in.^{2}).

TABLE V

AISI 321 STAINLESS STEEL DUCT TEST DATA

Test	Length, l (m)		Diameter, d (m)		Wall Thickness, t (m)	
I-A-1	1.53		0.0508		0.00124	
N	ϵ (x 10^6)	N/ϵ	ζ	Q	σ newtons/m^2 (x 10^{-7})	lb/in.^{2} (x 10^{-3})
1.1	184	5980	0.0224	22.4	3.55	5.15
1.3	227	5730	0.0215	23.3	4.39	6.36
1.9	298	6380	0.0208	24.0	5.75	8.34
2.2	360	6110	0.0230	21.8	6.97	10.1
3.2	550	5820	0.0218	22.9	10.6	15.4
3.8	650	5850	0.0220	22.8	12.6	18.2
5.0	810	6170	0.0231	21.6	15.7	22.7
6.0	1090	5500	0.0206	24.2	21.0	30.5
6.5	1220	5330	0.0200	25.0	23.6	34.2
7.6	1190	6390	0.0208	24.0	23.0	33.3
8.8	1550	5680	0.0213	23.5	29.9	43.4
9.0	1850	4860	0.0182	27.4	35.7	51.8
10.6	1950	5440	0.0204	24.5	37.7	54.6
11.2	2060	5440	0.0204	24.5	39.8	57.7
12.0	2125	5640	0.0212	23.6	41.1	59.5
13.5	2100	6430	0.0241	20.7	40.6	58.8
14.0	2220	6300	0.0236	21.2	42.9	62.2
15.2	2200	6910	0.0259	19.3	42.5	61.6
16.5	2410	6850	0.0257	19.5	46.6	67.5

TABLE V (Cont)

AISI 321 STAINLESS STEEL DUCT TEST DATA

Test	Length, l (m)		Diameter, d (m)		Wall Thickness, t (m)	
I-E-29	1.98		0.076		0.00124	
N	ϵ (x 10^6)	N/ϵ	ζ	Q	σ newtons/m^2 (x 10^{-7})	lb/in.^{2} (x 10^{-3})
1.0	145	6,900	0.0282	17.7	2.83	4.1
2.4	250	9,600	0.0393	12.7	4.83	7.0
4.4	360	12,220	0.0500	10.0	6.97	10.1
6.0	550	10,910	0.0447	11.2	10.6	15.4
6.8	565	12,040	0.0493	10.1	10.9	15.8
8.7	750	11,600	0.0475	10.5	14.5	21.0
9.4	835	11,260	0.0461	10.9	16.1	23.4
12.0	990	12,120	0.0496	10.1	19.1	27.7
15.0	1190	12,610	0.0516	9.7	23.0	33.3
16.0	1040	15,400	0.0630	7.9	20.1	29.1
17.0	1100	15,500	0.0632	7.9	23.1	30.8
22.0	1320	16,700	0.0682	7.3	25.5	37.0
24.0	1280	18,800	0.0768	6.5	24.7	35.8
29.5	1310	22,500	0.0922	5.4	25.3	36.7
36.0	1420	25,400	0.1038	4.8	27.5	39.8
39.0	1400	27,900	0.1140	4.8	27.0	39.2
40.0	1500	26,700	0.1092	4.6	29.0	42.0
42.0	1700	24,700	0.1012	4.9	32.8	47.6

TABLE V (Cont)

AISI 321 STAINLESS STEEL DUCT TEST DATA

Test	Length, l (m)		Diameter, d (m)		Wall Thickness, t (m)	
I-B-8	1.98		0.102		0.00124	
N	ϵ (x 10^6)	N/ϵ	ζ	Q	σ newtons/m^2 (x 10^{-7})	lb/in.^{2} (x 10^{-3})
3.0	130	23,100	0.0718	7.0	2.51	3.64
4.0	210	19,000	0.0590	8.5	4.06	5.88
5.0	250	20,000	0.0620	8.1	4.83	7.0
7.6	360	21,100	0.0655	7.6	7.45	10.8
8.6	425	20,200	0.0626	8.0	8.21	11.9
9.2	440	20,900	0.0648	7.7	8.49	12.3
11.8	525	22,500	0.0699	7.2	10.1	14.7
13.2	720	18,300	0.0568	8.8	13.9	20.2
13.5	680	19,900	0.0617	8.1	13.1	19.0
16.4	830	19.800	0.0614	8.1	16.0	23.2
18.2	860	21,200	0.0658	7.6	16.6	24.1
19.3	950	20,300	0.0630	7.9	18.4	26.6
23.7	960	24,700	0.0766	6.5	18.6	26.9
25.0	1080	23,100	0.0718	7.0	20.8	30.2
27.0	1130	23,900	0.0743	6.7	21.8	31.6
30.0	1190	25,200	0.0782	6.4	23.0	33.3
34.0	1260	27,000	0.0838	5.9	24.4	35.3
40.2	1350	29.800	0.0925	5.4	26.1	37.8

TABLE VI

INCONEL 718 DUCT TEST DATA

Test	Length, l (m)		Diameter, d (m)		Wall Thickness, t (m)	
I-A-2	1.53		0.0508		0.00124	
N	ϵ (x 10^6)	N/ϵ	ζ	Q	σ newtons/m^2 (x 10^{-7})	lb/in.^{2} (x 10^{-3})
1.0	175	5,710	0.0214	23.6	3.62	5.25
2.0	275	7,270	0.0273	18.3	5.69	8.25
3.0	460	6,520	0.0245	20.4	9.51	13.8
4.0	600	6,670	0.0250	20.0	12.4	18.0
6.0	775	7,740	0.0290	17.2	16.0	23.2
7.0	875	8,000	0.0300	17.2	18.1	26.2
8.0	1000	8,000	0.0300	16.7	20.7	30.0
10.0	1120	8,930	0.0335	14.9	23.2	33.6
12.0	1200	10,000	0.0375	13.3	24.8	36.0
14.0	1380	10,140	0.0380	13.2	28.5	41.3
16.0	1420	11,270	0.0423	11.8	29.3	42.5
18.0	1480	12,160	0.0456	11.0	30.6	44.4
20.0	1600	12,500	0.0469	10.7	33.1	48.0
22.0	1570	14,010	0.0525	9.5	32.5	47.1
I-A-2a	1.53		0.0508		0.00124	
0.7	130	5,380	0.0206	24.2	2.69	3.9
1.1	250	4,400	0.0169	29.6	5.18	7.5
2.0	380	5,280	0.0206	24.2	7.87	11.4
4.0	630	6,350	0.0244	20.4	13.05	18.9
5.5	750	7,320	0.0281	17.8	15.51	22.5

TABLE VI (Cont)

INCONEL 718 DUCT TEST DATA

Test	Length, l (m)		Diameter, d (m)		Wall Thickness, t (m)	
I-A-2a	1.53		0.0508		0.00124	
N	ϵ ($\times 10^{-6}$)	N/ϵ	ζ	Q	σ newtons/m^2 ($\times 10^{-7}$)	lb/in.^{2} ($\times 10^{-3}$)
8.0	930	8,600	0.0330	15.1	19.25	27.9
7.4	1190	6,200	0.0248	20.1	24.6	35.7
12.0	1380	8,700	0.0334	15.0	28.5	41.4
13.8	1650	8,360	0.0321	15.5	34.2	49.5
14.8	1840	8,050	0.0309	16.2	38.1	55.2
17.1	2000	8,550	0.0328	15.3	41.4	60.0
20.0	2300	8,700	0.0334	15.0	47.5	69.0
23.0	2400	9,600	0.0368	13.6	49.6	72.0
25.0	2550	9.800	0.0386	13.0	52.7	76.5
I-E-30	1.98		0.076		0.00124	
1.0	120	8,330	0.0341	14.7	2.48	3.60
3.8	250	15,200	0.0341	8.0	5.18	7.50
4.6	365	12,600	0.0516	9.7	7.56	11.0
6.6	610	10,800	0.0443	11.3	12.6	18.3
8.4	840	10,000	0.0409	12.2	17.4	25.2
8.7	925	9,400	0.0358	13.0	19.2	27.7
10.5	980	10,700	0.0438	11.4	20.3	29.4
12.0	1140	10,500	0.0431	11.6	23.6	34.2
14.9	1230	12,100	0.0496	10.1	25.5	36.9
18.5	1600	11,600	0.0473	10.6	33.1	48.0

TABLE VI (Cont)

INCONEL 718 DUCT TEST DATA

Test	Length, l (m)		Diameter, d (m)		Wall Thickness, t (m)	
I-E-30	1.98		0.076		0.00124	
N	ϵ (x 10^6)	N/ϵ	ζ	Q	σ newtons/m^2 (x 10^{-7})	lb/in.^{2} (x 10^{-3})
22.0	1800	12,200	0.0500	10.0	37.26	54.0
25.0	2020	12,400	0.0507	9.9	41.81	60.6
30.0	2580	11,600	0.0476	10.5	53.41	77.4
32.0	2750	11,600	0.0477	10.5	56.93	82.5
I-E-30a	1.98		0.076		0.00124	
0.7	100	7,000	0.0287	17.5	2.07	3.0
2.4	250	9,000	0.0393	12.7	5.18	7.5
5.5	500	11,000	0.0450	11.1	10.4	15.0
10.2	900	11,300	0.0464	10.7	18.6	27.0
14.5	1355	10,700	0.0438	11.4	28.1	40.7
22.0	1980	11,100	0.0455	11.0	41.0	59.4
26.3	2510	10,500	0.0429	11.6	52.0	75.3
27.0	2700	10,000	0.0409	12.2	55.9	81.0
30.0	3300	9,100	0.0372	13.4	68.3	99.0
31.0	3300	9,400	0.0384	13.0	68.3	99.0
35.0	3600	9,700	0.0398	12.6	74.5	108.

TABLE VI (Cont)

INCONEL 718 DUCT TEST DATA

Test	Length, l (m)		Diameter, d (m)		Wall Thickness, t (m)	
I-E-30a	1.98		0.076		0.00124	
N	ϵ (x 10^6)	N/ϵ	ζ	Q	σ newtons/m^2 (x 10^{-7})	lb/in.^{2} (x 10^{-3})
1.9	100	19,000	0.0590	8.5	2.07	3.00
3.2	175	18,300	0.0568	8.8	3.62	5.25
5.5	300	18.300	0.0568	8.8	6.21	9.00
15.5	650	23,800	0.0739	6.8	13.5	19.5
20.0	870	23,000	0.0714	7.0	18.0	26.1
22.0	1020	21,606	0.0670	7.5	21.1	30.6
24.0	1170	20,500	0.0636	7.9	24.2	35.1
29.5	1390	21,200	0.0658	7.6	28.8	41.7
35.0	1660	21,100	0.0655	7.6	34.4	49.8
36.0	1880	19,100	0.0593	8.5	38.9	56.4
41.0	2050	20,000	0.0620	8.0	42.4	61.5
50.0	2340	21,400	0.0664	7.5	48.4	70.2
54.0	2710	19,900	0.0615	8.1	56.1	81.3

TABLE VII

6Al-4V TITANIUM DUCT TEST DATA

Test	Length, l (m)		Diameter, d (m)		Wall Thickness, t (m)	
I-A-4	1.53		0.0508		0.00124	
N	ϵ (x 10^6)	N/ϵ	ζ	Q	σ newtons/m^2 (x 10^{-7})	lb/in.^{2} (x 10^{-3})
2.0	500	4000	0.0150	33.2	5.87	8.5
2.5	732	3400	0.0129	39.2	8.59	12.4
3.5	1250	2800	0.0104	48.2	14.7	21.3
4.0	976	4100	0.0154	32.8	11.5	16.6
4.5	1250	3600	0.0135	33.2	14.7	21.3
6.0	1450	4100	0.0154	32.5	17.0	24.7
7.0	1860	3800	0.0141	35.4	21.8	31.6
8.0	2200	3600	0.0135	37.0	25.8	37.3
9.0	2070	4300	0.0160	31.2	24.3	35.3
9.3	2230	4200	0.0157	31.9	26.1	37.8
10.0	2520	4000	0.0150	33.2	29.6	42.8
10.5	2440	4300	0.0160	31.2	28.6	41.5
11.0	2500	4400	0.0166	30.0	29.3	42.5
12.0	2750	4400	0.0166	30.0	32.2	46.7
14.5	3170	4600	0.0173	28.9	37.2	53.9
15.0	3290	4600	0.0173	28.9	38.6	56.0
15.8	3480	4500	0.0170	29.5	40.8	59.0
19.0	3780	5000	0.0188	26.5	44.4	64.3
22.5	4270	5300	0.0198	25.3	50.1	72.6

TABLE VII (Cont)

6Al-4V TITANIUM DUCT TEST DATA

Test	Length, l (m)		Diameter, d (m)		Wall Thickness, t (m)	
I-A-4	1.98		0.076		0.00124	
N	ϵ ($\times 10^6$)	N/ϵ	ζ	Q	σ newtons/m^2 ($\times 10^{-7}$)	lb/in.^{2} ($\times 10^{-3}$)
1.0	180	5.550	0.0227	22.0	2.11	3.06
3.8	550	6,910	0.0283	17.7	6.45	9.35
5.8	860	6,740	0.0276	18.1	10.1	14.6
9.4	1330	7,000	0.0287	17.5	15.6	22.6
10.5	1550	6,770	0.0277	18.0	18.2	26.4
12.0	2020	5,940	0.0243	20.6	23.7	34.3
16.2	2650	6,110	0.0250	20.0	31.1	45.0
20.0	3250	6,150	0.0252	19.9	38.1	55.3
21.6	3400	6,350	0.0260	19.2	39.9	57.8
26.2	4700	5,570	0.0228	21.9	55.1	79.9
I-B-11	1.98		0.102		0.00124	
1.2	110	10,900	0.0339	14.7	1.29	1.87
3.0	225	13,300	0.0413	12.1	2.64	3.83
3.6	300	12,000	0.0372	13.4	3.52	5.10
6.7	460	14,600	0.0454	11.0	5.40	7.82
7.6	500	15,200	0.0473	10.6	5.87	8.50
7.8	580	13,300	0.0413	12.1	6.86	9.95
8.4	710	11,700	0.0363	13.8	8.39	12.2
12.8	870	14,700	0.0457	10.9	10.2	14.8

TABLE VII (Cont)

6Al-4V TITANIUM DUCT TEST DATA

Test	Length, l (m)		Diameter, d (m)		Wall Thickness, t (m)	
I-B-11	1.98		0.102		0.00124	
N	ϵ (x 10^6)	N/ϵ	ζ	Q	σ newtons/m^2 (x 10^{-7})	lb/in.^{2} (x 10^{-3})
13.2	930	14,300	0.0444	11.3	10.9	15.7
14.0	990	14,100	0.0438	11.4	11.6	16.8
16.5	1300	12,700	0.0394	12.7	15.2	22.1
21.0	1630	12,900	0.0400	12.5	19.1	27.6
24.0	1740	13,800	0.0429	11.6	20.4	29.5
27.0	1850	14,600	0.0454	11.0	21.7	31.5
33.0	2700	12,000	0.0378	13.2	31.7	45.9
36.0	2820	12,800	0.0397	12.6	42.2	61.2
45.0	3440	13,100	0.0407	12.3	52.8	76.5

TABLE VIII

6061-T6 ALUMINUM DUCT TEST DATA

Test	Length, l (m)		Diameter, d (m)		Wall Thickness, t (m)	
I-A-3	1.53		0.0508		0.00124	
N	ϵ ($\times 10^6$)	N/ϵ	ζ	Q	σ newtons/m^2 ($\times 10^{-7}$)	lb/in.^{2} ($\times 10^{-3}$)
0.1	200	500	0.0019	265.3	1.38	2.00
0.3	320	940	0.0035	142.1	2.21	3.20
0.4	370	1080	0.0040	123.4	2.55	3.70
0.7	410	1710	0.0064	78.0	2.83	4.10
0.9	560	1610	0.0060	82.9	3.86	5.60
1.1	600	1830	0.0069	72.7	4.14	6.00
1.3	740	1760	0.0066	75.8	5.12	7.40
1.5	870	1720	0.0064	77.7	6.00	8.70
1.7	940	1810	0.0068	73.7	6.49	9.40
2.1	1020	2060	0.0077	64.7	7.05	10.2
3.1	1150	2700	0.0101	49.4	7.95	11.5
3.3	1340	2460	0.0092	54.1	9.25	13.4
3.5	1490	2350	0.0088	56.9	10.3	14.9
3.7	1830	2020	0.0076	66.0	12.6	18.3
4.2	1960	2140	0.0080	62.2	13.5	19.6
5.0	2240	2230	0.0084	59.8	15.5	22.4
6.3	3060	2060	0.0093	53.8	21.1	30.6
6.6	3730	1770	0.0066	75.4	25.8	37.3
9.7	5070	1910	0.0072	69.8	35.0	50.8

TABLE VIII (Cont)

6061-T6 ALUMINUM DUCT TEST DATA

Test	Length, l (m)		Diameter, d (m)		Wall Thickness, t (m)	
I-E-31	1.98		0.076		0.00124	
N	ϵ (x 10^6)	N/ϵ	ζ	Q	σ newtons/m^2 (x 10^{-7})	lb/in.^{2} (x 10^{-3})
0.3	190	1580	0.0065	77.3	1.31	1.90
0.8	310	2580	0.0106	47.4	2.14	3.10
1.7	440	3860	0.0158	31.6	3.04	4.40
3.8	1000	3800	0.0156	32.2	6.90	10.0
5.4	1100	4910	0.0201	24.9	7.59	11.0
6.4	1440	4440	0.0182	27.5	9.94	14.4
7.4	2000	3850	0.0154	32.6	13.8	20.0
9.5	2530	3850	0.0154	32.6	17.5	25.3
11.2	2730	4100	0.0168	29.8	18.8	27.3
13.5	3200	4220	0.0173	[illegible]	22.0	32.0
I-B-10	1.98		0.102		0.00124	
0.3	90	3300	0.0103	48.4	0.62	0.90
0.7	120	5830	0.0181	27.6	0.83	1.20
1.2	150	8000	0.0248	20.1	1.04	1.50
1.4	180	7780	0.0241	20.7	1.24	1.80
1.8	240	7500	0.0233	21.5	1.66	2.40
2.6	340	7650	0.0238	21.1	2.35	3.40
3.7	450	8220	0.0310	16.1	3.11	4.50
5.6	675	8300	0.0258	19.4	4.66	6.75

TABLE VIII (Cont)

6061-T6 ALUMINUM DUCT TEST DATA

Test	Length, l (m)		Diameter, d (m)		Wall Thickness, t (m)	
I-B-10	1.98		0.102		0.00124	
N	ϵ ($\times 10^6$)	N/ϵ	ζ	Q	σ newtons/m^2 ($\times 10^{-7}$)	lb/in.^{2} ($\times 10^{-3}$)
6.2	760	8160	0.0253	19.7	5.24	7.60
8.6	1040	8270	0.0310	16.1	7.18	10.4
9.8	1260	7780	0.0241	20.7	8.69	12.6
12.4	1750	7090	0.0220	22.7	12.0	17.5
15.0	2000	7500	0.0233	21.5	13.8	20.0
17.0	2240	7590	0.0236	21.2	15.5	22.4
20.0	2570	7780	0.0241	20.7	17.7	25.7
22.0	2920	7530	0.0234	21.4	20.1	29.2

Plots of ϵ versus N and σ versus N are given in Figures 14 through 17. Tangent Young's modulus values were used to convert measured strains to estimates of bending stresses. The values, ϵ versus N, for heat treated Inconel 718, 6061-T6, and 6A1-4V alloy ducts obey essentially linear relationships, which can be interpreted to mean that inelastic damping mechanisms are not dominant with these materials; however, the ϵ versus N relationships for AISI 321 stainless steel ducts are clearly nonlinear. Therefore, bending stresses for the stainless steel ducts should more properly have been computed on the basis of secant Young's modulus values. This approach was not followed because only static tensile stress-strain data are available for AISI 321 stainless steel. The 321 stainless steel stress data could be re-interpreted if dynamic stress-strain data became available in future tests.

To provide a common basis of comparison for the results obtained with the four test materials in terms useful to designers, an arbitrary design life of 3×10^5 load cycles was chosen. Fatigue stresses at 3×10^5 load cycles for an environment at a temperature of 21°C were determined from available fatigue curves. Equation 5 was used to predict damping ratios, ζ, at values of N/ϵ for the 3×10^5 load cycle design life. Results are summarized in Table IX. Nomographs in Figures 18 through 21 were used to obtain the tabulated damping ratio values.

If the single degree of freedom model used in deriving the Test Series I damping ratio prediction equation (Equation 5) is valid, the damping ratios in Table IX should follow a general linear relationship (on a log-log plot of ζ versus N/ϵ at a slope of unity with logarithmic modules of equal length). Figure 22 represents such a plot, in which experimental values of ζ versus N/ϵ for a 3×10^5 cycle design life are compared with a dashed line at a slope of unity.

4.3 TEST SERIES II RESULTS

A total of 20 duct sections was fabricated for evaluation of one inelastic damping sleeve configuration. In the configuration, damping sleeves of uniform thicknesses and with a 360 degree angle of wrap were bonded to the midspan portions of the ducts. Details of the duct and damping sleeve geometries are listed in Table I. Two sleeve thicknesses, 0.13 and 0.25 millimeters, and sleeve lengths in the range 25 to 41 centimeters were investigated. AISI 321 stainless steel was selected as the damping sleeve material in each case. Three duct materials, Inconel 718, 6Al-4V titanium, and 6061-T6 aluminum, were used.

TABLE IX

VALUES OF DAMPING RATIO, ζ, AND ACCELERATION LOAD FACTOR/STRAIN RATIO, N/ϵ, AT LOAD LIMIT, N, FOR 3 X 10^5 CYCLE DESIGN LIFE

Material and 3 x 10^5 Cycle Fatigue Limit Stress	Test	Length (m)	Diameter (m)	N	ϵ	N/ϵ	ζ
AISI 321 Stainless Steel	I-A-1	1.53	0.0508	7.0	1250×10^{-6}	5.6×10^{3}	0.020
$\sigma_f = 24.2 \times 10^7$	I-E-29	1.98	0.076	20.3	1250×10^{-6}	16.2×10^{3}	0.065
(newtons/m^2)	I-B-8	1.98	0.102	32.0	1250×10^{-6}	25.6×10^{3}	0.080
Inconel 718	I-A-2a	1.53	0.0508	25.0	2530×10^{-6}	9.9×10^{3}	0.036
$\sigma_f = 52.3 \times 10^7$	I-E-30a	1.98	0.076	30.0	2530×10^{-6}	11.8×10^{3}	0.049
(newtons/m^2)	I-B-9	1.98	0.102	52.3	2530×10^{-6}	20.8×10^{3}	0.065
6Al-4V Titanium	I-A-4	1.53	0.0508	14.5	3300×10^{-6}	4.4×10^{3}	0.016
$\sigma_f = 38.6 \times 10^7$	I-E-32	1.98	0.076	21.0	3300×10^{-6}	6.4×10^{3}	0.026
(newtons/m^2)	I-B-11	1.98	0.102	43.3	3300×10^{-6}	13.1×10^{3}	0.041
6061-T6 Aluminum	I-A-3	1.53	0.0508	5.7	2700×10^{-6}	2.1×10^{3}	0.0076
$\sigma_f = 18.6 \times 10^7$	I-E-31	1.98	0.076	11.0	2700×10^{-6}	4.1×10^{3}	0.017
(newtons/m^2)	I-B-10	1.98	0.102	20.5	2700×10^{-6}	7.6×10^{3}	0.024

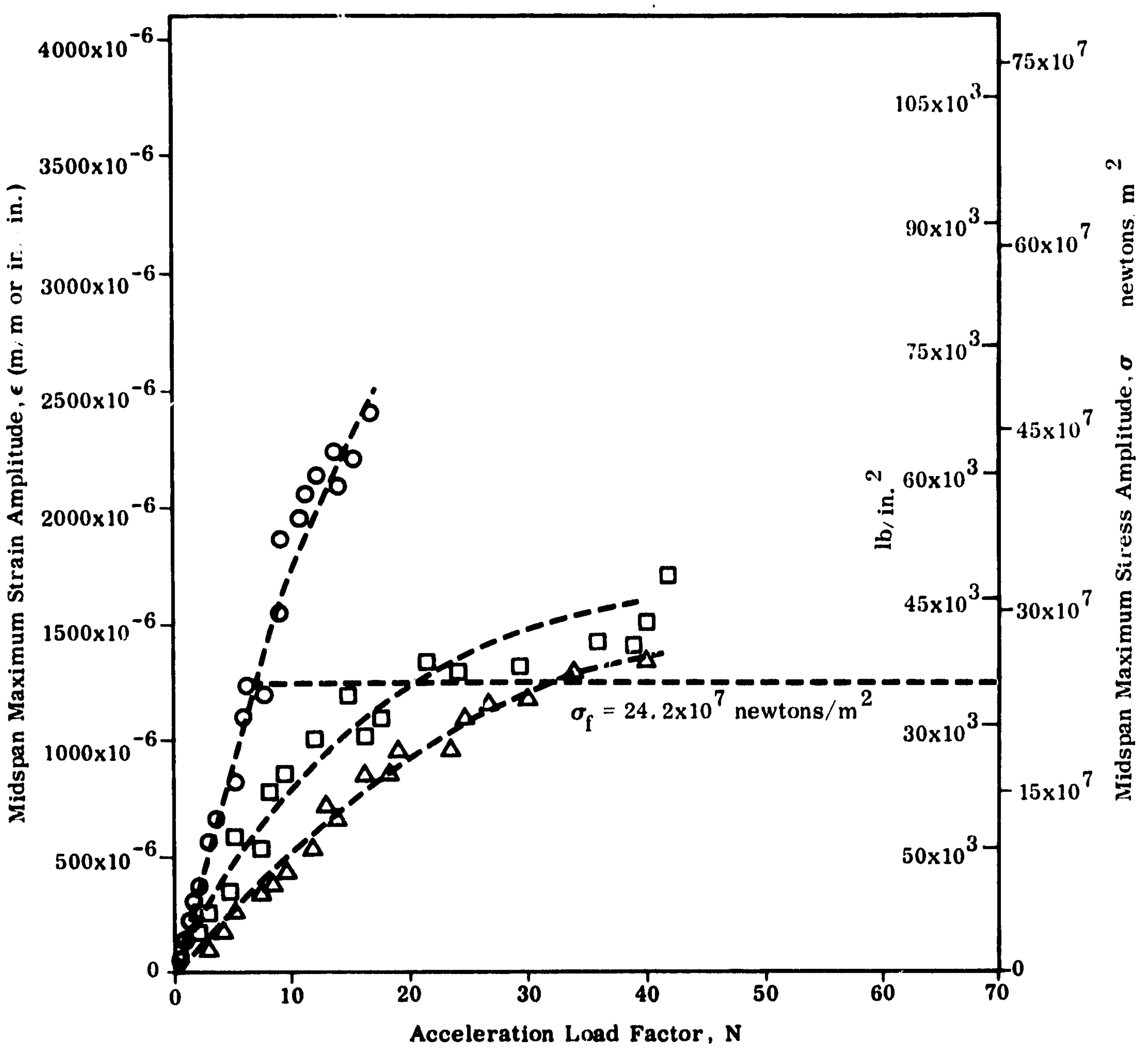

σ_f = Fatigue Limit at 21°C and 3 x 10^5 Load Cycles

$\sigma = E\epsilon$; E = 19.3 x 10^{10} newtons/m^2

Test	Symbol	Length (m)	Diameter (m)
I-A-1	○	1.53	0.025
I-E-29	□	1.98	0.037
I-B-8	△	1.98	0.050

Duct Wall Thickness = 1.24 x 10^{-3}m

FIGURE 14. MIDSPAN MAXIMUM STRAIN AND STRESS AMPLITUDES VERSUS ACCELERATION LOAD FACTOR FOR AISI 321 STAINLESS STEEL DUCTS

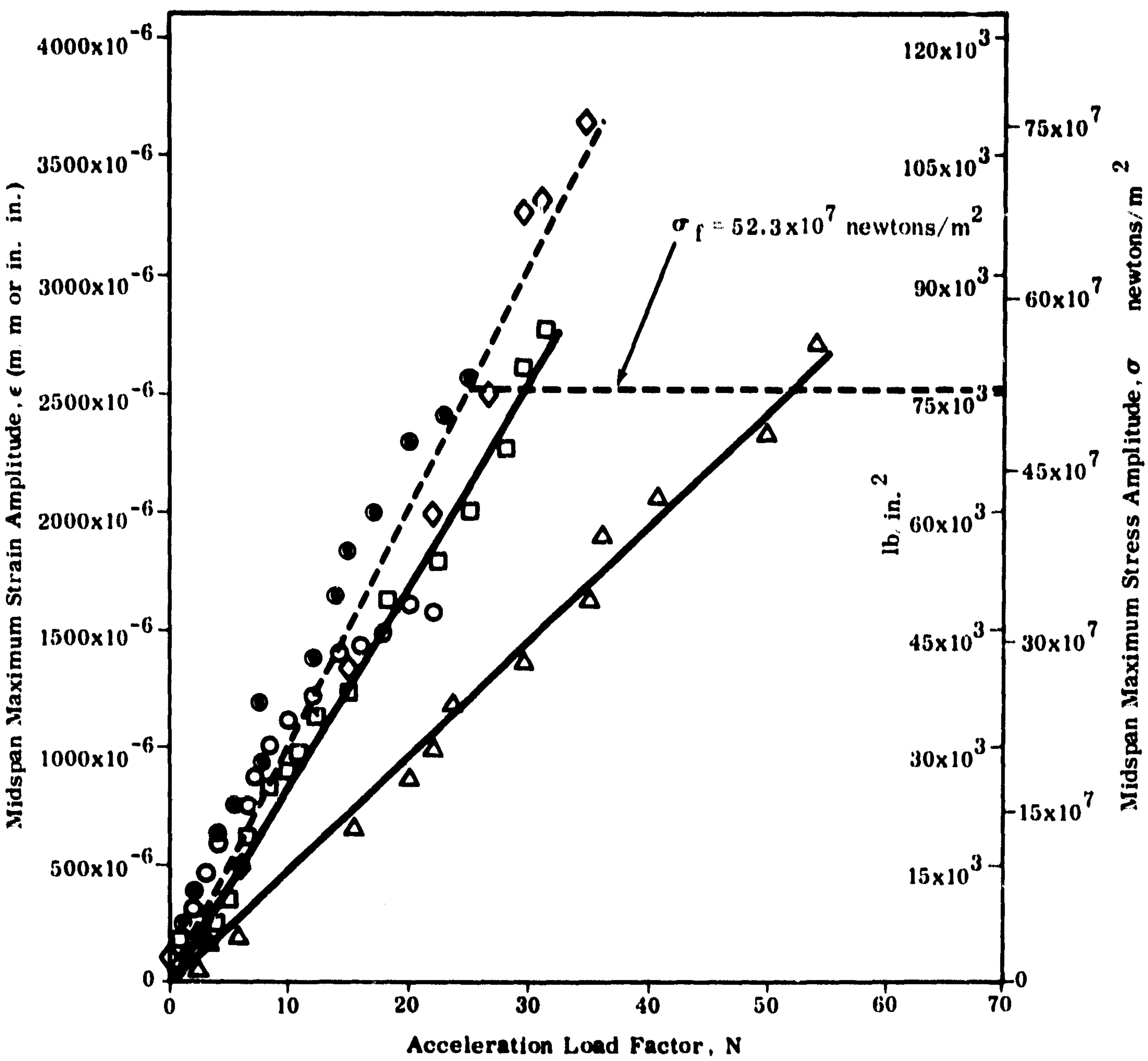

σ_f = Fatigue Limit at 21°C and 3×10^5 Load Cycles

$\sigma = E\epsilon$; $E = 20.7 \times 10^{10}$ newtons/m^2

Test	Symbol	Length (m)	Diameter (m)	Condition
I-A-2	○	1.53	0.025	Annealed
I-A-2a	●	1.53	0.025	Heat Treated
I-E-30	□	1.98	0.037	Annealed
I-E-30a	◇	1.98	0.037	Heat Treated
I-B-9	△	1.98	0.050	Annealed

Duct Wall Thickness = 1.24×10^{-3}m

FIGURE 15. MIDSPAN MAXIMUM STRAIN AND STRESS AMPLITUDES VERSUS ACCELERATION LOAD FACTOR FOR INCONEL 718 DUCTS

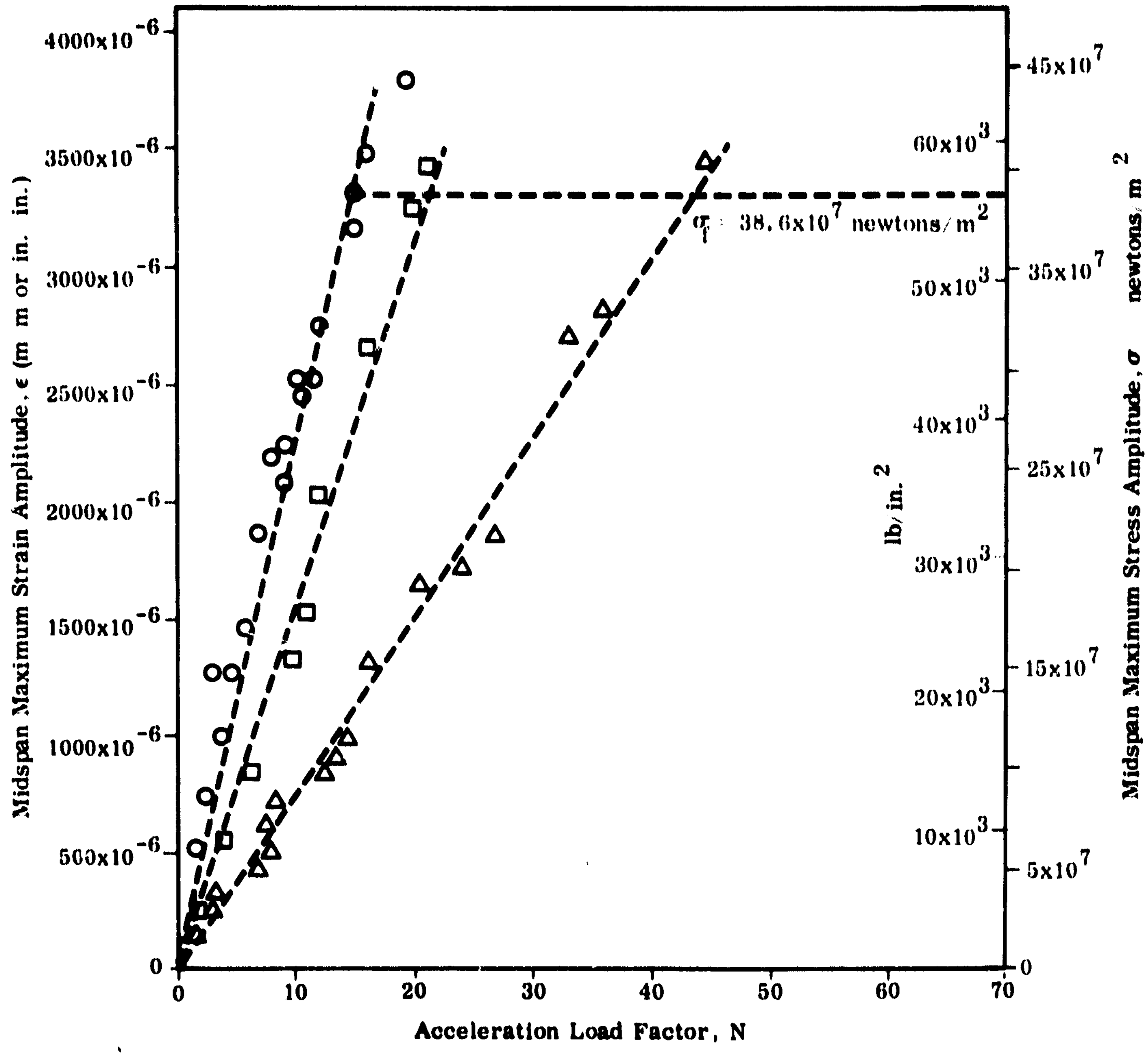

σ_f = Fatigue Limit at 21°C and 3×10^5 Load Cycles

$\sigma = E\epsilon$; $E = 11.7 \times 10^{10}$ newtons/m^2

Test	Symbol	Length (m)	Diameter (m)
I-A-4	○	1.53	0.025
I-E-32	□	1.98	0.037
I-B-11	△	1.98	0.050

Duct Wall Thickness = 1.24×10^{-3} m

FIGURE 16. MIDSPAN MAXIMUM STRAIN AND STRESS AMPLITUDES VERSUS ACCELERATION LOAD FACTOR FOR 6Aℓ-4V TITANIUM DUCTS

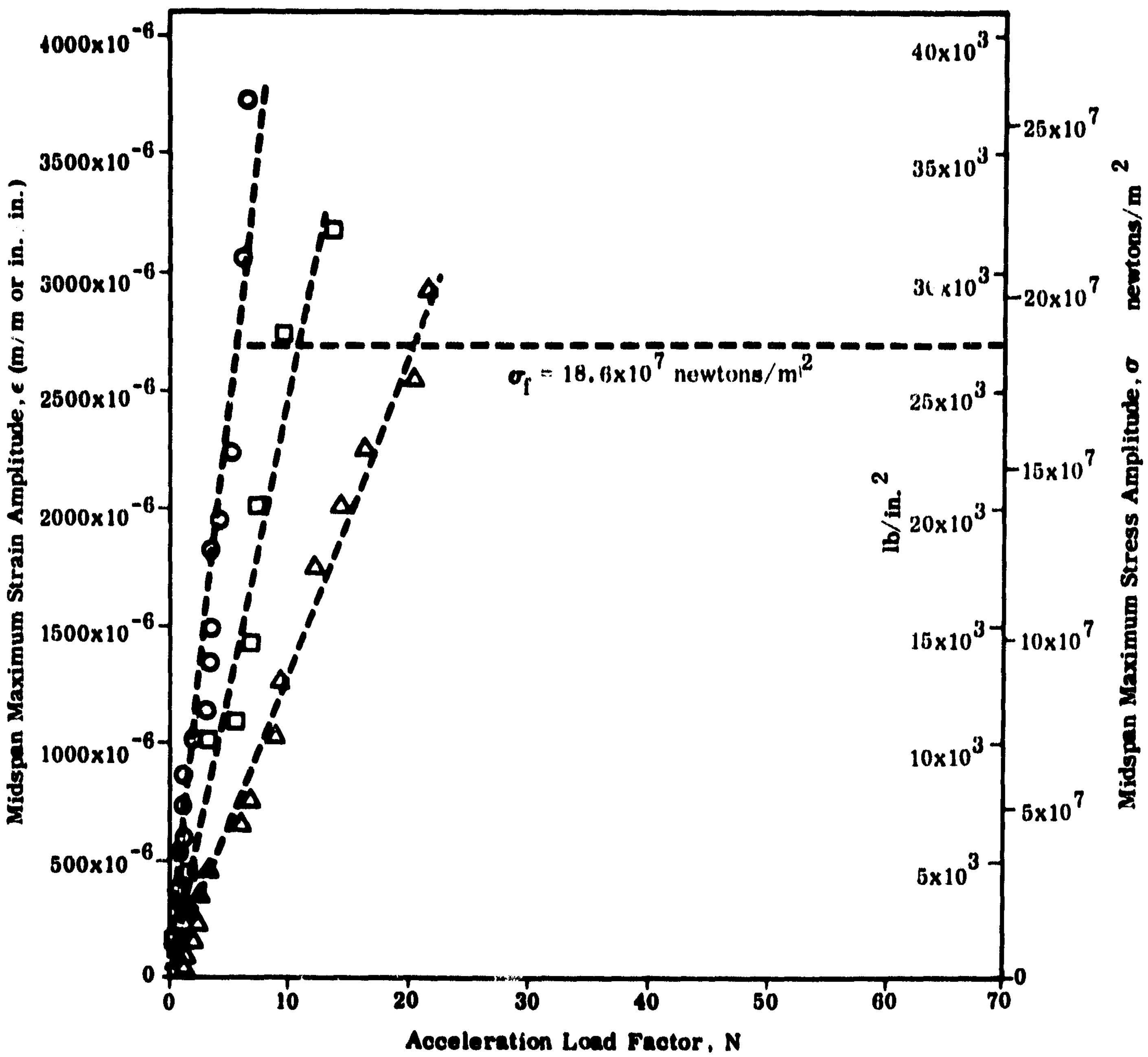

σ_f = Fatigue Limit at 21°C and 3×10^5 Load Cycles

$\sigma = E\epsilon$; $E = 6.9 \times 10^{10}$ newtons/m^2

Test	Symbol	Length (m)	Diameter (m)
I-A-3	○	1.53	0.025
I-E-31	□	1.98	0.037
I-B-10	△	1.98	0.050

Duct Wall Thickness = 1.24×10^{-3}m

FIGURE 17. MIDSPAN MAXIMUM STRAIN AND STRESS AMPLITUDES VERSUS ACCELERATION LOAD FACTOR FOR 6061-T6 ALUMINUM DUCTS

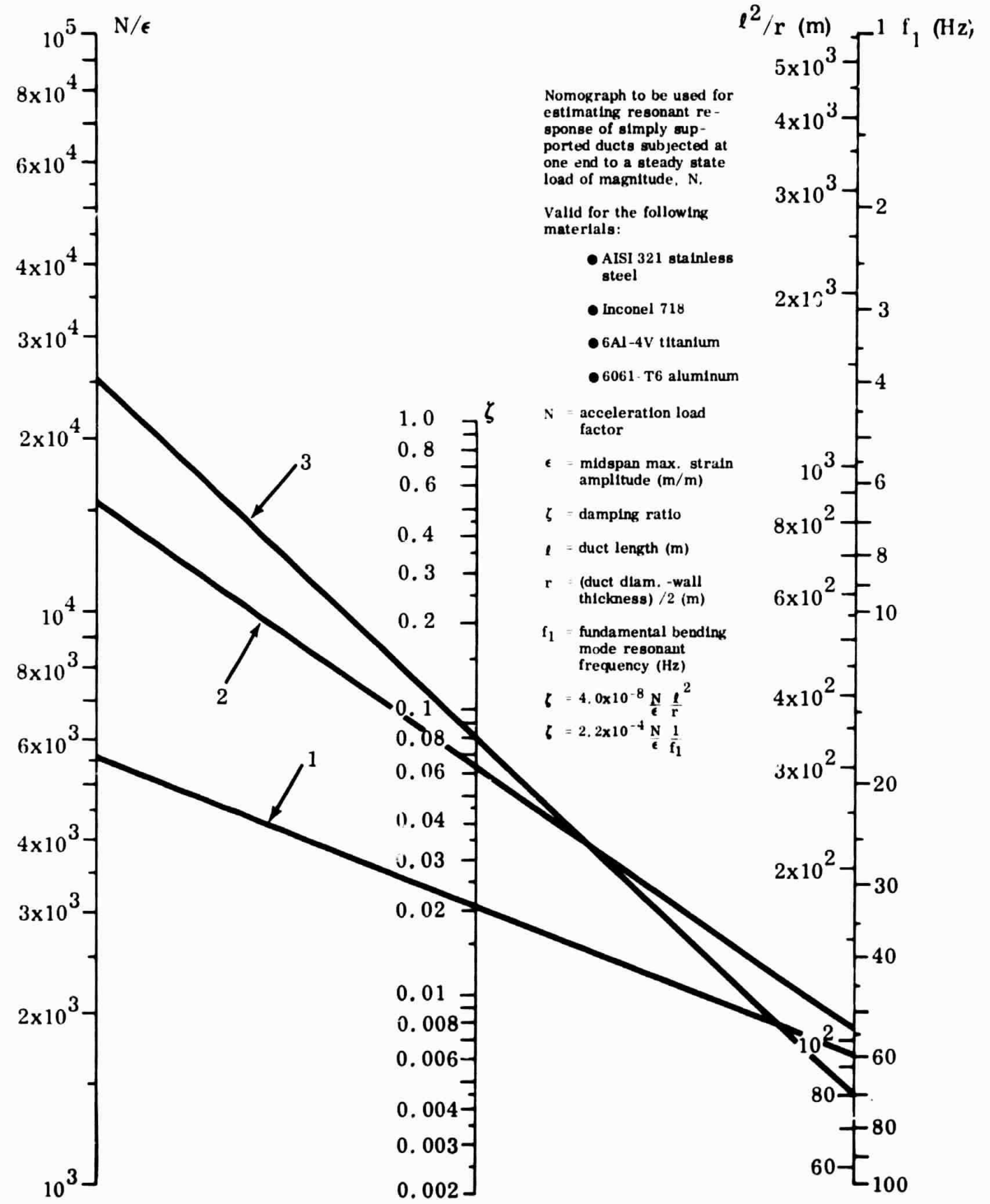

Curve	Test	Life Load Factor, N, at 21°C and 3×10^5 Cycle Design	Length, (m)	Diameter, d (m)	Wall Thickness, t (m)
1	I-A-1	7.0	1.53	0.0508	0.00124
2	I-E-29	20.3	1.98	0.076	0.00124
3	I-B-8	32.0	1.98	0.102	0.00124

FIGURE 18. DAMPING RATIOS FOR AISI 321 STAINLESS STEEL DUCTS

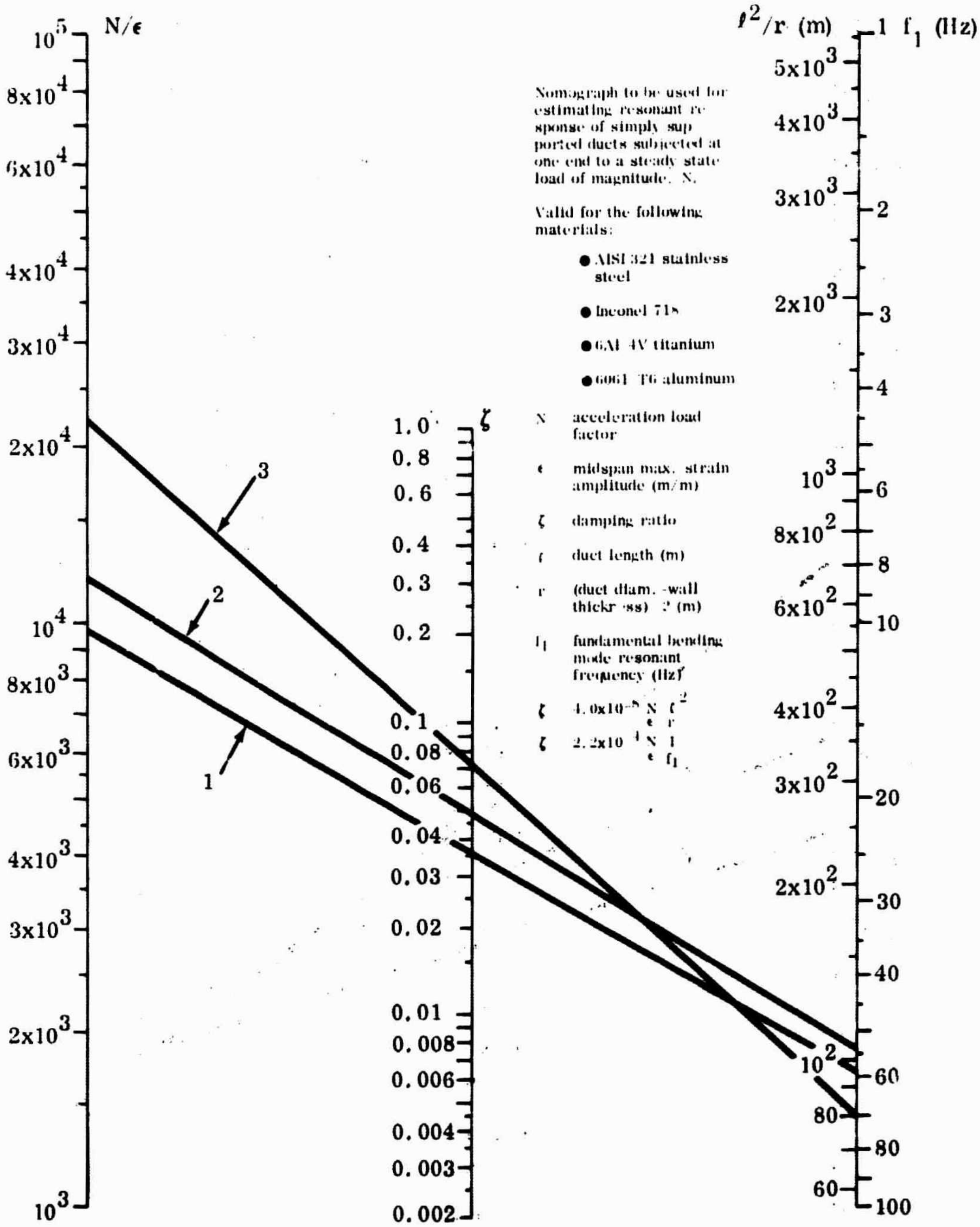

Curve	Test	Life Load Factor, N, at 21°C and 3×10^5 Cycle Design	Length, (m)	Diameter, d (m)	Wall Thickness, t (m)
1	I-A-2a	25.0	1.53	0.0508	0.00124
2	I-E-30a	30.0	1.98	0.076	0.00124
3	I-B-9	52.3	1.98	0.102	0.00124

FIGURE 19. DAMPING RATIOS FOR INCONEL 718 DUCTS

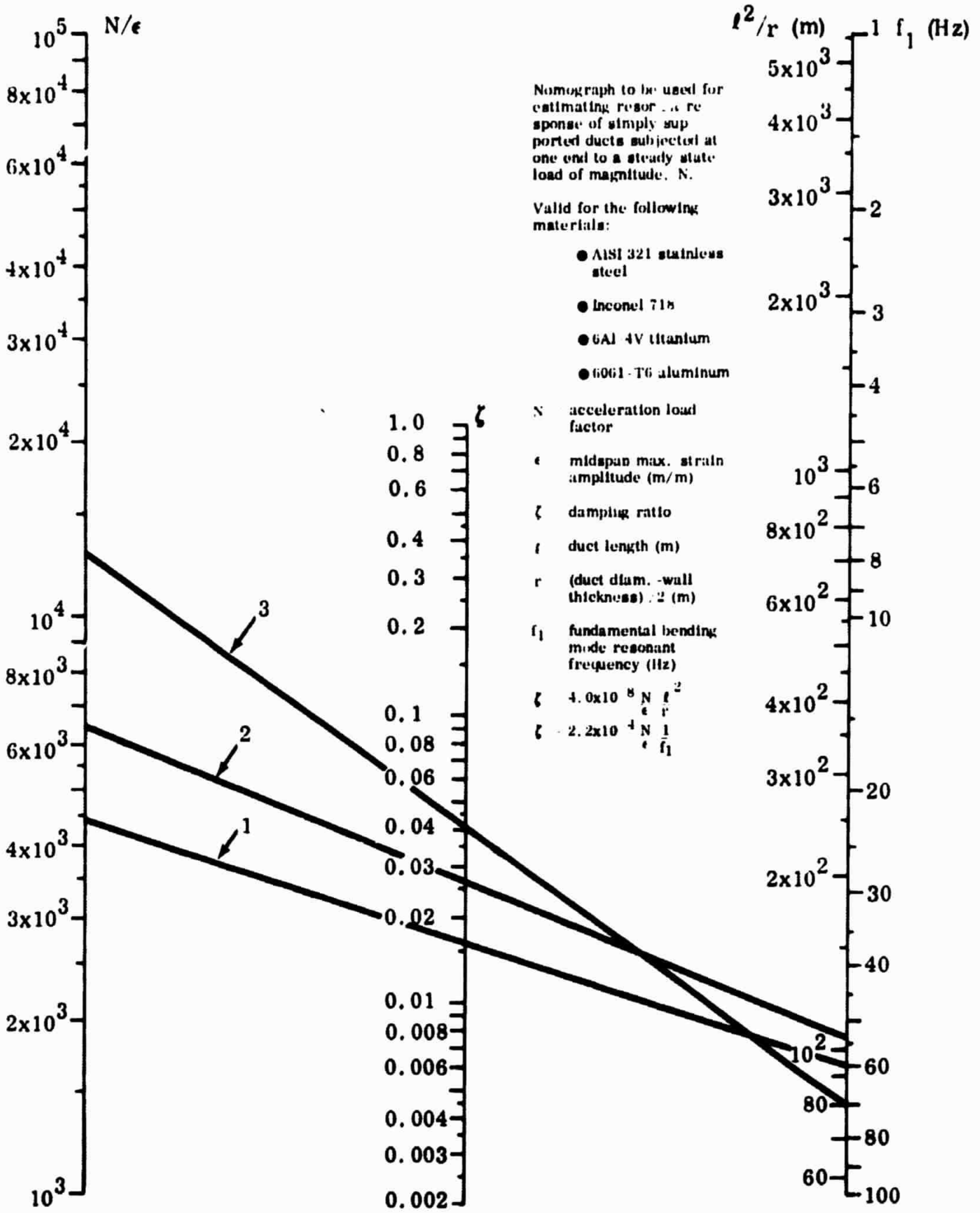

Curve	Test	Life Load Factor, N, at 21°C and 3x10^5 Cycle Design	Length, (m)	Diameter, d (m)	Wall Thickness, t (m)
1	I-A-4	14.5	1.53	0.0508	0.00124
2	I-E-32	21.0	1.98	0.076	0.00124
3	I-B-11	43.3	1.98	0.102	0.00124

FIGURE 20. DAMPING RATIOS FOR 6Aℓ-4V TITANIUM DUCTS

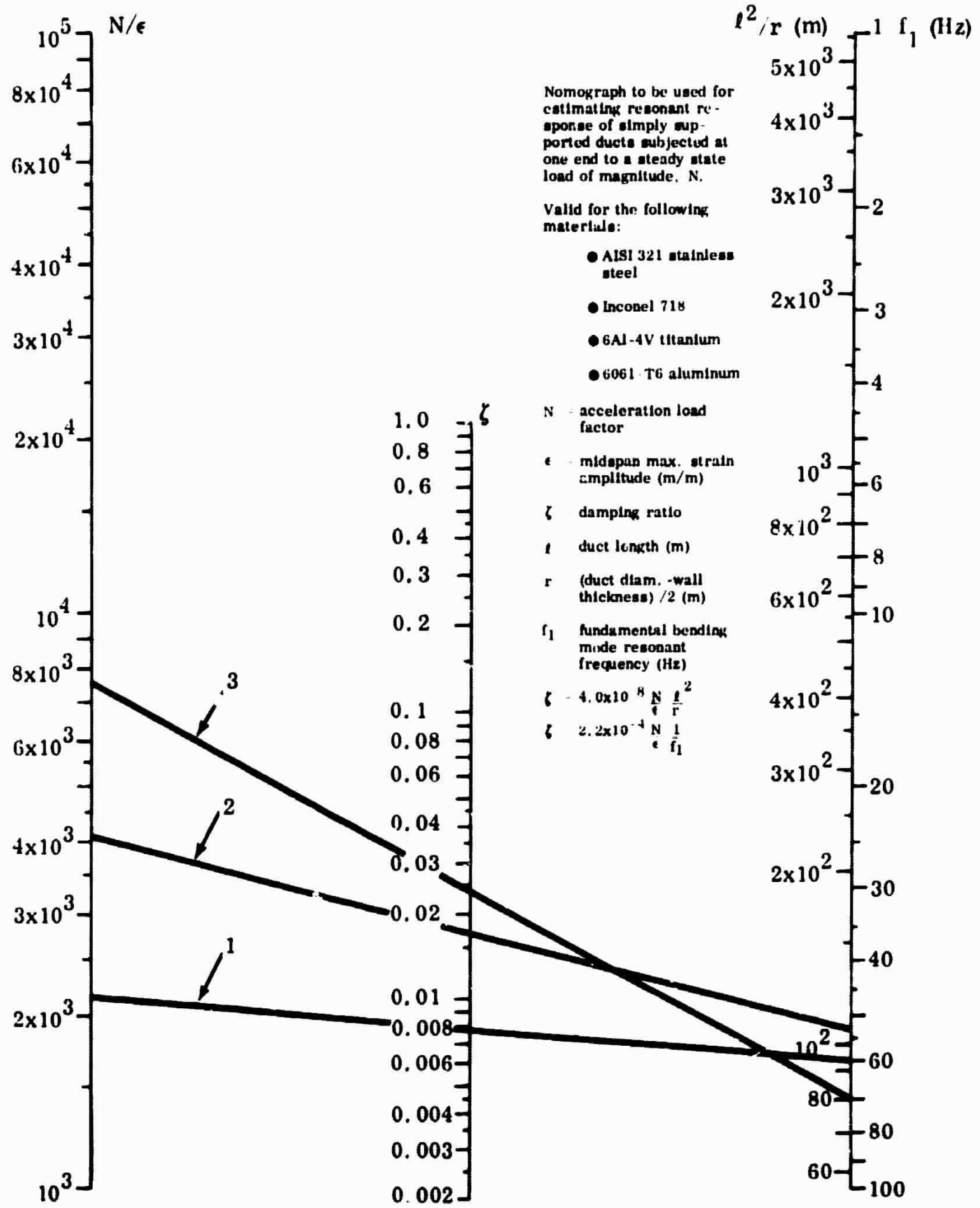

Curve	Test	Life Load Factor, N, at 21°C and 3×10^5 Cycle Design	Length, (m)	Diameter, d (m)	Wall Thickness, t (m)
1	I-A-3	5.7	1.53	0.0508	0.00124
2	I-E-31	11.0	1.98	0.076	0.00124
3	I-B-10	20.5	1.98	0.102	0.00124

FIGURE 21. DAMPING RATIOS FOR 6061-T6 ALUMINUM DUCTS

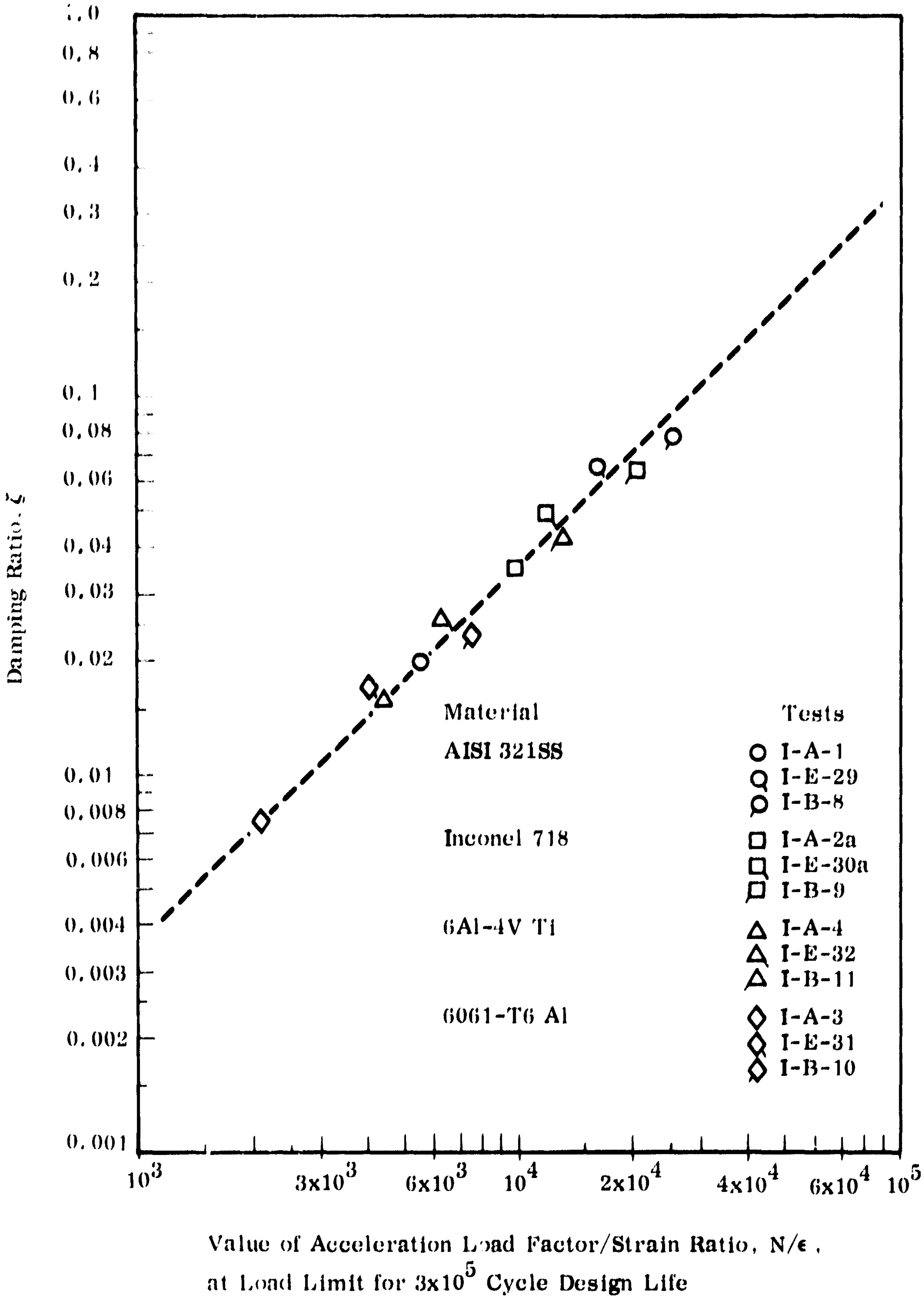

FIGURE 22. DAMPING RATIO, ζ, VERSUS ACCELERATION LOAD FACTOR/STRAIN RATE, N/ϵ, AT LOAD LIMIT FOR 3 X 10^5 CYCLE DESIGN LIFE

Both dynamic response and fatigue life experiments were performed on the Test Series II ducts. To provide a basis for comparison of Test Series I and II results, the following criterion was defined: A Test Series II duct, differing from a Test Series I duct only by the addition of a damping sleeve, should have a fatigue life equal to or greater than 3 x 10^5 cycles at an acceleration load level that could be expected to yield a 3 x 10^5 cycle life for the Test Series I duct.

The appropriate acceleration load factors for a 3 x 10^5 cycle design life of the test ducts are given in Table IX. Acceleration load factors and fatigue lives of the Test Series II ducts are given in Table X. Two Inconel 718 ducts (Tests II-E-42 and II-B-12) and one 6061-T6 aluminum duct (Test II-A-6) had fatigue lives greater than 3 x 10^5 cycles.

Seventeen ducts had fatigue lives less than 3 x 10^5 cycles. Two 6061-T6 aluminum ducts (Tests II-E-34 and II-E-44) failed before significant numbers of loading cycles were accumulated. The average fatigue life of the remaining 15 ducts was 0.75 x 10^5 cycles, with the lowest and highest values being 0.17 x 10^5 and 2.14 x 10^5 cycles, respectively.

Data in Table II reveal that most of the fatigue failures on the Test Series II ducts occurred near the ends of damping sleeves. Addition of a damping sleeve to a duct caused a nonuniform redistribution of duct bending strain in the length direction. To illustrate the nature of the strain redistribution, consider the results obtained in Test II-E-46a. In this test, a 7.6-centimeter OD 6Al-4V titanium duct with a length of 1.98 meters and a wall thickness of 1.24 millimeters had a 41-centimeter long, 0.254-millimeter thick AISI 321 stainless steel damping sleeve. Maximum strain amplitudes were measured at three locations:

- Duct center
- 25.4 centimeters from duct center
- 49.5 centimeters from duct center.

In Figure 23, the three measured strains for an acceleration load factor N = 16.5 are plotted as a function of duct position. The solid curve in the figure represents a theoretical strain distribution of the form sin ($\pi x/\ell$), which is typical of the distributions which were obtained in the bare Test Series I ducts.

TABLE X

TEST SERIES II FATIGUE DATA

Test Number	Duct Material	Duct Outer Diameter (cm)	Sleeve Thickness (mm)	Sleeve End	Test Acceleration Load Factor, N	Cycles to Failure, N ($\times 10^{-3}$)	Stress in Sleeve newtons/m^2 ($\times 10^{-7}$)	Stress in Parent Duct newtons/m^2 ($\times 10^{-7}$)	Stress in Bare Duct for 3×10^5 Cycle Life newtons m^2 ($\times 10^{-7}$)
5	Inconel 718	5.08	0.127	Plain	34.4	69.4	28.6	26.2	52.5
33	Inconel 718	7.62	0.127	Plain	26.5	214	20.7	42.8	52.5
12	Inconel 718	10.16	0.127	Plain	37.0	350(1)	20.7	29	52.5
38	Inconel 718	5.08	0.254	Plain	24.3	123.2	26.9	52.5	52.5
39	Inconel 718	5.08	0.254	Chevron	24.3	59.9	26.9	52.5	52.5
42	Inconel 718	7.62	0.254	Plain	26.5	350(1)	20.7	28.3	52.5
43	Inconel 718	7.62	0.254	Chevron	26.5	137	20.7	28.3	52.5
8	6061-T6Al	5.08	0.127	Plain	6.0	320	14.8	13.3	18.6
34	6061-T6Al	7.62	0.127	Plain	Failed During Response Test	--	--	--	18.6
13	6061-T6Al	10.16	0.127	Plain	21.0	113	17.6	12.4	18.6
40	6061-T6Al	5.08	0.254	Plain	6.0	57.2	14.8	9.60	18.6
41	6061-T6Al	5.08	0.254	Chevron	6.0	75.8	14.8	8.60	18.6
44	6061-T6Al	7.62	0.254	Plain	Failed During Response Test	--	--	--	18.6
45	6061-T6Al	7.62	0.254	Chevron	11.0	17.0	16.5	8.30	18.6
7	6Al-4VTi	5.08	0.127	Plain	Failed During Response Test	57.7	--	--	38.6
35	6Al-4VTi	7.62	0.127	Plain	20.0	25.1	19.3	24.8	38.6
14	6Al-4VTi	10.16	0.127	Chevron	Failed During Response Test	36.9	--	--	38.6
46	6Al-4VTi	7.62	0.254	Plain	20.0	100	19.3	27.2	38.6
47	6Al-4VTi	7.62	0.254	Chevron	20.0	45.2	19.3	27.2	38.6

1. Did not fail.

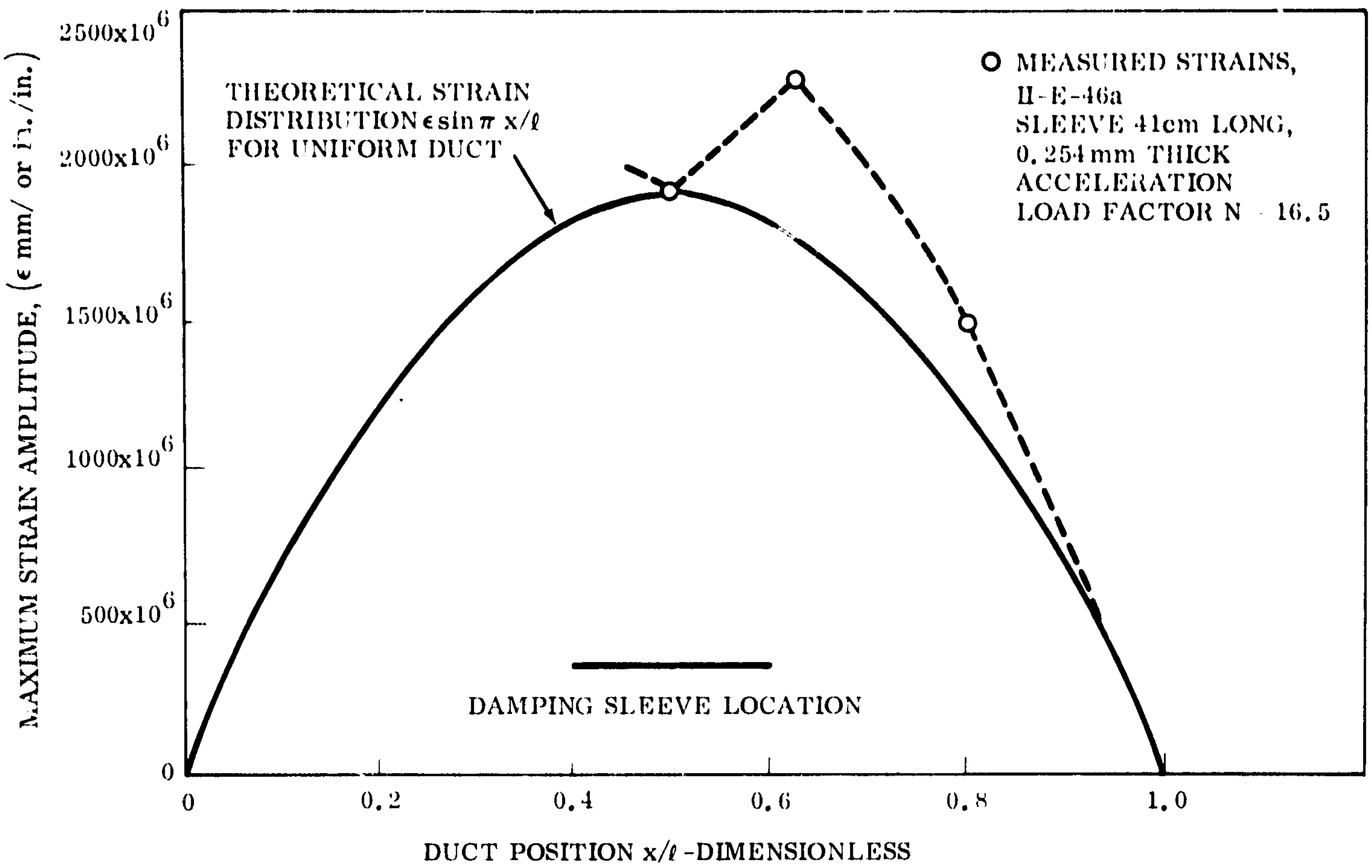

FIGURE 23. COMPARISON OF THEORETICAL AND MEAS''RED STRAINS AS A FUNCTION OF DUCT POSITION FOR 7.6-CENTIMETER OD 6Al-4V TITANIUM DUCT WITH AISI STAINLESS STEEL DAMPING SLEEVE

The single degree of freedom model used in deriving the damping ratio prediction equation

$$\zeta = \frac{1}{\pi^2} \frac{\gamma}{E} \frac{N}{\epsilon} \frac{\ell^2}{r}$$

for interpretation of the Test Series I results cannot be applied to the Test Series II results for the following reasons:

- The shape of a damped Test Series II duct fundamental bending mode is not of the form $\sin(\pi x/\ell)$.

- The maximum bending strain in a damped duct at a given acceleration load level is not necessarily at midspan.

All of the Test Series II response data are given in Tables XI through XIII. Symbols ϵ_c and σ_c identify midspan maximum bending strain and stress amplitude in the parent ducts. The symbol ϵ_d identifies maximum bending strain amplitudes in parent ducts at a distance of 25.4 centimeters from the midspan location.

TABLE XI

TEST SERIES II - INCONEL 718 DUCTS

Test Number	Length, l (m)	Diameter, d (cm)	Wall Thickness, t (mm)	Sleeve Length, l_s (cm)	Sleeve Thickness, t_s (mm)
II-A-5	1.52	5.08	1.24	30.5	0.127
N	ϵ_c ($\times 10^6$)	ϵ_d ($\times 10^6$)	N/ϵ_c	σ_c newtons/m^2 ($\times 10^{-7}$)	lb/in.^{2} ($\times 10^{-3}$)
2	100		0.0200	2.07	3.00
3	150		0.0200	3.10	4.50
4	225		0.0178	4.65	6.75
5	300		0.0167	6.21	9.00
6	340		0.0176	6.95	10.2
7	430		0.0163	8.90	12.9
8	500		0.0160	10.8	15.0
9	575		0.0157	11.9	17.3
10	650		0.0154	13.5	19.5
12	725		0.0166	15.1	21.8
14	800		0.0175	16.6	24.0
16	850		0.0188	17.6	25.5
18	950		0.0189	19.7	28.5
20	1000		0.0200	20.7	30.0
22	1060		0.0207	21.6	31.2
24	1110		0.0216	23.1	33.4
26	1150		0.0226	23.8	34.5

TABLE XI (Cont)

TEST SERIES II - INCONEL 718 DUCTS

Test Number	Length, l (m)	Diameter, d (cm)	Wall Thickness, t (mm)	Sleeve Length, l_s (cm)	Sleeve Thickness, t_s (mm)
II-A-38	1.52	5.08	1.24	30.5	0.254
N	ϵ_c (x 10^6)	ϵ_d (x 10^6)	N/ϵ_c	σ_c newtons/m^2 (x 10^{-7})	lb/in.^{2} (x 10^{-3})
2.4	160		0.0150	3.32	4.80
4.2	340		0.0124	7.05	10.2
6.2	720		0.0086	14.9	21.6
7.5	980		0.0076	20.2	29.4
10.0	1300		0.0077	20.7	30.0
13.0	1530		0.0085	31.6	45.9
16.0	1840		0.0087	38.1	55.2
18.0	2100		0.0085	42.8	62.0
21.0	2200		0.0095	45.5	66.0
II-A-38a	1.52	5.08	1.24	35.4	0.254
2.1	125		0.0168	2.59	3.75
4.7	450		0.0105	9.30	13.5
7.0	1050		0.0066	21.7	31.5
10.0	960		0.0104	19.2	27.8
12.4	1020		0.0121	21.1	30.6
16.2	1350		0.0120	28.0	40.5
18.1	1700		0.0106	35.2	51.0
20.5	2000		0.0102	41.4	60.0

TABLE XI (Cont)

TEST SERIES II - INCONEL 718 DUCTS

Test Number	Length, l (m)	Diameter, d (cm)	Wall Thickness, t (mm)	Sleeve Length, l_s (cm)	Sleeve Thickness, t_s (mm)
II-A-38b	1.52	5.08	1.24	25.4	0.127
N	ϵ_c (x 10^6)	ϵ_d (x 10^6)	N/ϵ_c	σ_c newtons/m^2 (x 10^{-7})	lb/in.^{2} (x 10^{-3})
1.8	250		0.0072	5.17	7.50
2.9	350		0.0083	7.25	10.5
4.2	460		0.0091	9.50	13.8
5.9	910		0.0059	18.8	27.3
8.9	1190		0.0075	24.6	35.7
13.0	1630		0.0079	33.7	48.9
16.0	2050		0.0078	42.5	61.5
18.0	2100		0.0085	43.5	63.0
20.0	2400		0.0083	49.5	72.0
II-E-33a	1.98	7.62	1.24	40.6	0.127
1.0	70		0.0143	1.45	2.10
2.9	200		0.0145	4.14	6.00
5.0	390		0.0128	8.08	11.7
9.5	690		0.0138	14.3	20.7
13.4	1100		0.0122	22.8	33.0
18.0	1300		0.0139	26.9	39.0
21.5	1600		0.0134	33.2	48.0
23.5	1970		0.0119	40.8	59.2
28.0	2150		0.0130	44.5	64.5
29.7	2520		0.0117	52.3	75.7

TABLE XI (Cont)

TEST SERIES II - INCONEL 718 DUCTS

Test Number	Length, l (m)	Diameter, d (cm)	Wall Thickness, t (mm)	Sleeve Length, l_s (cm)	Sleeve Thickness, t_s (mm)
II-E-33	1.98	7.62	1.24	38.1	0.127
N	ϵ_c (x 10^6)	ϵ_d (x 10^6)	N/ϵ_c	σ_c newtons/m^2 (x 10^{-7})	lb/in.^{2} (x 10^{-3})
1.0	85		0.0118	1.76	2.55
2.4	190		0.0127	3.94	5.7
4.1	350		0.0117	7.25	10.5
6.2	530		0.0116	11.2	16.1
9.0	730		0.0124	15.0	21.8
11.5	940		0.0093	19.4	28.2
15.0	1240		0.0121	25.7	37.2
20.5	1760		0.0117	36.4	52.8
22.8	1940		0.0118	40.1	58.2
24.5	2400		0.0102	49.6	72.0
27.5	2500		0.0110	51.8	75.0
33.0	2570		0.0128	68.3	99.0
II-E-33b	1.98	7.62	1.24	35.6	0.127
3.8	300		0.0127	6.20	9.0
7.6	450		0.0169	9.31	13.5
8.6	650		0.0132	13.4	19.5
12.0	980		0.0123	20.2	29.3
16.5	1330		0.0125	27.4	39.8
23.0	1780		0.0130	36.8	53.3
23.8	1950		0.0122	40.3	58.5
25.4	2150		0.0118	44.5	64.5

TABLE XI (Cont)

TEST SERIES II - INCONEL 718 DUCTS

Test Number	Length, l (m)	Diameter, d (cm)	Wall Thickness, t (mm)	Sleeve Length, l_s (cm)	Sleeve Thickness, t_s (mm)
II-E-33b	1.98	7.62	1.24	35.6	0.127
N	ϵ_c ($\times 10^6$)	ϵ_d ($\times 10^6$)	N/ϵ_c	σ_c newtons/m^2 ($\times 10^{-7}$)	lb/in.^{2} ($\times 10^{-3}$)
28.5	2380		0.0120	49.2	71.3
29.0	2400		0.0121	49.6	72.0
34.0	2880		0.0118	59.5	86.3
II-E-42a	1.98	7.62	1.24	40.6	0.254
2.4	170	210	0.0141	3.52	5.10
5.1	290	380	0.0176	6.00	8.70
6.5	400	520	0.0163	8.28	12.0
8.2	530	680	0.0156	10.9	15.8
10.3	610	800	0.0169	12.6	18.3
13.2	760	1030	0.0174	15.7	22.8
15.1	880	1210	0.0173	18.2	26.3
16.6	940	1350	0.0176	19.4	28.2
18.6	1000	1500	0.0186	20.7	30.0
21.8	1110	1660	0.0195	23.0	33.3
26.8	1400	2180	0.0191	29.0	42.0
28.8	1480	2330	0.0195	30.4	44.0
32.0	1620	2520	0.0198	33.6	48.6

TABLE XI (Cont)

TEST SERIES II - INCONEL 718 DUCTS

Test Number	Length, l (m)	Diameter, d (cm)	Wall Thickness, t (mm)	Sleeve Length, l_s (cm)	Sleeve Thickness, t_s (mm)
II-E-42	1.98	7.62	1.24	35.6	0.254
N	ϵ_c (x 10^6)	ϵ_d (x 10^6)	N/ϵ_c	σ_c newtons/m^2 (x 10^{-7})	lb/in.^{2} (x 10^{-3})
2.0	140	190	0.0143	2.90	4.20
4.0	230	300	0.0174	4.75	6.90
6.4	370	500	0.0173	7.65	11.1
8.6	500	670	0.0172	10.3	15.0
10.0	570	770	0.0175	11.8	17.1
14.0	610	870	0.0229	12.6	18.3
17.0	690	960	0.0246	14.3	20.7
19.5	1140	1610	0.0171	23.6	34.2
23.0	1180	1690	0.0195	24.4	35.4
27.0	1220	1780	0.0223	25.2	36.6
30.0	1540	2230	0.0195	31.9	46.2
31.0	1600	2250	0.0194	33.1	48.0
II-E-42b	1.98	7.62	1.24	30.5	0.254
2.4	130	150	0.0185	2.69	3.90
4.2	290	370	0.0145	6.00	8.70
6.0	400	510	0.0150	8.30	12.0
9.2	550	700	0.0167	11.4	16.5
14.0	850	1100	0.0165	17.6	25.5
18.0	1130	1540	0.0159	23.4	33.9
24.0	1380	1870	0.0174	26.5	38.4

TABLE XI (Cont)

TEST SERIES II - INCONEL 718 DUCTS

Test Number	Length, l (m)	Diameter, d (cm)	Wall Thickness, t (mm)	Sleeve Length, l_s (cm)	Sleeve Thickness, t_s (mm)
II-E-42b	1.98	7.62	1.24	30.5	0.254
N	ϵ_c (x 10^6)	ϵ_d (x 10^6)	N/ϵ_c	σ_c newtons/m^2 (x 10^{-7})	lb/in.^{2} (x 10^{-3})
29.0	1620	2070	0.0179	33.6	48.6
34.0	1760	2220	0.0193	36.4	52.8
II-B-12	1.98	10.2	1.24	38.1	0.127
1.35	75	80	0.0180	1.76	2.25
25	100	120	0.0225	2.07	3.00
4.1	180	190	0.0228	3.72	5.40
6.6	280	300	0.0236	5.80	8.40
8.2	310	350	0.0265	6.40	9.30
9.0	380	425	0.0212	7.85	11.4
11.5	420	470	0.0247	8.70	12.6
13.8	480	540	0.0291	9.85	14.3
15.8	610	670	0.0260	12.6	18.3
19.5	800	830	0.0244	16.6	24.0
22.0	880	960	0.0250	18.2	26.4
24.0	970	1020	0.0247	20.1	29.1
26.5	1050	1140	0.0252	21.8	31.5
29.0	1220	1320	0.0238	25.2	36.6
36.0	1330	1420	0.0277	26.9	39.0
41.0	1530	1680	0.0268	31.6	45.9
46.0	1640	1790	0.0280	33.9	49.2
50.0	1870	2040	0.0267	38.8	56.1
57.0	2110	2300	0.0270	43.6	63.3
58.0	2290	2500	0.0253	47.4	68.7

TABLE XII

TEST SERIES II - 6Al-4V TITANIUM DUCTS

Test Number	Length, l (m)	Diameter, d (cm)	Wall Thickness, t (mm)	Sleeve Length, l_s (cm)	Sleeve Thickness, t_s (mm)
II-A-7	1.52	5.08	1.24	30.5	0.127
N	ϵ_c (x 10^6)	ϵ_d (x 10^6)	N/ϵ_c	σ_c newtons/m^2 (x 10^{-7})	lb/in.^{2} (x 10^{-3})
0.1	130	160	0.0008	1.64	2.38
0.5	160	190	0.0031	1.88	2.72
1.4	310	350	0.0045	3.64	5.27
1.8	510	560	0.0035	5.97	8.67
2.6	640	700	0.0041	7.45	10.8
3.0	740	810	0.0041	8.70	12.6
5.0	1000	1120	0.0050	11.7	17.0
5.6	1160	1290	0.0048	13.6	19.7
6.6	1410	1570	0.0047	16.5	24.0
7.3	1500	1670	0.0044	17.6	25.5
7.8	1700	1900	0.0046	19.9	28.9
8.4	1820	2000	0.0045	21.3	30.9
9.5	1930	2150	0.0049	22.6	32.8
10.4	2000	2240	0.0052	23.5	34.0
11.8	2230	2460	0.0053	26.2	37.9
12.2	2330	2600	0.0052	27.3	39.6
13.0	2460	2730	0.0053	28.8	41.8

TABLE XII (Cont)

TEST SERIES II - 6Al-4V TITANIUM DUCTS

Test Number	Length, l (m)	Diameter, d (cm)	Wall Thickness, t (mm)	Sleeve Length, l_s (cm)	Sleeve Thickness, t_s (mm)
II-E-35a	1.98	7.62	1.24	40.6	0.127
N	ϵ_c (x 10^6)	ϵ_d (x 10^6)	N/ϵ_c	σ_c newtons/m^2 (x 10^{-7})	lb/in.^{2} (x 10^{-3})
0.8	130		0.0062	1.45	2.21
2.1	250		0.0084	2.93	4.25
4.0	440		0.0091	5.16	7.48
5.8	700		0.0083	8.21	11.9
8.0	1020		0.0078	11.9	17.3
12.0	1270		0.0095	14.9	21.6
14.0	1500		0.0093	17.6	25.5
16.5	1750		0.0094	20.6	29.8
18.0	1900		0.0095	22.3	32.3
21.0	2430		0.0086	28.5	41.3
25.0	2700		0.0093	31.7	45.9
II-E-35	1.98	7.62	1.24	35.5	0.127
1.4	200		0.0070	2.35	3.40
3.7	410		0.0090	4.81	6.97
7.1	740		0.0096	8.35	12.1
8.6	940		0.0091	11.1	16.0
10.0	1060		0.0094	12.4	18.0
13.5	1630		0.0083	19.2	27.8
19.2	2030		0.0095	23.9	34.6

TABLE XII (Cont)

TEST SERIES II - 6Al-4V TITANIUM DUCTS

Test Number	Length, l (m)	Diameter, d (cm)	Wall Thickness, t (mm)	Sleeve Length, l_s (cm)	Sleeve Thickness, t_s (mm)
II-E-35	1.98	7.62	1.24	35.5	0.127
N	ϵ_c (x 10^6)	ϵ_d (x 10^6)	N/ϵ_c	σ_c newtons/m^2 (x 10^{-7})	lb/in.^{2} (x 10^{-3})
17.2	1900		0.0091	22.3	32.3
23.0	2500		0.0092	29.4	42.5
21.0	2220		0.0095	26.1	37.8
22.8	2480		0.0092	29.2	42.2
27.5	2950		0.0093	34.6	50.2
II-E-35b	1.98	7.62	1.24	30.5	0.127
1.1	150		0.0073	1.76	2.55
1.2	200		0.0060	2.34	3.40
4.2	450		0.0093	5.28	7.65
6.7	760		0.0088	7.05	10.4
8.8	980		0.0090	11.5	16.7
12.2	1200		0.0101	14.1	20.4
16.0	1680		0.0095	19.7	28.6
18.0	2000		0.0090	23.4	34.0
21.0	2520		0.0084	29.6	42.8
26.0	2350		0.0101	27.6	40.0

TABLE XII (Cont)

TEST SERIES II - 6Al-4V TITANIUM DUCTS

Test Number	Length, l (m)	Diameter, d (cm)	Wall Thickness, t (mm)	Sleeve Length, l_s (cm)	Sleeve Thickness, t_s (mm)
II-E-46a	1.98	7.62	1.24	40.6	0.254
N	ϵ_c (x 10^6)	ϵ_d (x 10^6)	N/ϵ_c	σ_c newtons/m^2 (x 10^{-7})	lb/in.^{2} (x 10^{-3})
1.8	200	260	0.0090	2.35	3.40
2.7	400	530	0.0068	4.70	6.80
3.8	500	680	0.0076	5.86	8.50
5.5	760	1000	0.0072	8.90	12.9
7.8	950	1220	0.0082	11.2	16.2
10.2	1170	1510	0.0087	13.7	19.9
14.5	1670	2080	0.0087	19.6	28.4
16.5	1900	2310	0.0087	22.3	32.3
19.6	2610	2750	0.0075	30.6	44.4
23.0	2800	2850	0.0082	32.9	47.6
26.0	3170	3000	0.0082	37.2	53.9
II-E-46	1.98	7.62	1.24	35.6	0.254
1.3	230	300	0.0057	2.70	3.91
2.5	340	450	0.0074	3.98	5.78
3.6	405	540	0.0089	4.75	6.89
5.8	550	730	0.0105	6.45	9.35
8.0	890	1100	0.0090	10.4	15.1
10.2	1260	1550	0.0081	14.8	21.4
12.1	1280	1600	0.0095	15.0	21.7

TABLE XII (Cont)

TEST SERIES II - 6Al-4V TITANIUM DUCTS

Test Number	Length, l (m)	Diameter, d (cm)	Wall Thickness, t (mm)	Sleeve Length, l_s (cm)	Sleeve Thickness, t_s (mm)
II-E-46	1.98	7.62	1.24	35.6	0.254
N	ϵ_c (x 10^6)	ϵ_d (x 10^6)	N/ϵ_c	σ_c newtons/m^2 (x 10^{-7})	lb/in.^{2} (x 10^{-3})
17.0	1900	2100	0.0089	22.3	32.3
20.5	2310	2430	0.0089	27.1	39.3
25.2	2930	2860	0.0086	34.4	49.8
II-E-46b	1.98	7.62	1.24	30.5	0.254
1.6	190	250	0.0084	2.23	3.23
2.8	310	460	0.0090	3.64	5.27
3.8	370	520	0.0104	4.28	6.21
6.8	690	930	0.0099	8.08	11.7
8.8	990	1350	0.0089	11.6	16.8
10.6	1310	1750	0.0081	15.4	22.3
14.9	1700	2120	0.0088	19.9	28.9
18.0	2200	2540	0.0082	25.8	37.4
21.5	3920	3600	0.0055	46.0	66.6
26.0	3800	3550	0.0068	44.6	64.6

TABLE XIII

TEST SERIES II - 6061-T6 ALUMINUM DUCTS

Test Number	Length, l (m)	Diameter, d (cm)	Wall Thickness, t (mm)	Sleeve Length, l_s (cm)	Sleeve Thickness, t_s (mm)
II-A-6	1. 52	5. 08	1. 24	28. 4	0. 127
N	ϵ_c $(\times 10^6)$	ϵ_d $(\times 10^3)$	N/ϵ_c	σ_c newtons/m^2 $(\times 10^{-7})$	lb/in.^{2} $(\times 10^{-3})$
0. 3	200		0. 0015	1. 38	2. 00
0. 5	240		0. 0021	1. 66	2. 40
0. 8	390		0. 0021	2. 69	3. 90
1. 0	420		0. 0024	2. 90	4. 20
1. 3	440		0. 0030	3. 04	4. 40
1. 5	620		0. 0024	4. 28	6. 20
2. 8	950		0. 0030	6. 55	9. 50
2. 9	1000		0. 0029	6. 99	10. 0
3. 5	1180		0. 0030	8. 15	11. 8
4. 8	1220		0. 0039	8. 42	12. 2
5. 0	1350		0. 0037	9. 32	13. 5
5. 6	1500		0. 0037	10. 4	15. 0
6. 2	1580		0. 0039	10. 9	15. 8
6. 8	1860		0. 0036	12. 8	18. 6
II-A-40a	1. 52	5. 08	1. 24	35. 6	0. 254
0. 6	200		0. 0030	1. 38	2. 0
1. 6	360		0. 0169	2. 48	3. 6
1. 8	510		0. 0035	3. 52	5. 1
1. 7	600		0. 0028	4. 15	6. 0

TABLE XIII (Cont)

TEST SERIES II - 6061-T6 ALUMINUM DUCTS

Test Number	Length, l (m)	Diameter, d (cm)	Wall Thickness, t (mm)	Sleeve Length, l_s (cm)	Sleeve Thickness, t_s (mm)
II-A-40a	1 52	5.08	1.24	35.6	0.254
N	ϵ_c (x 10^6)	ϵ_d (x 10^6)	N/ϵ_c	σ_c newtons/m^2 (x 10^{-7})	lb/in.^{2} (x 10^{-3})
4.4	970		0.0045	6.69	9.7
2.7	650		0.0041	4.48	6.5
3.8	800		0.0047	5.52	8.0
4.2	1070		0.0039	7.40	10.7
4.6	1260		0.0036	8.70	12.6
6.4	1270		0.0050	8.77	12.7
5.8	1400		0.0041	9.66	14.0
II-A-40	1.52	5.08	1.24	30.5	0.254
0.6	170		0.0035	1.17	1.7
1.2	350		0.0035	2.42	3.5
2.2	540		0.0040	3.72	5.4
2.8	730		0.0038	5.04	7.3
3.8	940		0.0039	6.48	9.4
7.0	1400		0.0050	9.75	14.0
7.8	1480		0.0052	10.2	14.8
II-A-40b	1.52	5.08	1.24	25.4	0.254
0.4	190		0.0021	1.31	1.9
1.4	450		0.0031	3.10	4.5
2.5	580		0.0043	4.00	5.8

TABLE XIII (Cont)

TEST SERIES II - 6061-T6 ALUMINUM DUCTS

Test Number	Length, l (m)	Diameter, d (cm)	Wall Thickness, t (mm)	Sleeve Length, l_s (cm)	Sleeve Thickness, t_s (mm)
II-A-40b	1.52	5.08	1.24	25.4	0.254
N	ϵ_c (x 10^6)	ϵ_d (x 10^6)	N/ϵ_c	σ_c newtons/m^2 (x 10^{-7})	lb/in.^{2} (x 10^{-3})
3.2	810		0.0039	5.60	8.1
3.9	930		0.0041	6.41	9.3
4.4	1130		0.0038	7.80	11.3
5.3	1330		0.0042	9.20	13.3
7.2	1520		0.0047	10.5	15.2
8.2	1610		0.0050	11.1	16.1
II-E-34	7.62	1.98	1.24	40.6	0.127
0.3	150		0.0020	1.03	1.5
1.2	200		0.0060	1.38	2.0
1.7	290		0.0059	2.00	2.9
2.1	350		0.0060	2.52	3.5
2.7	520		0.0052	3.58	5.2
4.8	740		0.0065	5.10	7.4
7.0	1010		0.0069	6.97	10.1
8.4	1250		0.0067	8.62	12.5
9.4	1370		0.0069	9.45	13.7
10.8	1700		0.0064	11.7	17.0

TABLE XIII (Cont)

TEST SERIES II - 6061-T6 ALUMINUM DUCTS

Test Number	Length, l (m)	Diameter, d (cm)	Wall Thickness, t (mm)	Sleeve Length, l_s (cm)	Sleeve Thickness, t_s (mm)
II-E-34a	7.62	1.98	1.24	35.6	0.127
N	ϵ_c (x 10^6)	ϵ_d (x 10^6)	N/ϵ_c	σ_c newtons/m^2 (x 10^{-7})	lb/in.^{2} (x 10^{-3})
0.3	110		0.0027	0.76	1.1
1.2	200		0.0060	1.38	2.0
1.6	310		0.0052	2.14	3.1
2.2	500		0.0044	3.45	5.0
5.1	720		0.0071	4.96	7.2
		(Duct Failed Here)			
II-E-44	1.98	7.62	1.24	35.6	0.254
1.0	160	250	0.0063	1.10	1.60
1.8	250	380	0.0072	1.72	2.50
3.2	430	700	0.0075	2.96	4.30
4.5	610	1000	0.0074	4.20	6.10
4.7	740	1150	0.0064	5.10	7.40
6.6	900	1400	0.0073	6.20	9.00
7.2	910	1420	0.0079	6.27	9.10
8.4	960	1500	0.0088	6.61	9.60
9.6	1000	1560	0.0096	6.69	10.00
12.0	1410	2210	0.0085	9.72	14.1
14.1	1350	2100	0.0108	9.30	13.5

TABLE XIII (Cont)

TEST SERIES II - 6061-T6 ALUMINUM DUCTS

Test Number	Length, l (m)	Diameter, d (cm)	Wall Thickness, t (mm)	Sleeve Length, l_s (cm)	Sleeve Thickness, t_s (mm)
II-E-44a	1.98	7.62	1.24	30.5	0.254
N	ϵ_c (x 10^6)	ϵ_d (x 10^6)	N/ϵ_c	σ_c newtons/m^2 (x 10^{-7})	lb/in.^{2} (x 10^{-3})
1.2	150	250	0.0080	1.03	1.50
1.9	300	510	0.0063	2.07	3.00
3.2	450	750	0.0071	3.10	4.50
5.0	600	990	0.0083	4.13	6.00
6.4	830	1350	0.0077	5.71	8.30
7.0	900	1500	0.0078	6.20	9.00
8.2	1100	1770	0.0074	7.60	11.0
10.2	1170	1900	0.0087	8.05	11.7
11.5	1350	2210	0.0085	9.30	13.5
II-E-44b	1.98	7.62	1.24	25.4	0.254
0.7	100	140	0.0070	0.69	1.00
1.2	200	310	0.0060	1.38	2.00
2.7	430	690	0.0063	2.96	4.30
3.0	435	700	0.0069	3.00	4.35
3.8	600	930	0.0063	4.13	6.00
II-B-13	1.98	10.16	1.24	38.1	0.127
0.2	70	90	0.0029	0.48	0.70
1.2	105	170	0.0114	0.76	1.10
1.9	180	200	0.0109	1.21	1.75

TABLE XIII (Cont)

TEST SERIES II - 6061-T6 ALUMINUM DUCTS

Test Number	Length, l (m)	Diameter, d (cm)	Wall Thickness, t (mm)	Sleeve Length, l_s (cm)	Sleeve Thickness, t_s (mm)
II-B-13	1. 98	10. 16	1. 24	38. 1	0. 127
N	ϵ_c ($\times 10^6$)	ϵ_d ($\times 10^6$)	N/ϵ_c	σ_c newtons/m^2 ($\times 10^{-7}$)	lb/in.^{2} ($\times 10^{-3}$)
2. 8	240	290	0. 0117	1. 65	2. 40
3. 2	290	330	0. 0112	1. 97	2. 85
4. 1	330	400	0. 0124	2. 28	3. 30
5. 2	490	530	0. 0106	3. 38	4. 90
5. 8	500	590	0. 0116	3. 44	5. 00
7. 1	630	740	0. 0113	4. 34	6. 30
10. [illegible]	900	1050	0. 0111	6. 20	9. 00
11. 0	1070	1280	0. 0103	7. 37	10. 7
13. 2	1100	1570	0. 0120	7. 58	11. 0
14. 0	1240	1460	0. 0113	8. 55	12. 4
14. 6	1280	1520	0. 0114	8. 83	12. 8
16. 0	1550	1830	0. 0103	10. 7	15. 5
21. 8	1630	2180	0. 0134	11. 2	16. 3

The Test Series II results demonstrate that even though a uniform damping sleeve may produce an undesirable length distribution of bending strain in a duct, the midspan maximum strain amplitude can be reduced significantly with respect to that of a Test Series I duct at the same acceleration load level. Table XIV lists values of N/ϵ at selected values of N for both Test Series I and II ducts. In most instances, the value of N in the table for a given duct material and geometry was selected as one which would be expected to yield a 3×10^5 cycle design life in a Test Series I duct. In some cases, Test Series II response measurements were not made at sufficiently large values of N to make this choice possible without extrapolation. Accordingly, the values of N in these cases, identified by a superscript star * in Table XIV, were chosen to be the largest values for which N/ϵ values could be selected from the tabulated data for a given duct material and geometry.

To demonstrate graphically the effects of the addition of damping sleeves on midspan response of Test Series II ducts in comparison with Test Series I ducts, values of N/ϵ for the former ducts were plotted in Figure 24 versus N/ϵ values for the latter. Symbols used in the graph are identified in Table XIV. A parameter ζ^* was defined as follows:

$\zeta^* = (N/\epsilon)$ for a Test Series II duct/(N/ϵ) for a Test Series I duct of the same material and geometry.

The following comparisons can be made:

If $\zeta^* = 1$, no improvement in midspan response was obtained

If $\zeta^* < 1$, midspan response was not reduced by addition of a damping sleeve

If $\zeta^* > 1$, addition of a damping sleeve reduced midspan response.

The parameter ζ^* may be used to rank order the Test Series II response test results. For example, addition of a 0.127-millimeter thick damping sleeve to 5.1-centimeter OD Inconel 718 ducts reduced midspan response, while addition of a 0.254-millimeter sleeve to a similar duct increased the response (Fig. 24). The most significant reductions in midspan response were obtained with addition of 0.254-millimeter thick sleeves to 5.1- and 7.6-centimeter OD 6061-T6 aluminum ducts. It can be conjectured from the increases in ζ^*, obtained by increasing the sleeve thickness from 0.127 to 0.254 millimeter with 5.1- and 7.6-centimeter OD 6061-T6 aluminum ducts, that a similar increase would be obtained by increasing the sleeve thickness for a 10.2-centimeter OD aluminum duct from 0.127 to 0.254 millimeter. It can also be seen that for the ranges over which sleeve lengths were varied, changes in ζ^* were not significant.

TABLE XIV

N/ϵ VALUES FOR TEST SERIES I AND II DUCTS

Test	Symbol	Duct Material	Length (m)	Diameter (m)	Sleeve Length (m)	Sleeve Thickness (mm)	N	$\epsilon \times 10^6$	N/ϵ
I-A-2a		Inconel 718	1.52	0.0508			20.0*	1800	11.1×10^3
II-A-5		Inconel 718	1.52	0.0508	0.305	0.127	20.0*	1000	20.0×10^3
II-A-38a		Inconel 718	1.52	0.0508	0.356	0.254	20.0*	1950	10.2×10^3
II-A-38		Inconel 718	1.52	0.0508	0.305	0.254	20.0*	2160	9.27×10^3
II-A-38b		Inconel 718	1.52	0.0508	0.254	0.254	20.0*	2400	8.34×10^3
I-E-30a		Inconel 718	1.98	0.0762			30.0	3000	10.0×10^3
II-E-33a		Inconel 718	1.98	0.0762	0.406	0.127	30.0	2550	11.8×10^3
II-E-33		Inconel 718	1.98	0.0762	0.381	0.127	30.0	2550	11.8×10^3
II-E-33b		Inconel 718	1.98	0.0762	0.356	0.127	30.0	2550	11.8×10^3
II-E-42		Inconel 718	1.98	0.0762	0.406	0.254	30.0	1550	19.4×10^3
II-E-42a		Inconel 718	1.98	0.0762	0.356	0.254	30.0	1550	19.4×10^3
II-E-42b		Inconel 718	1.98	0.0762	0.305	0.254	30.0	1650	18.2×10^3
I-B-9		Inconel 718	1.98	0.102			52.3	2530	20.7×10^3
II-B-12		Inconel 718	1.98	0.102	0.381	0.127	52.3	1970	26.5×10^3
I-A-4		6Al-4V Ti	1.52	0.0508			11.5*	2620	4.4×10^3
II-A-7		6Al-4V Ti	1.52	0.0508	0.305	0.127	11.5*	1880	6.1×10^3
I-E-32		6Al-4V Ti	1.98	0.0762			21.0	3300	6.4×10^3
II-E-35a		6Al-4V Ti	1.98	0.0762	0.406	0.127	21.0	2430	8.6×10^3
II-E-35		6Al-4V Ti	1.98	0.0762	0.356	0.127	21.0	2220	9.5×10^3
II-E-35b		6Al-4V Ti	1.98	0.0762	0.305	0.127	21.0	2200	9.5×10^3
II-E-46a		6Al-4V Ti	1.98	0.0762	0.406	0.254	21.0	2250	9.3×10^3
II-E-46		6Al-4V Ti	1.98	0.0762	0.356	0.254	21.0	2250	9.3×10^3
II-E-46b		6Al-4V Ti	1.98	0.0762	0.305	0.254	21.0	2250	9.3×10^3
I-B-11		6Al-4V Ti	1.98	0.102			41.0*	3160	13.0×10^3
II-B-14		6Al-4V Ti	1.98	0.102	0.356	0.127	41.0*	2040	20.0×10^3
I-A-3		6061-T6 Al	1.52	0.0508			5.7	2700	2.1×10^3
II-A-6 Rerun		6061-T6 Al	1.52	0.0508	0.284	0.127	5.7	1510	3.8×10^3
II-A-40a		6061-T6 Al	1.52	0.0508	0.356	0.254	5.7	1250	4.6×10^3
II-A-40		6061-T6 Al	1.52	0.0508	0.305	0.254	5.7	1250	4.6×10^3
II-A-40b		6061-T6 Al	1.52	0.0508	0.254	0.254	5.7	1250	4.6×10^3
I-E-31		6061-T6 Al	1.98	0.0762			11.0	2700	4.1×10^3
II-E-34		6061-T6 Al	1.98	0.0762	0.406	0.127	11.0	1700	6.5×10^3
II-E-34a		6061-T6 Al	1.98	0.0762	0.356	0.127	11.0	1700	6.5×10^3
II-E-44		6061-T6 Al	1.98	0.0762	0.356	0.254	11.0	1200	9.2×10^3
II-E-44a		6061-T6 Al	1.98	0.0762	0.305	0.254	11.0	1200	9.2×10^3
II-E-44b		6061-T6 Al	1.98	0.0762	0.254	0.254	11.0	1200	9.2×10^3
I-B-10		6061-T6 Al	1.98	0.102			20.5	2700	7.6×10^3
II-B-13		6061-T6 Al	1.98	0.102	0.356	0.127	20.5	1610	12.7×10^3

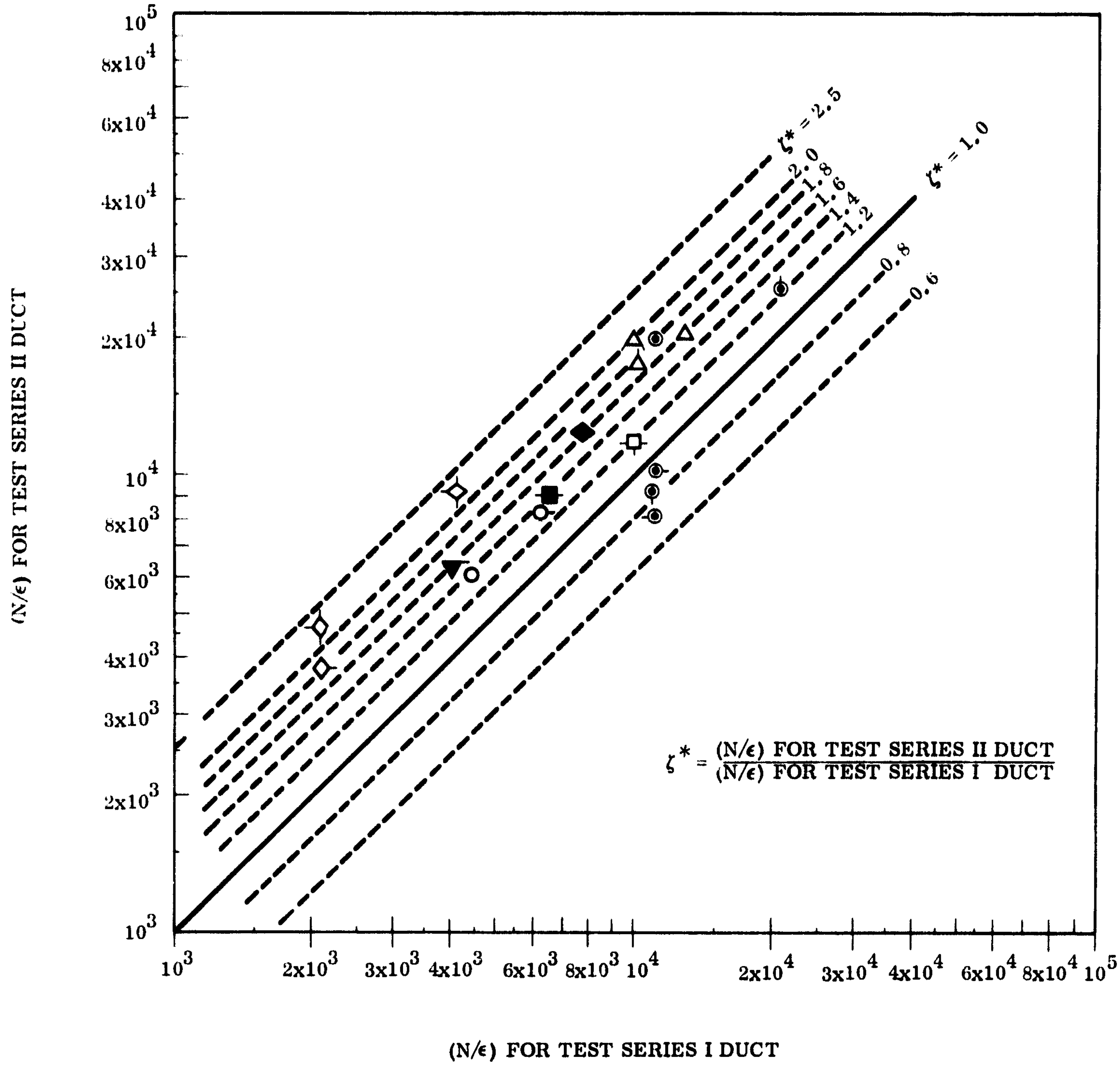

FIGURE 24. COMPARISON OF (N/ϵ) VALUES FOR TEST SERIES I AND II DUCTS

4.3.1 Evaluation of Fatigue Failures

Results of the fatigue tests are summarized in Tables II and X. The failures can be identified with a combination of causes which differ in relative importance for each test:

- Bending stress concentrations at or near sleeve ends
- Degradation of parent duct material properties during the brazing cycle
- Local imperfections in braze alloy distribution
- Fatigue damage of the 321 stainless steel sleeve material
- Fatigue damage of parent duct material

Comparisons of results obtained with similar damped ducts having either plain or one-inch chevron sleeve ends indicate that more extensive changes in sleeve geometry are required to achieve significant improvements in fatigue lives.

Metallographic and tensile test specimens were removed from five of the fatigued ducts. The following discussion is categorized by duct material in the order Inconel 718, 6Al-4V titanium, and 6061-T6 aluminum.

Inconel 718

Test Duct No. 38 was selected for examination of a representative Inconel 718 duct failure. This duct cracked near the center of the damping sleeve after 1.23×10^5 cycles at 52.3×10^7 newtons/m^2 midspan stress level in the duct. The pattern of fracture is similar to that of Test Ducts 5 and 33. Ducts 12 and 42 did not fracture in the requisite 3×10^5 cycles, although the damping sleeves developed numerous cracks; and the failure of Ducts 39 and 43 initiated at resistance welded tacks.

Tensile Properties. A longitudinal sample was sectioned from Duct 38, in the central portion of the damper sleeve. The 321 stainless steel sleeve material was peeled away and the Inconel 718 machined to a standard 1.27 centimeter wide tensile specimen. By coincidence, the reduced section of the tensile specimen was located in an area of the duct which had not been wet by the silver braze alloy; therefore, it was possible to determine the mechanical properties of the Inconel 718 as affected solely by the thermal history rather than the braze alloy. Results were as follows:

Area (Nominal) (cm)	Ultimate Strength (newtons/m^2)	0.2 Percent Yield (newtons/m^2)	Elongation Percent in 2.54 cm
0.124 x 1.27	152×10^7	130×10^7	18.0

These results are typical of handbook values for the parent material and show acceptable strength and ductility in the age-hardened condition, indicating that no significant degradation occurred during the braze cycle of the duct material.

Hardness. Rockwell superficial hardness tests on cross sections of the Inconel 718 duct from the center brazed area, the adjacent heat-affected area, and the end unaffected areas all showed identical hardness, approximately 15N 83.5, corresponding to the above reported tensile properties and again indicative of no damage by brazing heat.

Metallographic Examination. Metallographic sections through the brazed sleeve area revealed a normal microstructure of heat-treated and aged Inconel 718. The 321 stainless steel sleeve was seen to have cracked in several places, with fatigue damage proceeding from the outside diameter inward (Fig. 25).

Figure 26 is a photomicrograph of a section through the actual tube fracture. The coincidence of this fracture with two cracks in the damping sleeve was noted. Progression is transgranular from the outside diameter inward.

There appears to be a second mode of failure not related to propagation of cracks from the outer sleeve. Several areas (Fig. 27) show incipient fatigue cracks initiated in the Inconel 718 duct at its interface with the braze alloy and apparently not associated with any deficiency in the damping sleeve.

The point of initiation appears to be an area of braze alloy erosion into the Inconel 718, which evidence can be correlated with the location of failures in Ducts 5 and 33. The latter ducts failed at the end of the damping sleeve where the buildup of braze alloy is heaviest due to the squeezing action which accompanies differential thermal expansion of restraining bands.

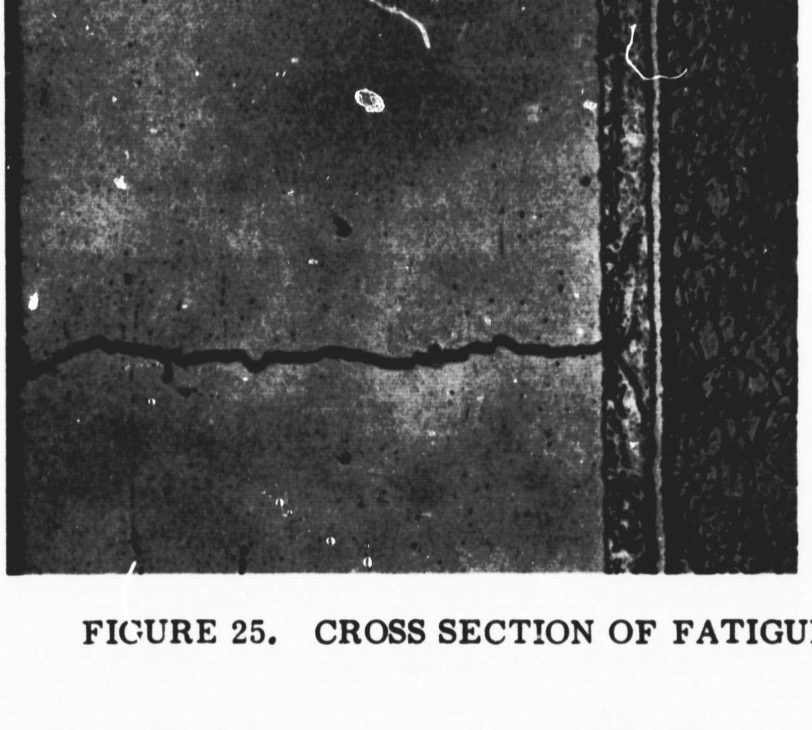

Etch: Electrolytic Oxalic Acid

Magnification: 250X

FIGURE 25. CROSS SECTION OF FATIGUE CRACK IN DAMPING SLEEVE

Etch: Electrolytic Oxalic Acid

Magnification: 50X

FIGURE 26. FAILURE IN WALL OF DUCT 38, COINCIDENT WITH FATIGUE CRACKS IN STAINLESS STEEL DAMPING SLEEVE

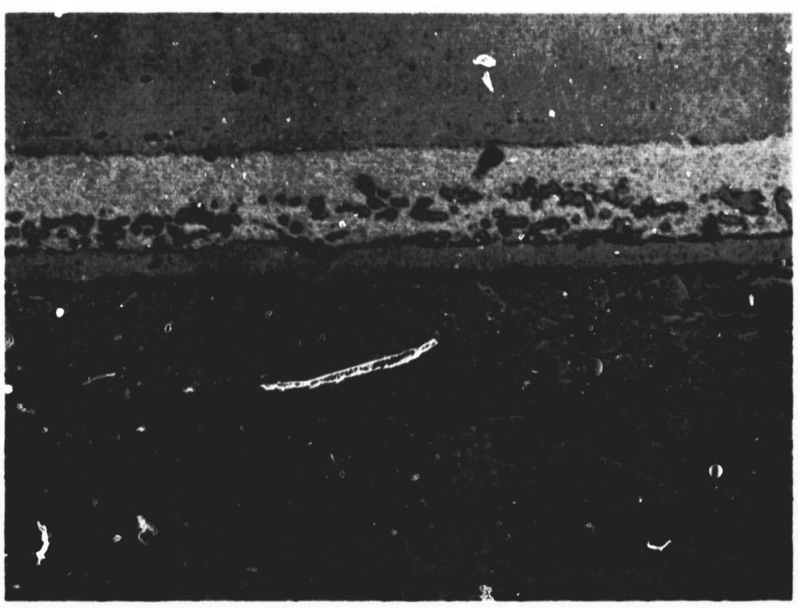

Etch: Electrolytic Oxalic Acid

Magnification: 500X

FIGURE 27. INCIPIENT FATIGUE CRACK INITIATED IN INTERFACE OF INCONEL 718 DUCT AND SILVER BRAZE ALLOY

Etch: Electrolytic Oxalic Acid

Magnification: 400X

321 Stainless Steel, DPH 192
Sta-Flow, DPH 69
Interface. DPH 104. 5
Inconel 718, DPH 357

FIGURE 28. MICROHARDNESS TESTS IN BRAZE ZONE OF INCONEL 718 DUCT

Figure 28 shows a section through the braze zone which includes a number of microhardness impressions. It can be seen that there are no anomalies in hardness to indicate zones of brittle intermetallics. (The very light impression load, five grams, precludes conversion of these results to more conventional hardness standards; however, a valid qualitative relationship exists.)

6Al-4V Titanium

Failures of the five titanium ducts were similar in that all cracked at damping sleeve ends in less than the requisite number of cycles. The two having the lowest and highest fatigue lives, Ducts 35 and 46, were selected for examination.

Hardness. Both ducts had equivalent variations of hardness in the three areas tested in cross section.

	DPH (500-gram)	
	Duct 35	Duct 46
Unbrazed parent metal	334	344
Braze heat-affected zone	317	317
Braze section under sleeve	287	303

Metallographic Examination. Metallographic examination of the titanium ducts confirmed the variation in hardness of the several sections as duct annealing conditions during the brazing heat. Figure 29 shows parent metal, heat-affected zone, and brazed zone corresponding to maximum processing temperatures of about 220, 700, and 900°C. Progression from the standard basket-weave alpha-beta type structure through spheroidization and equiaxed alpha structure is noted.

Figure 30 is a section of Duct 35 under the brazed sleeve and is typical also of Duct 46. Diamond pyramid hardness impressions show the wide variation in hardness through the brazed section. Most significant are the formation of a hard intermetallic zone between the silver alloy and the titanium; and the segregation of the braze alloy into two distinct phases, one very hard and the other very soft.

Unlike the Inconel 718 test ducts, the only cracks noted in the damping sleeves of the titanium alloy ducts were those which initiated at the inside surface and were associated with unbrazed sections of the sleeve (Fig. 31).

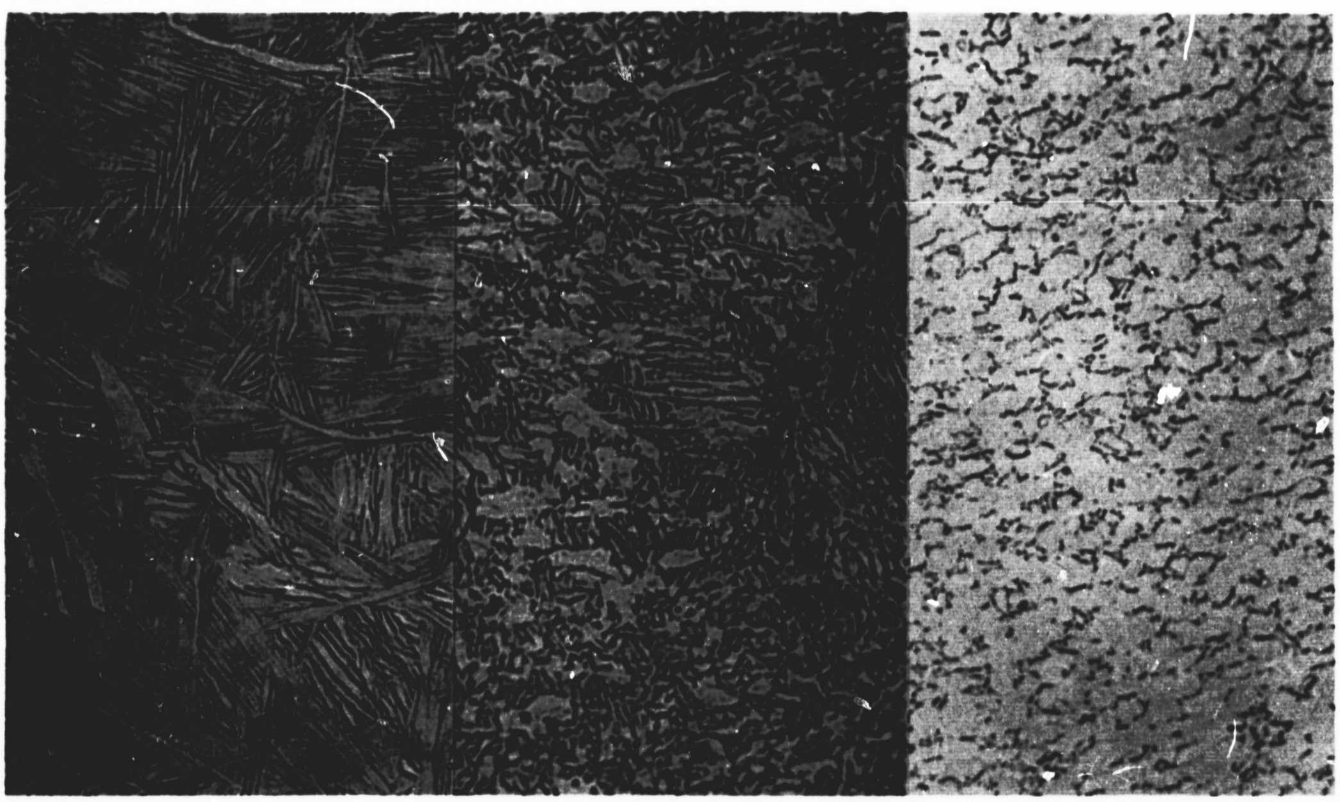

A. Parent Metal B. Heat-Affected Zone C. Braze Area

Etch: Kroll's

Magnification: 500X

FIGURE 29. MICROSTRUCTURE OF 6Al-4V TITANIUM ALLOY AS AFFECTED BY BRAZE CYCLE

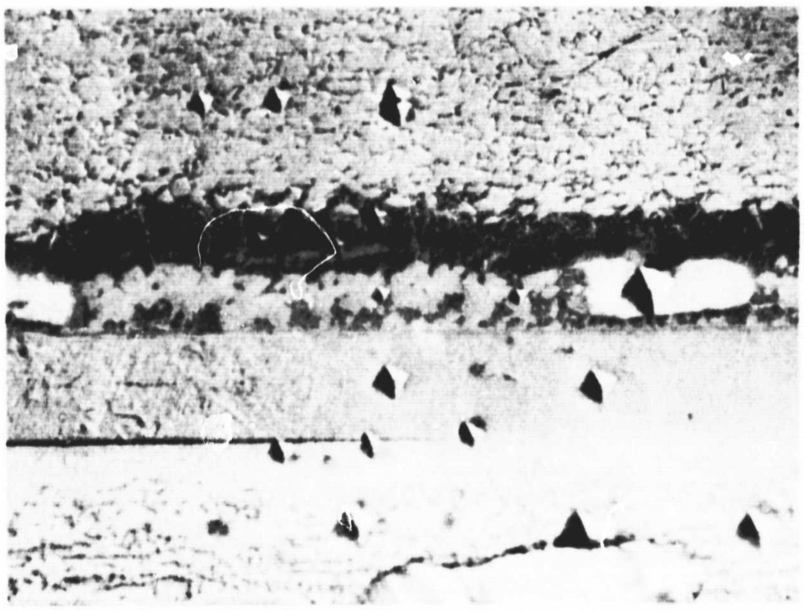

Etch: Kroll's -
Oblique Elimination

Magnification: 400X

10gm DPN Hardness

Ti-6Al-4V, DPH 259
Braze Affected Ti-6Al-4V, DPH 273
Intermediate, DPH 439
Braze Alloy, Hard Phase DPH 563
Soft Phase DPH 68
Diffusion Barrier Foil, DPH 152
Interface, DPH 203
Braze Alloy, DPH 88

FIGURE 30. TITANIUM DUCT HARDNESS TESTS

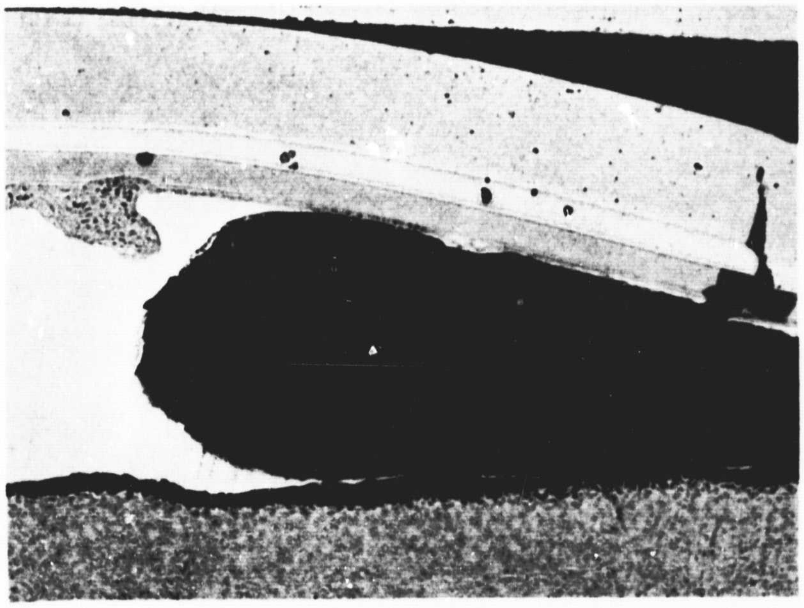

Etch: Kroll's

Magnification: 100X

FIGURE 31. FRACTURE OF STAINLESS STEEL DAMPING SLEEVE FROM INSIDE DIAMETER OUTWARD, COINCIDENT WITH UNBRAZED SECTION

6061-T6 Aluminum

All brazed aluminum alloy ducts failed at the end of the sleeve sections. The duct to which the sleeve was epoxy bonded did not fail, although the sleeve cracked after failure of the epoxy joint. The two ducts selected for examination were No. 6, which sustained more cycles in resonant fatigue than any other, 320 and 400; and No. 41, which failed at about the average of the other tubes, 75 and 800 cycles. The sleeve-to-duct braze of Duct 6 was the most marginal of any tested because of the manner in which the differential thermal expansion restraining bands were attached.

Tensile Properties. Longitudinal specimens were sectioned from the central portion of the ducts and the 321 stainless steel sleeve sections were peeled away from the aluminun. The specimens were machined to a standard 1.27-centimeter configuration and tested in tension. Results were:

Tube	Area (Nominal) (cm)	Ultimate Strength newtons/m^2 ($x\ 10^{-7}$)	0.2 Percent Yield newtons/m^2 ($x\ 10^{-7}$)	Elongation Percent In 2.54 cm
6	0.124 x 1.27	29.6	28.2	4.5
41	0.124 x 1.27	28.5	26.3	3.0

Tensile and yield strengths are of approximately the proper magnitude but there is a marked loss of ductility. Typical elongation for 6061-T6 extruded tubing is about eight percent.

Metallographic Examination. Figures 32 and 33 show cross sections of the braze joints in aluminum ducts, No. 6 and 41 respectively, the latter at the point of fracture. The condition most obvious in both is the degree to which the aluminum-silicon braze alloy has alloyed with the 6061 aluminum. The braze to the damping sleeve is of very marginal quality and includes many voids. This irregularity of the surface provides severe notches for amplification of the cyclic stress. At the ends of the sleeves there is an excess of braze alloy which has been squeezed out of the joint by differential thermal expansion against the restraining bands. Due to the inefficiency of banding on Duct 6, the braze alloy had less buildup and the damage which it caused was less, probably contributing to the longer life of this particular duct in the fatigue test.

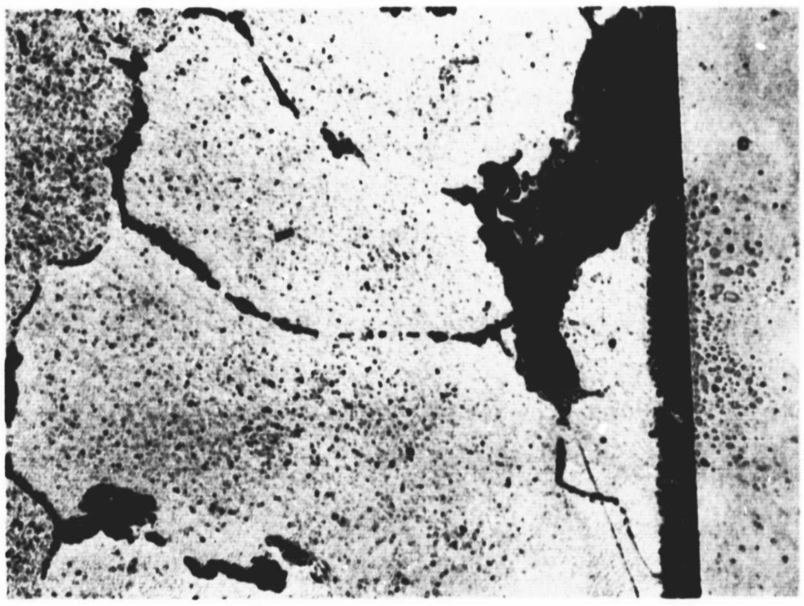

Etch: Flick's

Magnification: 250X

FIGURE 32. TYPICAL SECTION OF SLEEVE TO ALUMINUM ALLOY DUCT BRAZE JOINT

Etch: Flick's

Magnification: 50X

Note excess of braze alloy on ID

FIGURE 33. FRACTURE THROUGH WALL OF ALUMINUM ALLOY DUCT 41, NEAR END OF DAMPING SLEEVE

SECTION V

DISCUSSION

Procedures for including material damping calculations in the preliminary design phase of engineering structures are not available in the literature commonly used by structural designers. This report represents a transition between the level of communication in the extensive general review by B. J. Lazan (Ref. 1) and the strength of materials language in day-to-day use by designers. The damping ratio prediction equation used here in the presentation of Test Series I response data has been translated into graphical formats (Fig. 12 and 22), and these formats are of immediate value when comparing the dynamic response of ducts made of four materials and with three different geometries. However, it must be acknowledged that a considerable amount of work remains to provide designers with procedures for predicting damping ratios for beams or ducts of arbitrary lengths, cross sections, and of differing materials without recourse to experimental results obtained on full-scale structures. The present authors believe that extension of the design procedure outlined in Appendix A, which is based on integration of unit material damping through the volume of a beam, is the best available technique and should be followed in future studies.

The Test Series II response and fatigue results demonstrate that application of a uniform damping sleeve can yield a substantial reduction in midspan maximum strain amplitude of a duct vibrating in the fundamental bending mode. This configuration is not recommended for use on full-scale structures because it can result in an undesirable length distribution of maximum strain amplitudes. Modifications could be made in the sleeve geometry that would retain the desirable reduction in midspan response without introducing strain concentrations. Design and evaluation of additional sleeve configurations could be accomplished as a logical extension of the experience gained in conducting the Test Series II experimental program.

The art of metallurgical bonding dissimilar structural alloys to achieve improved structural damping in engineering structures must be considered to be in an early stage of development. The practices adopted in this study were not in all instances optimum from a metallurgical viewpoint, but were considered to be sufficiently refined for evaluation of the Test Series II uniform damping sleeve configuration.

PRECEDING PAGE BLANK NOT FILMED.

VI

CONCLUSIONS

The following conclusions were reached during the course of this study program.

- An improvement in the communication level for the presentation of uniform duct damping test results has been accomplished.

- Techniques for predicting midspan response of uniform ducts of arbitrary length, cross section, and of differing structural alloy materials are available but require translation into language readily usable by designers.

- Application of a uniform AISI 321 stainless steel sleeve to Inconel 718, 6Al-4V titanium, and 6061-T6 aluminum ducts by metallurgical bonding techniques can yield significant reductions in midspan maximum strain amplitudes.

- Modifications of the present uniform damping sleeve geometry are required to avoid undesirable lengthwise redistribution of maximum strain amplitudes.

REFENCES

1. Lazan, B. J., Damping of Materials and Members in Structural Mechanics. Pergamon Press, London (1968).

2. Crandall, S. H., On Scaling Laws for Material Damping. NASA TN D-1467 (December 1962).

PRECEDING PAGE BLANK NOT FILMED.

APPENDIX A

PREDICTION OF DAMPING IN UNIFORM DUCTS

PRECEDING PAGE BLANK NOT FILMED

APPENDIX A

PREDICTION OF DAMPING IN UNIFORM DUCTS

In the present series of experiments, ducts were placed in a horizontal position with one end free to rotate in a pinned joint and the other free to rotate and slide in a pinned/slotted joint. A driving force was imposed on the pinned end in a direction perpendicular to the beam axis and at a frequency which caused the beam to vibrate in the first fundamental mode. The total system damping, in units of m-newtons/cycle, consists of separate external and internal parts which contribute additively to the total damping,

i. e., $D_o^s = D_o^e + D_o^i$, m-newtons/cycle,

where D_o^s = total system damping

D_o^e = external damping

D_o^i = internal damping

The external damping, D_o^e, can be further divided into components due to air friction and friction in the grips at the ends of the beam,

i. e., $D_o^e = D_o^a + D_o^g$, m-newtons/cycle,

where D_o^a = damping due to air friction

D_o^g = damping due to grips.

When $D_o^e << D_o^i$, the total system damping can be approximated by computing or measuring the total internal damping, D_o^i. No attempt was made in this study to predict the contributions due to air friction and friction in the grips.

The total internal damping in the first fundamental beam vibration mode of a uniform beam is a function of beam geometry, the stress distribution in the beam, and the specific damping D in units of m-newtons/m^3-cycle of the beam material. When uniaxial test specimens of typical structural materials are subjected to alternating stress, it is found that the specific damping, D, is dependent on stress amplitude in a manner that can be described in terms of three stress amplitude regimes. At low stress amplitude levels, D is found to be frequency and temperature dependent and to be proportional to the square of stress amplitude. At stress amplitude levels in the order of 7×10^5-7×10^6 newtons/m^2 there is a transition to a medium stress level regime in which specific damping for a given material is a single valued function of stress amplitude, σ, in the form

$$D = J\sigma^n$$

where J and n depend on the material. In this regime, it is commonly found that $2 \leq n \leq 3$. At stress amplitude levels in the order of 7×10^7 - 7×10^8 newtons/m^2 there is a transition at a cyclic stress sensitivity level, to a regime in which D is dependent on the number of vibration cycles that a specimen has undergone.

It is assumed here that the maximum stress amplitude is in the medium stress regime. J. S. Whittier[1] indicated that the specific damping energy in a uniaxial test is composed of a component due to change of shape or distortion, and one due to change in volume or dilatation. In an isotropic material, the distortional strain energy may be expressed as a function of an effective stress $\bar{\sigma}$ and the dilatational strain energy as a function of an effective stress $\bar{\bar{\sigma}}$. If it is assumed that the specific damping is a function of these effective stresses, we may write

$$D = D(\bar{\sigma}, \bar{\bar{\sigma}}).$$

If there is no physical coupling between dilatational and distortional damping mechanisms, we may assume that

$$D(\bar{\sigma}, \bar{\bar{\sigma}}) = D(\bar{\sigma}) + D(\bar{\bar{\sigma}}).$$

If it is further assumed that for a material obeying a uniaxial damping law of the form

$$D = J\sigma^n$$

the two types of damping behavior are equally effective, then the specific damping at a point of a stressed object made of that material may be expressed in the form

$$D(\bar{\sigma}, \bar{\bar{\sigma}}) = J_1\bar{\sigma}^n + J_2\bar{\bar{\sigma}}^n,$$

where J_1, J_2, and n are material constants.

---

1. Whittier, J. S., Phenomenological Theories of Hysteretic Material Damping with Application to the Vibrations of Circular Plates. ASD Technical Report 61-264 (November 1961).

In a uniaxial test specimen, or in a vibrating beam, $\sigma = \bar{\bar{\sigma}} = \sigma$, say. In this case,

$$D = J\sigma^n = D(\bar{\sigma}, \bar{\bar{\sigma}}) = D(\sigma, \sigma) = J_1\sigma^n + J_2\sigma^n,$$

where the terms with coefficients J_1, J_2 correspond to distortional and dilatational contributions, respectively. If the equal-damping-effectiveness assumption is considered to be too restrictive in a beam vibration experiment, a damping law of the form

$$D(\sigma, \sigma) = J_1\sigma^{n_1} + J_2\sigma^{n_2}$$

can be assumed. In this case, the constants J_1, J_2, n_1, and n_2 can be found by a semi-inverse method in which ranges of values of the constants are assumed and theoretical predictions of total internal damping, D_o^i, based on assumed values of $D(\sigma, \sigma)$ are compared with experimental results.

Computation of Total Damping

The logarithmic decrement due to material damping for vibration decay is defined as

$$\delta = \frac{D_o^i}{2W}$$

where D_o^i is the total internal energy loss per cycle and W is the maximum elastic energy per cycle. D_o^i is the volume integral through a duct section of the unit damping, D

i.e., $$D_o^i = \iiint D\,dV = \iiint J\,\sigma_a^n\,dV$$

When a cylindrical coordinate system (r, θ, x) is used to describe positions of the duct and the stress distribution is given by

$$\sigma_a = \sigma_{max}\frac{y}{r_2}\sin\frac{\pi x}{\ell} = \sigma_{max}\frac{r}{r_2}\sin\theta\sin\frac{\pi x}{\ell},$$

where σ_{max} is the stress amplitude at $y = r_2$ and $x = \ell/2$, the following results are obtained.

$$D_o^i = 2J\,\sigma_{max}^n\,\frac{\ell}{\pi}\,r_2^2\,\frac{\left[1-\left(\frac{r_1}{r_2}\right)^{n+2}\right]}{n+2}\left[\int_o^{\pi}\sin^n\theta d\theta\right]^2$$

and
$$2W = \frac{\sigma_{max}^2}{2E}\,\frac{\ell}{\pi}\,r_2^2\left[1-\left(\frac{r_1}{r_2}\right)^4\right]\left[\int_o^{\pi}\sin^2\theta d\theta\right]^2$$

and, therefore
$$\delta = \frac{D_o^i}{2W} = \frac{4EJ\,\sigma_{max}^{n-2}}{n+2}\left[\frac{1-\left(\frac{r_1}{r_2}\right)^{n+2}}{1-\left(\frac{r_1}{r_2}\right)^4}\right]\left[\frac{\int_o^{\pi}\sin^n\theta d\theta}{\int_o^{\pi}\sin^2\theta d\theta}\right]^2$$

$$= \frac{4EJ\,\sigma_{max}^{n-2}}{n+2}\left(\frac{2}{\pi}\right)^2 f_1\,(r_1/r_2,\ n)\,f_2^2\,(n)$$

where
$$f_1\,(r_1/r_2,\ n) = \frac{1-\left(\frac{r_1}{r_2}\right)^{n+2}}{1-\left(\frac{r_1}{r_2}\right)^4}$$

and
$$f_2\,(n) = \int_o^{\pi}\sin^n\theta d\theta\ .$$

Figure 34 shows values of f_2 (n) as a function of the damping exponent n. As a numerical check on this result the function f (θ, n) = $\sin^n\theta$ was plotted versus θ in Figure 35 for a particular value n = 6.7. The area under the curve was found by planimetry to be

$$f_2\ (n = 6.7) = 0.93$$

The function f_1 $(r_1/r_2,\ n)$ is shown versus r_1/r_2 in Figure 36 for n = 2, 4, 6, 8, 10 in the range $0 \le r_1/r_2 \le 0.99$. For the baseline 7.6 cm OD stainless steel duct section (Test II-E-29) n = 6.7, J = 3.25×10^{-51}, and r_1/r_2 = 0.968. In this case f_1 = 2.02.

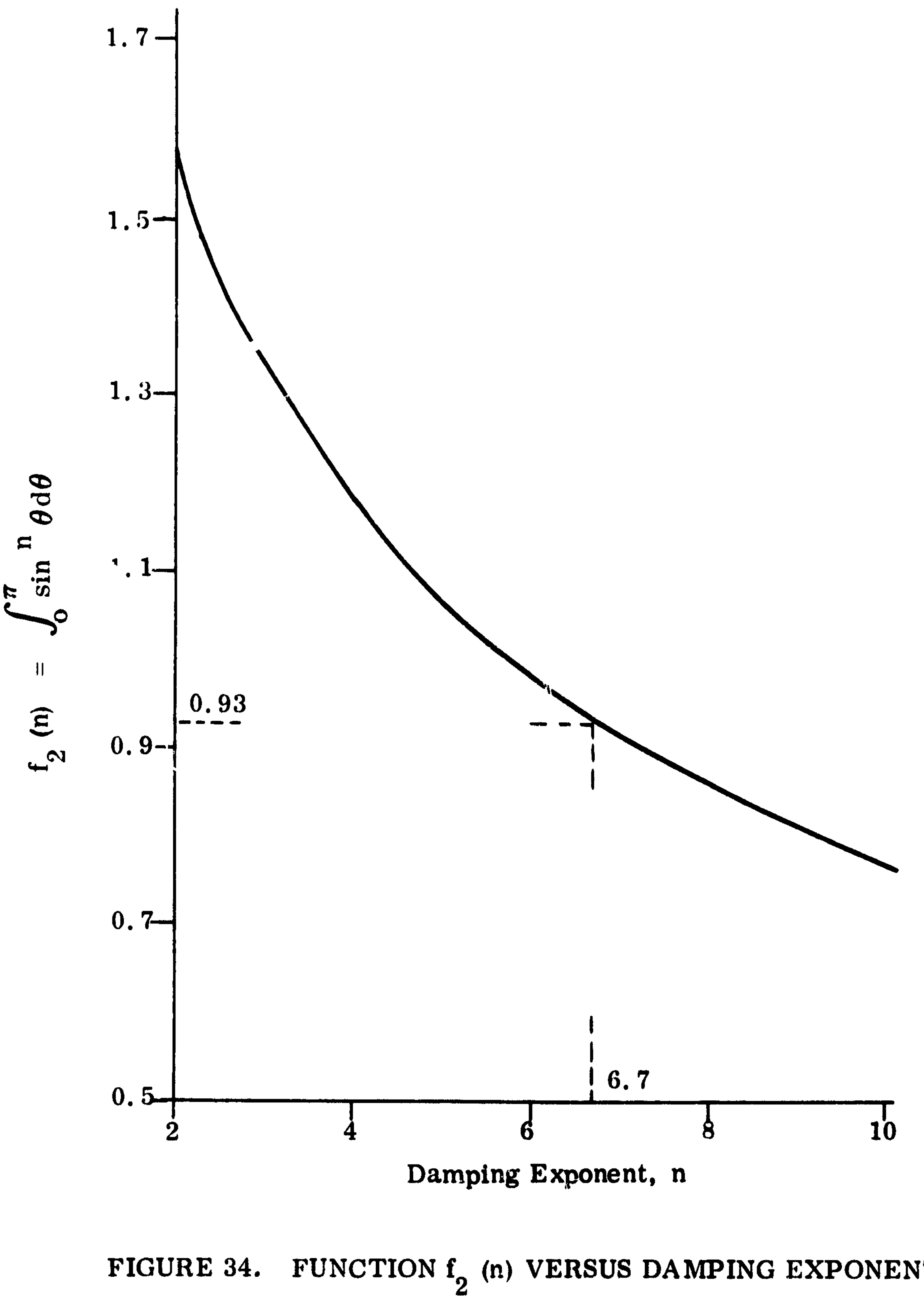

FIGURE 34. FUNCTION f_2 (n) VERSUS DAMPING EXPONENT, n

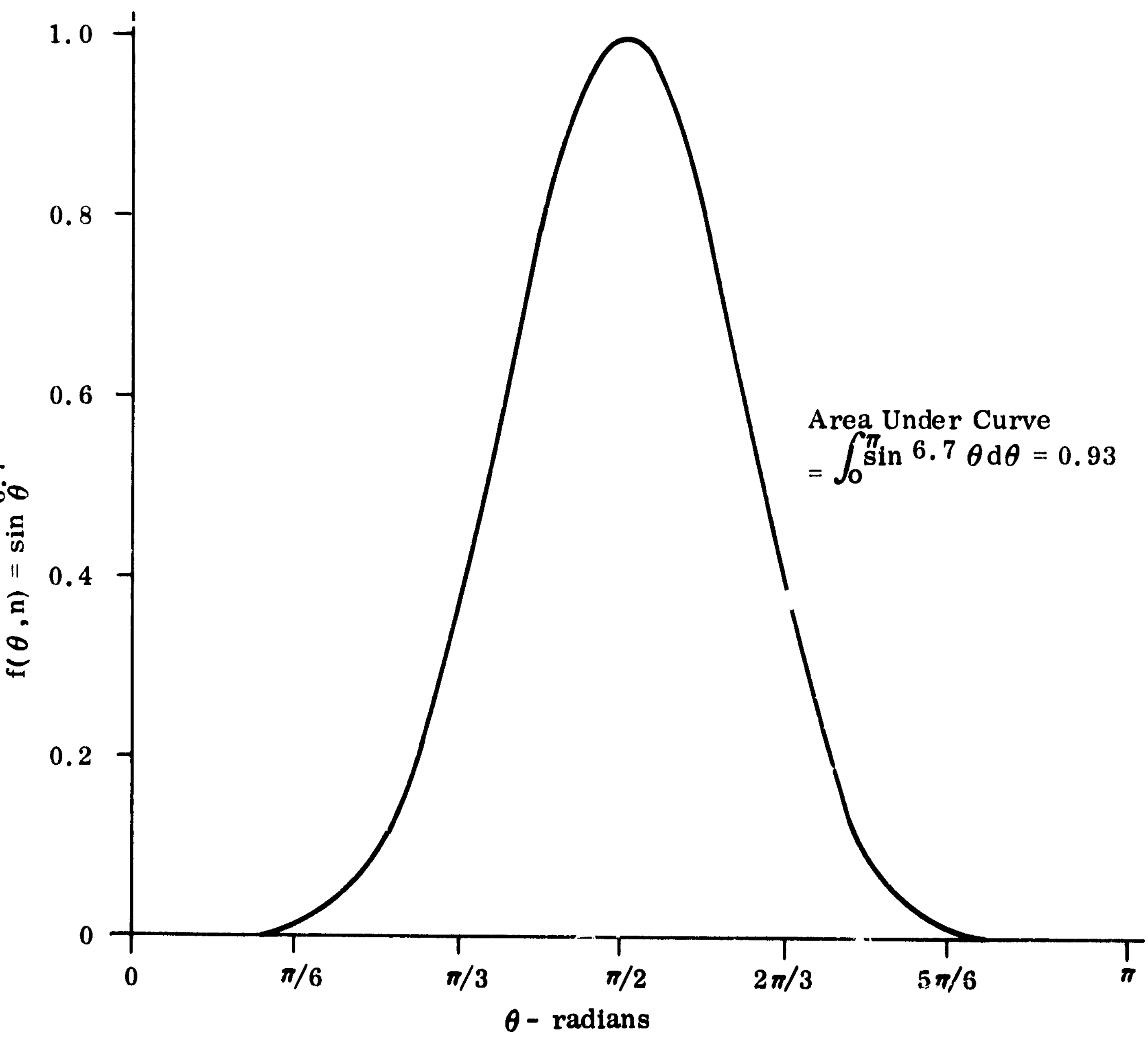

FIGURE 35. ANGULAR DISTRIBUTION FUNCTION VERSUS θ FOR DAMPING EXPONENT $n = 6.7$

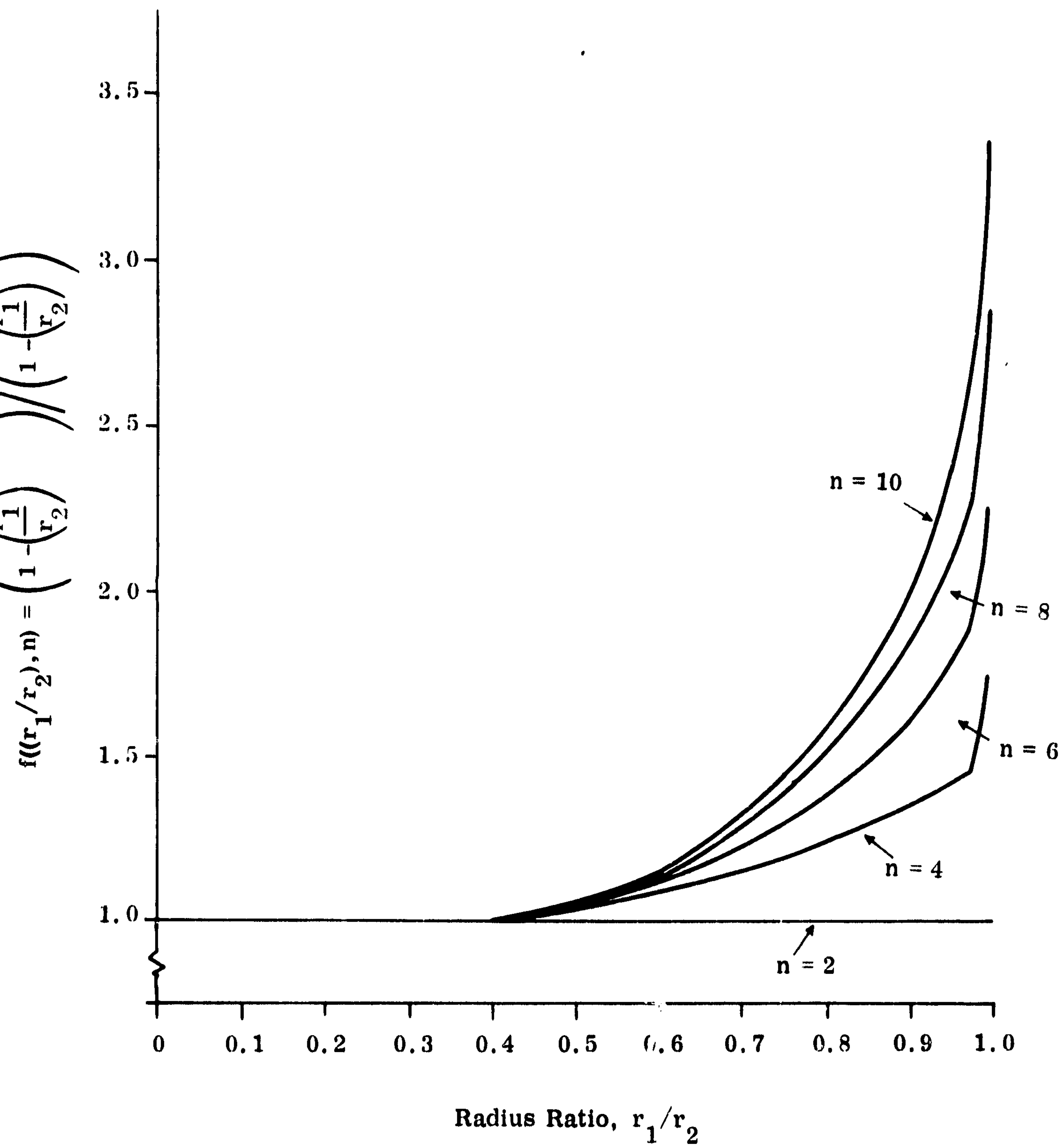

FIGURE 36. RADIUS RATIO FUNCTION $f((r_1/r_2), n)$ VERSUS DIAMETER RATIO FOR DIFFERENT VALUES OF THE DAMPING EXPONENT, n

To illustrate the results, the 321 stainless steel damping ratio ζ was computed for $O \le \sigma_{max} \le 25 \times 10^7$ newtons/m^2 using the relation

$$\zeta = \delta / 2\pi.$$

Figure 37 shows a solid curve computed for Test II-E-29 321 stainless steel duct and a comparison with results obtained by substitution of measured values of N and ϵ in the damping ratio prediction equation $\zeta = \frac{1}{\pi^2} \frac{\gamma}{E} \frac{N}{\epsilon} \frac{\ell^2}{r}$.

The theory of this section is considered to be remarkably successful at higher stress levels in preducting the change in slope of the ζ - σ relation found by experiment. There is considerable disagreement at stress amplitudes less than 20×10^7 newtons/m^2, indicating that future experimental and theoretical work on uniform ducts is warranted.

Comparison of Predicted and Measured Values of ζ

An attempt was made to compare predictions of ζ with direct measurements of damping in experiments on a 6061-T6 aluminum duct section. The duct diameter, length, and wall thickness were 5.1 centimeters, 1.52 meters, and 0.124 millimeter, respectively. Two different standard techniques were used. In the first, the duct was mounted with one pinned end on a shaker head and the other in a pinned/slotted wall bracket. Motion of the shaker head was prevented by means of clamps and blocks. A 45.4-kilogram weight was suspended at midspan of the duct with a support that included a section of safety wire. A strain gage was attached to the outer duct wall at midspan. It was found that consistent vibration decay curves could be obtained on an oscillograph by cutting the support wire in repeated tests. The vibration decay test setup is shown in Figure 38. The vibration decay data were reduced as follows. Logarthmic decrement values were computed over four vibration cycles at average peak strain values of 230, 400, 610, and 700 x 10^{-6} meter/meter. The measurements were repeated eight times. Damping ratios were computed according to the relation

$$\zeta = \delta / 2\pi, \text{ where}$$

$$\delta = \text{logarthmic decrement} = \frac{1}{4} \ln \frac{\epsilon_n}{\epsilon_{n+4}}$$

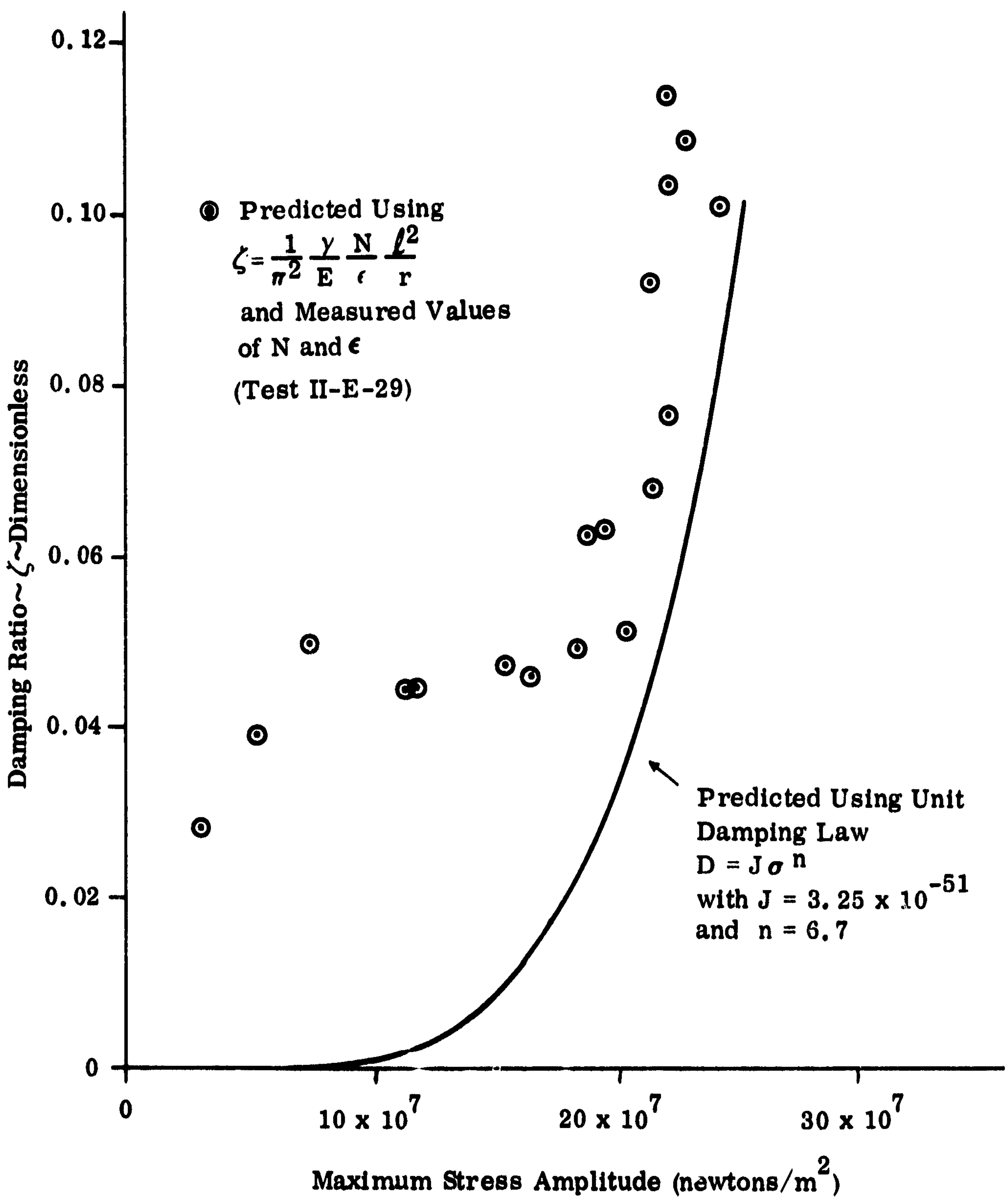

FIGURE 37. DAMPING RATIO VERSUS STRESS FOR 7.6 CENTIMETER OD AISI 321 STAINLESS STEEL DUCT; (Test II-E-29)

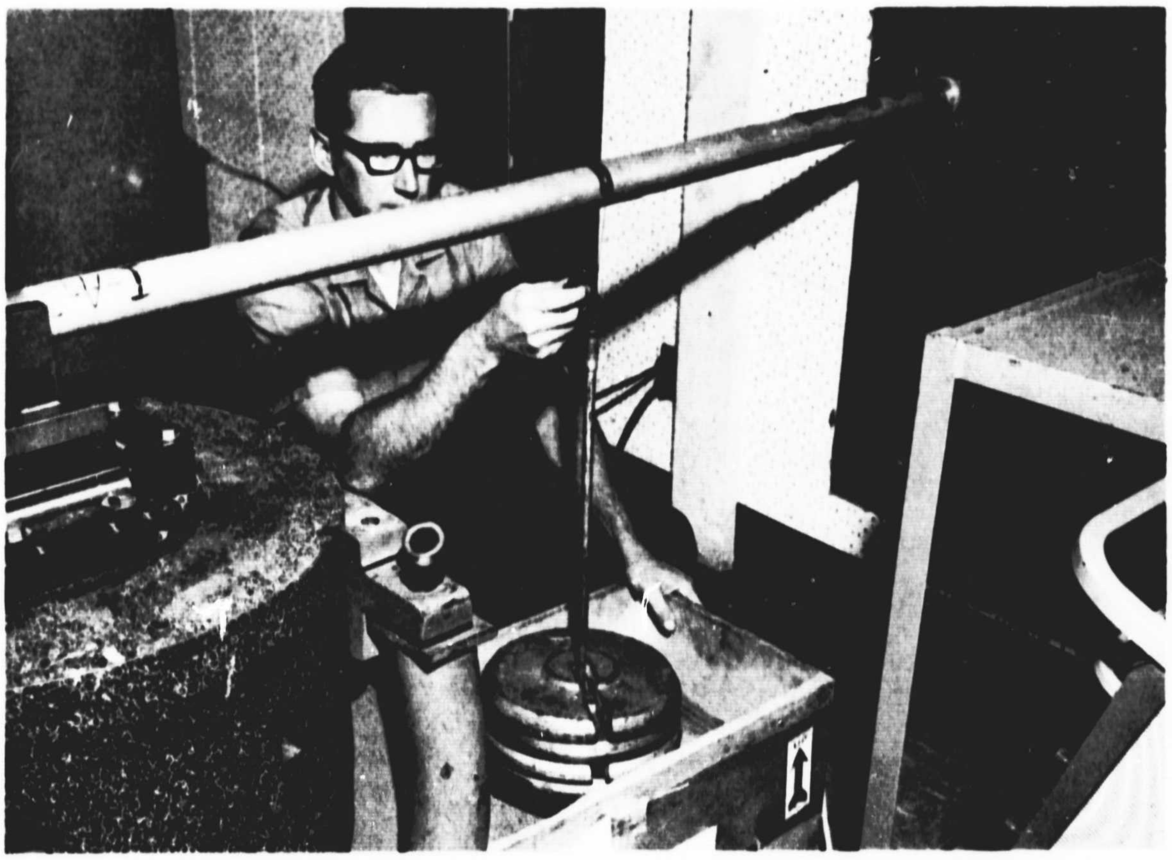

FIGURE 38. METHOD OF RELEASING DEAD WEIGHT LOAD FOR RECORDING OF VIBRATION DECAY

Sample standard deviations for ζ at each of the four strain values were computed using the formula

$$\sigma \zeta = \left(\frac{1}{7} \sum_{i=i}^{8} (\zeta_i - \bar{\zeta})^2 \right)^{1/2}$$

where ζ_i represents an individual measurement and $\bar{\zeta}$ an average over eight measurements. Figure 39 shows the average damping ratio results, together with curves at levels of $\pm$ one standard deviation. The results show a maximum in ζ at a strain in the range $400 < \epsilon < 500 \times 10^{-6}$ meter/meter with lower values at lower and higher strains.

The second series of damping measurements was made by using what is known as the frequency/half-power bandwidth method. The shaker mounted end of the duct was subjected to swept-sine frequency excitation at resonant peak strain levels in the range $680 < \epsilon < 1100 \times 10^{-6}$ meter/meter. A typical peak strain versus frequency response curve is shown in Figure 40. The frequency bandwidth, Δf, at a strain amplitude equal to 0.707 times the amplitude at resonance was measured and damping ratios were computed using the formula

$$\zeta = \frac{\Delta f}{2 f_1}, \text{ where } f_1 = \text{ frequency at resonance.}$$

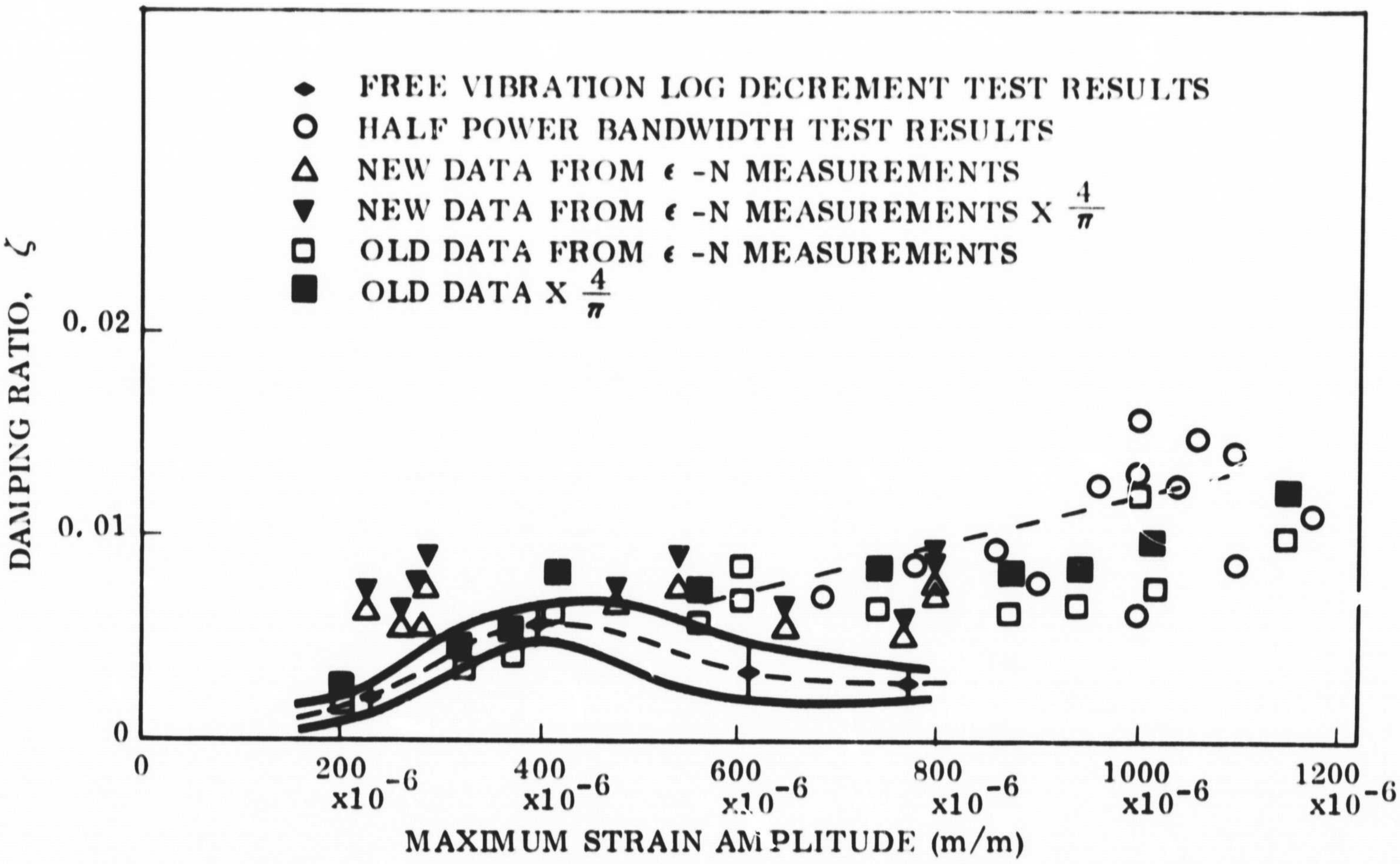

FIGURE 39. DAMPING RATIO VERSUS STRAIN OBTAINED BY DIFFERENT TECHNIQUES WITH 5.2-CENTIMETER OD ALUMINUM DUCT

A total of 14 response curves was obtained. Measured values of ζ are plotted as circled dots in Figure 39. The dashed line represents a least squares straight line fit on the ζ values.

The two sets of measured ζ values tend to converge at a peak strain in the order of 600×10^{-6} meter/meter, but diverge at higher strains. The ζ values obtained by the vibration decay method are consistently lower than those obtained in the swept-sine tests at higher strain levels.

In a third series of measurements, peak strain, ϵ, and acceleration load factor, N, values were obtained at resonance of the duct in the fundamental mode for strain amplitudes in the range $220 < \epsilon < 800 \times 10^{-6}$ meter/meter. These measurements represent a repeat of experiment I-A-3 with a different duct of the same material. Damping ratios were computed using the alternate formulae of the preceding section for both the newly obtained and previous results. The open triangles in Figure 39 represent data computed according to the formula

$$\zeta = \frac{1}{\pi^2} \frac{\gamma}{E} \frac{N}{\epsilon} \frac{\ell^2}{r}$$

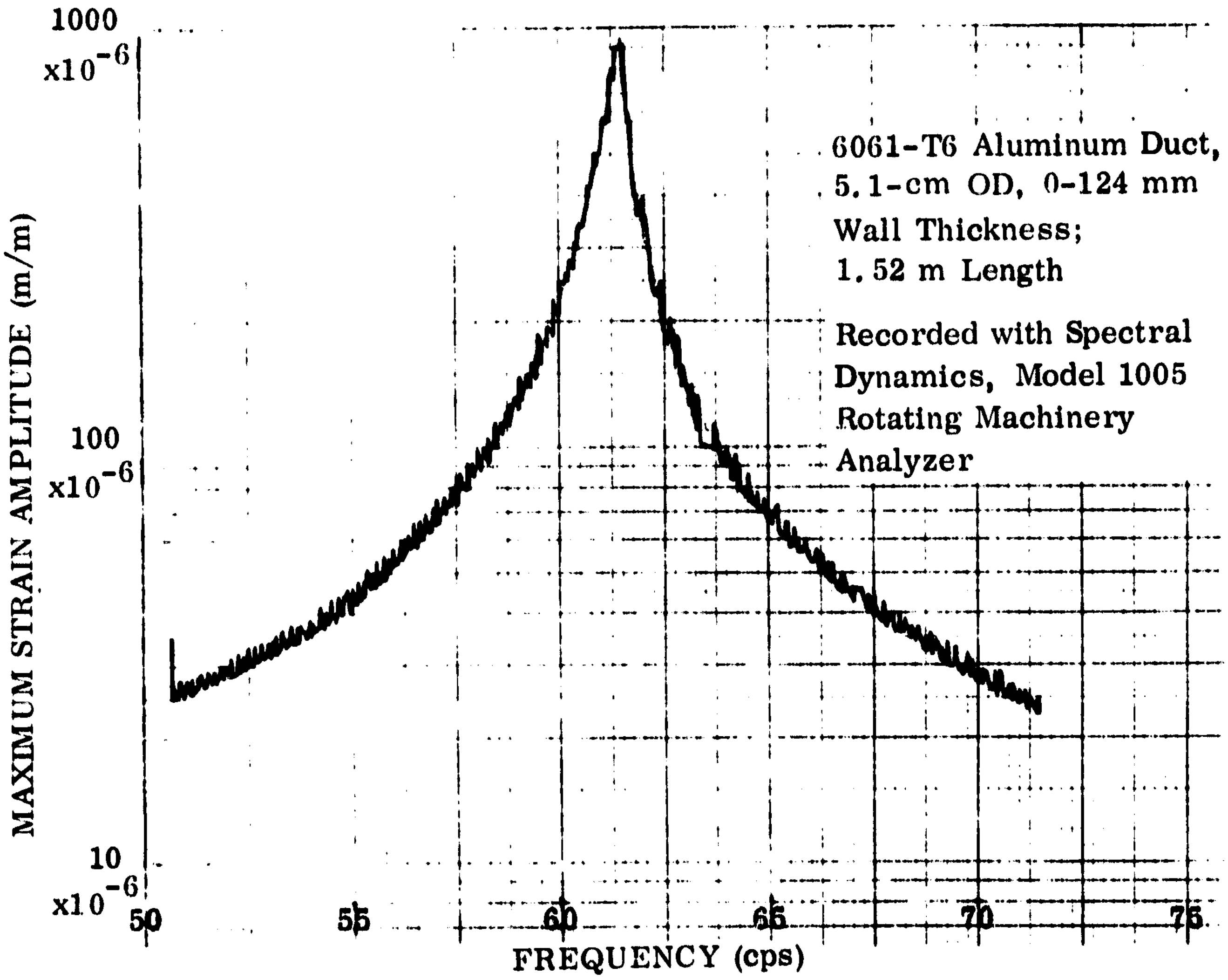

FIGURE 40. FREQUENCY SWEEP THROUGH FIRST RESONANT MODE

and the solid triangles are greater by a factor of $4/\pi$. The previous data are plotted as open and closed squares. The two sets of computed ζ values for the different ducts agree reasonably well for strains greater than 400 x 10^{-6} meter/meter. The disagreement at lower strains is attributed to lack of precision in measurement of low values of N.

This exercise points out the need for taking extreme care in obtaining direct measurements of damping by the two alternate techniques. No firm conclusion can be made regarding the advisability of changing the prediction equation for damping ratio ζ by a factor of $4/\pi$ on the basis of the data presented here. Either form of the prediction equation yields damping ratios that are in fair agreement with the vibration decay results at strain levels lower than 500 x 10^{-6} meter/meter and with the values obtained by the frequency/half-power bandwidth method at strains in the range $500 < \epsilon < 1000 \times 10^{-6}$ meter/meter.

Technique for Scaling Values of the Damping Ratio, ζ

The baseline duct material identified in this program is AISI 321 stainless steel. Values of the damping ratio, ζ, have been obtained for the following ducts.

Test	Diameter (cm)	Length (m)	Wall Thickness (mm)
I-A-1	5.08	1.52	0.124
I-E-29	7.6	1.98	0.124
I-B-8	10.2	1.98	0.124

In the experiments, one end of a pinned/pinned duct was subjected to a transverse excitation at the fundamental bending mode resonant frequency. Values for the damping ratio, ζ, were predicted using the formula

$$\zeta = \frac{1}{\pi^2} \frac{\gamma}{E} \frac{N}{\epsilon} \frac{\ell^2}{r}$$

When damping ratios for two different ducts are considered, one approach is to compare them at the same strain level at midspan to assure that the portions of the ducts subjected to the highest stress levels are behaving according to the same unit damping law of the form

$$D = J\sigma^n .$$

If subscripts 1 and 2 are used to denote two different ducts and the condition $\epsilon_1 = \epsilon_2$ is imposed, we can write

$$\zeta_1 = \frac{1}{\pi^2} \frac{\gamma_1}{E_1} \frac{N_1}{\epsilon_1} \frac{\ell_1^2}{r_1}$$

and

$$\zeta_2 = \frac{1}{\pi^2} \frac{\gamma_2}{E_2} \frac{N_2}{\epsilon_1} \frac{\ell_2^2}{r_2} .$$

If the ducts are of the same material, $\gamma_1 = \gamma_2$ and $E_1 = E_2$. The relationship between damping ratios ζ_1 and ζ_2 at the same strain level is then

$$\zeta_2 = \frac{r_1}{r_2} \frac{N_2}{N_1} \left(\frac{\ell_2}{\ell_1}\right)^2 \zeta_1$$

The following procedure has been adopted to check the internal consistency of experimental results obtained with different 321 stainless steel ducts. Subscript 1 was used to denote results obtained with the 5.1-centimeter OD duct and subscript 2 to denote results obtained with the 7.6-centimeter OD duct and then with the 10.2-centimeter OD duct, in comparison with those of the 5.1-centimeter OD duct. Ratios N_2/N_1 at the strain levels observed in the 5.1-centimeter OD duct tests were computed and experimental test points with values ζ and ϵ in the 5.1-centimeter OD duct tests were then scaled to predict ζ versus ϵ values for the larger ducts. The scaled values for the latter ducts are shown in Figure 41 as open triangles and circles, respectively. The dashed lines represent least-squares-straight-line fits on ζ as functions of ϵ. These results, therefore, represent predictions of damping ratios for the larger diameter ducts based on N versus ϵ curves and the results of the 5.1 centimeter OD duct tests.

The solid triangles and circles in Figure 41 represent ζ versus ϵ values at strain levels observed in Tests I-E-29 and I-B-8, respectively. The solid lines are least-squares fits to the data points. It can be concluded, from comparison of the two sets of straight line fits to the data, that within the limits of data scatter observed in the experiments, a good correlation exists between ζ values for 7.6-centimeter OD and 10.2-centimeter OD ducts when results are scaled on the basis of 5.1 centimeter OD duct tests, and then computed directly using the damping ratio prediction equation.

Suppose that a designer needs estimates of ζ, N, and ϵ values for a larger diameter duct, in the order of 20 centimeters. Let subscripts 1 and 2 denote 5.1- and 20-centimeter OD ducts, respectively. If no shaker tests had been performed on pinned/pinned 20-centimeter OD ducts, a relationship between N_2 and ϵ_2 would not be available. One approach that could be used would be to conduct vibration decay tests on the larger duct. Compare ζ and N values for the two ducts at the same strain levels, i.e., let

$$\epsilon_1 = \epsilon_2.$$

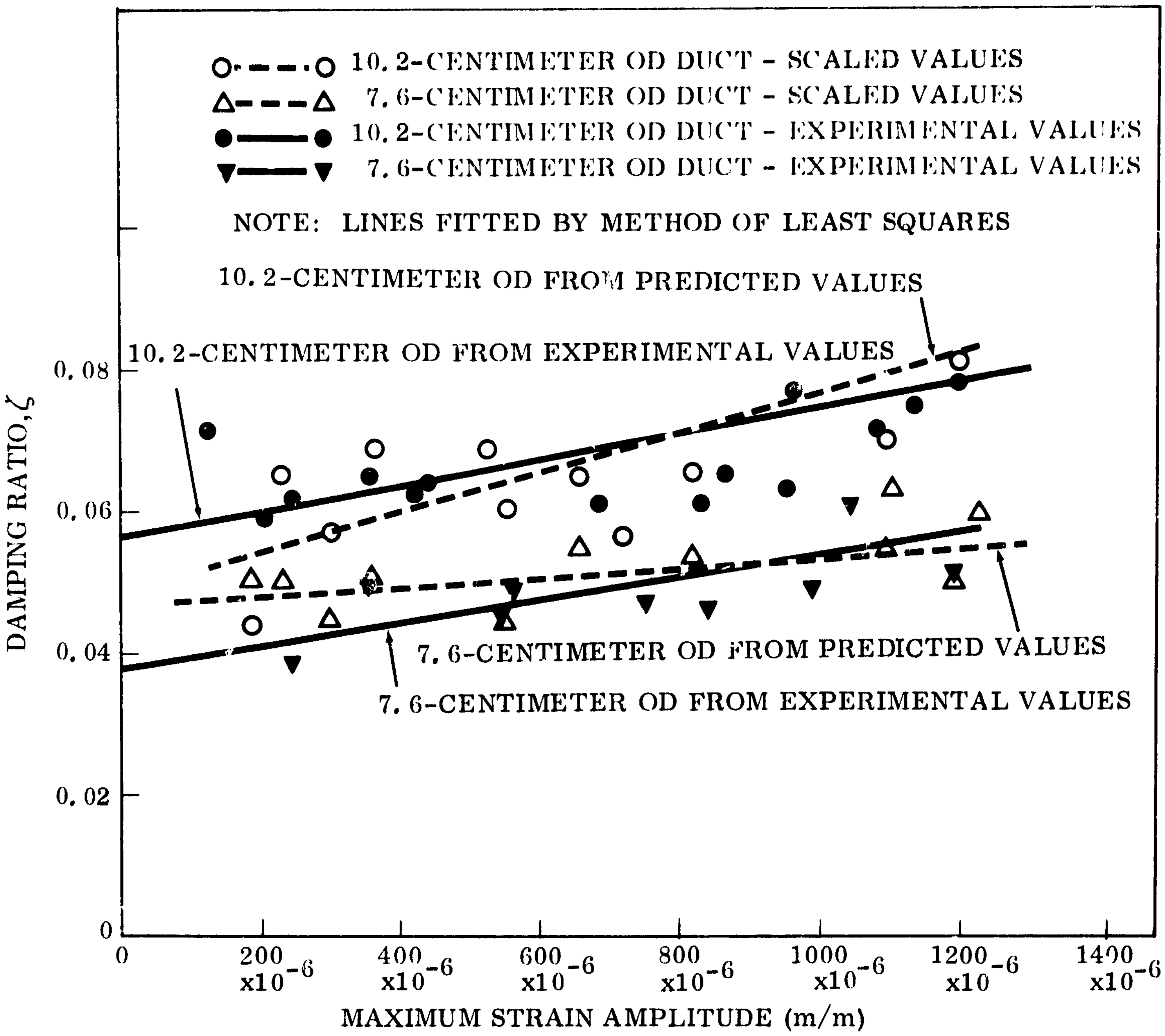

FIGURE 41. VALUES OF ζ-PREDICTED VERSUS MEASURED FOR 7.6- AND 10.2-CENTIMETER OD DUCTS; Predicted Values Scaled From Experimental Data Obtained on 5.1-Centimeter OD AISI 321 Stainless Steel Duct

Write

$$\zeta_2 = \frac{\delta_2}{2\pi} \frac{1}{\pi^2} \frac{\gamma_2}{E_2} \frac{N_2}{\epsilon_1} \frac{\ell_2^{\,2}}{r_2},$$

where ζ_2 represents measured values of logarithmic decrement for the 20-centimeter OD duct. For the 5.1-centimeter OD duct,

$$\zeta_1 = \frac{1}{\pi^2} \frac{\gamma_1}{E_1} \frac{N_1}{\epsilon_1} \frac{\ell_1^2}{r_1}.$$

The latter two expressions may then be used to obtain values of N_2 for the larger duct at strain levels ϵ_1.

$$N_2 (\epsilon_1) = \frac{1}{2\pi} \frac{r_2}{r_1} \frac{\ell_1^2}{\ell_2^2} \frac{\delta_2 (\epsilon_1)}{\zeta_1 (\epsilon_1)} N_1 (\epsilon_1).$$

In using this approach, ζ_2 versus ϵ_2 values for the larger diameter duct would therefore be obtained from vibration decay tests, and the corresponding acceleration load factors, N2, would be obtained by scaling results obtained with the smaller diameter duct. If the method is proven to be successful, shaker tests on the larger diameter duct would only be required to check the predicted results.

APPENDIX B

DERIVATION OF AN IMPULSE RESPONSE FUNCTION BY TRANSFORMATION OF A TRANSFER FUNCTION

PRECEDING PAGE BLANK NOT FILMED

PRECEDING PAGE BLANK NOT FILMED

APPENDIX B

DERIVATION OF AN IMPULSE RESPONSE FUNCTION BY TRANSFORMATION OF A TRANSFER FUNCTION

A single degree of freedom model for the deflections at midspan of a pinned ended duct can be expressed by the solution of the equation

$$\frac{d^2Y(t)}{dt^2} + \omega_1^2 (1 + 2\zeta i)\, Y(t) = f(t)$$

The transfer function for the model may be derived by finding the response to an input $f(t) = e^{st}$, where $s = \sigma + i\omega$ is a complex frequency parameter that is defined for ease of computation in terms of Laplace transform techniques. It is assumed that the system is at rest for time $t < 0$.

Substitution of the particular solution $Y(t) = Ae^{st}$ in the equation

$$\frac{d^2Y(t)}{dt^2} + \omega_1^2 (1 + 2\zeta i)\, Y(t) = e^{st}$$

yields the result

$$A = \frac{1}{s^2 + \omega_1^2 (1 + 2\zeta i)}.$$

The function

$$H(s) = A = \frac{1}{s^2 + \omega_1^2 (1 + 2\zeta i)}$$

is described as the transfer function for the single degree of freedom model. The impulse response function h(t) is the inverse Laplace transform of $H(s)e^{st}$. Let $z_o = \omega_1^2 (1 + 2\zeta i)$. The polar form of z_o is given by

$$z_o = r_o e^{i\theta o} = (\omega_1^{\,4} + \omega_1^{\,4}\, 4\zeta^2)^{1/2} e^{i\theta o}$$

where $\qquad \tan\theta_o = 2\zeta.$

For the problems of interest here, θ_o can be restricted to the range $0 < \theta_o < 2\pi$. The transfer function, H(s), may be factored as follows:

$$H(s) = \frac{1}{s^2 + z_o} = \frac{1}{2s(s - i\sqrt{z_o})} + \frac{1}{2s(s + i\sqrt{z_o})}$$

The function

$$f_1(s) = \frac{e^{st}}{2s(s - i\sqrt{z_o})}$$

is analytic in the region of the s-plane, except at the pole $s = i\sqrt{z_o}$ if a branch cut is made on the positive imaginary axis and the origin $s = 0$ is excluded. Then the inverse Laplace transform of $f_1(s)$ is given by the residue of $f_1(s)$ at the pole $s = i\sqrt{z_o}$.

i.e., $$L^{-1}\left[f_1(s)\right] = \frac{e^{i\sqrt{z_o}t}}{2i\sqrt{z_o}}$$

By a similar argument, the inverse transform of

$$f_2(s) = \frac{e^{st}}{2s(s + i\sqrt{z_o})}$$

is the residue of $f_2(s)$ at the pole $s = -i\sqrt{z_o}$.

Thus,

$$L^{-1}\left[H(s)e^{st}\right] = \frac{e^{i\sqrt{z_o}t} - e^{-i\sqrt{z_o}t}}{2i\sqrt{z_o}}$$

For problems of physical interest, h(t) is a real function of t.

Since

$$\sqrt{z_o} = (\omega_1^4 + \omega_1^4 4\zeta^2)^{1/4} e^{i\theta_o/2}$$

$$= (\omega_1^4 + \omega_1^4 4\zeta^2)^{1/4} \left(\cos\frac{\theta_o}{2} + i \sin\frac{\theta_o}{2}\right),$$

then $$e^{i\sqrt{z_o}\,t} = e^{(\omega_1^4 + \omega_1^4 4\zeta^2)^{1/4}\left(i \cos\frac{\theta_o}{2} - \sin\frac{\theta_o}{2}\right)t}$$

$$\left[\cos\left((\omega_1^4 + \omega_1^4 4\zeta^2)^{1/4} \left(\cos\frac{\theta_o}{2}\right)t\right) + i \sin\left((\omega_1^4 + \omega_1^4 4\zeta^2)^{1/4} \left(\cos\frac{\theta_o}{2}\right)t\right)\right]$$

$$\times\, e^{-(\omega_1^4 + \omega_1^4 4\zeta^2)^{1/4}}$$

and $$L^{-1}\left|H(s)e^{st}\right|$$

$$= \frac{\left[\sin\left((\omega_1^4 + \omega_1^4 4\zeta^2)^{1/4} \left(\cos\frac{\theta_o}{2}\right)t\right)\right] e^{-(\omega_1^4 + \omega_1^4 4\zeta^2)^{1/4}\left(\sin\frac{\theta_o}{2}\right)t}}{(\omega_1^4 + \omega_1^4 4\zeta^2)^{1/4}\left(\cos\frac{\theta_o}{2} + i \sin\frac{\theta_o}{2}\right)}$$

The real part of $L^{-1}\left|H(s)e^{st}\right|$

$$= \frac{\left[\left(\cos\frac{\theta_o}{2}\right) \sin\left((\omega_1^4 + \omega_1^4 4\zeta^2)^{1/4} \left(\cos\frac{\theta_o}{2}\right)t\right)\right] e^{-(\omega_1^4 + \omega_1^4 4\zeta^2)^{1/4}\left(\sin\frac{\theta_o}{2}\right)t}}{(\omega_1^4 + \omega_1^4 4\zeta^2)^{1/4}}$$

If the model is lightly damped, $2\zeta << 1$

and $\tan\theta_o = 2\zeta \approx \theta_o$.

In this case, $\sin\frac{\theta_0}{2} = \frac{\theta_0}{2}$ and $\cos\frac{\theta_0}{2} = 1$

and the impulse response function, h(t) is given by

$$h(t) = \frac{e^{-\omega_1 \zeta t} \sin \omega_1 t}{\omega_1}$$

The impulse response is seen to be a damped sine wave with period $\tau = \frac{2\pi}{\omega_1}$. Positive peaks occur at time intervals

$$t = \frac{(\frac{\pi}{2} + 2n\pi)}{\omega_1}, \quad n = 0, 1, 2, 3, -----.$$

The ratio is successive peaks h_n and h_{n+1} is given by

$$\frac{h_n}{h_{n+1}} = \frac{e^{-\zeta(\frac{\pi}{2} + 2n\pi)}}{e^{-\zeta(\frac{\pi}{2} + 2(n+1)\pi)}} = e^{2\pi\zeta} = e^{\delta},$$

where $\delta = 2\pi\zeta$ is called the logarithmic decrement.

The damping ratio, ζ, for an equivalent single degree of freedom model with light viscous damping can be obtained, therefore, from measurements of the logarithmic degrement by using the relation

$$\delta = 2\pi\zeta$$

APPENDIX C

NEW HIGH FRICTION GIMBAL

PRECEDING PAGE BLANK NOT FILMED

APPENDIX C

NEW HIGH FRICTION GIMBAL

A part of this program was devoted to the consideration of various ways to increase the total damping capacity in ducting systems. Ducting systems normally include a number of gimbals which can contribute to the total system damping. Special characteristics of a high friction gimbal capable of a large dissipation of vibratory energy would include:

- Very large diameter gimbal pins to produce a large frictional resisting moment
- A large gimbal pre-stress force to produce a frictional resisting moment in addition to that from dynamic shear on the pins
- Close tolerance between the pin and lug holes to enhance uniform frictional effects
- Careful selection of pin and lug materials to acquire the maximum kinetic coefficient of friction.

A comprehensive study resulted during the process of this program. Consideration of factors such as the reduction of manufacturing costs, improved reliability, and the incorporation of more simplified machining processes led to the design concept shown in Figure 42. Here an isometric cut-away view of the high friction, lightweight gimbal is shown incorporating the features outlined above. A view of the detailed components machined for the high friction gimbals are shown in Figure 43, with the assembly of the components shown in Figure 44.

As indicated by the isometric view, the gimbal ring is placed entirely outside the flanges. Insertion of the flanges on the inside of the ring provides several significant advantages.

- No slots are required in the gimbal ring as with the more conventional design which means that the thickness of the ring can be minimized.
- The elimination of slots helps reduce manufacturing costs since the gimbal ring is made entirely of circular machine parts.
- The size of the overall gimbal is reduced and produces weight savings through more efficient utilization of materials.
- During preflight certification testing, the flange lugs which were inserted in the gimbal slots constituted an area of high stress.

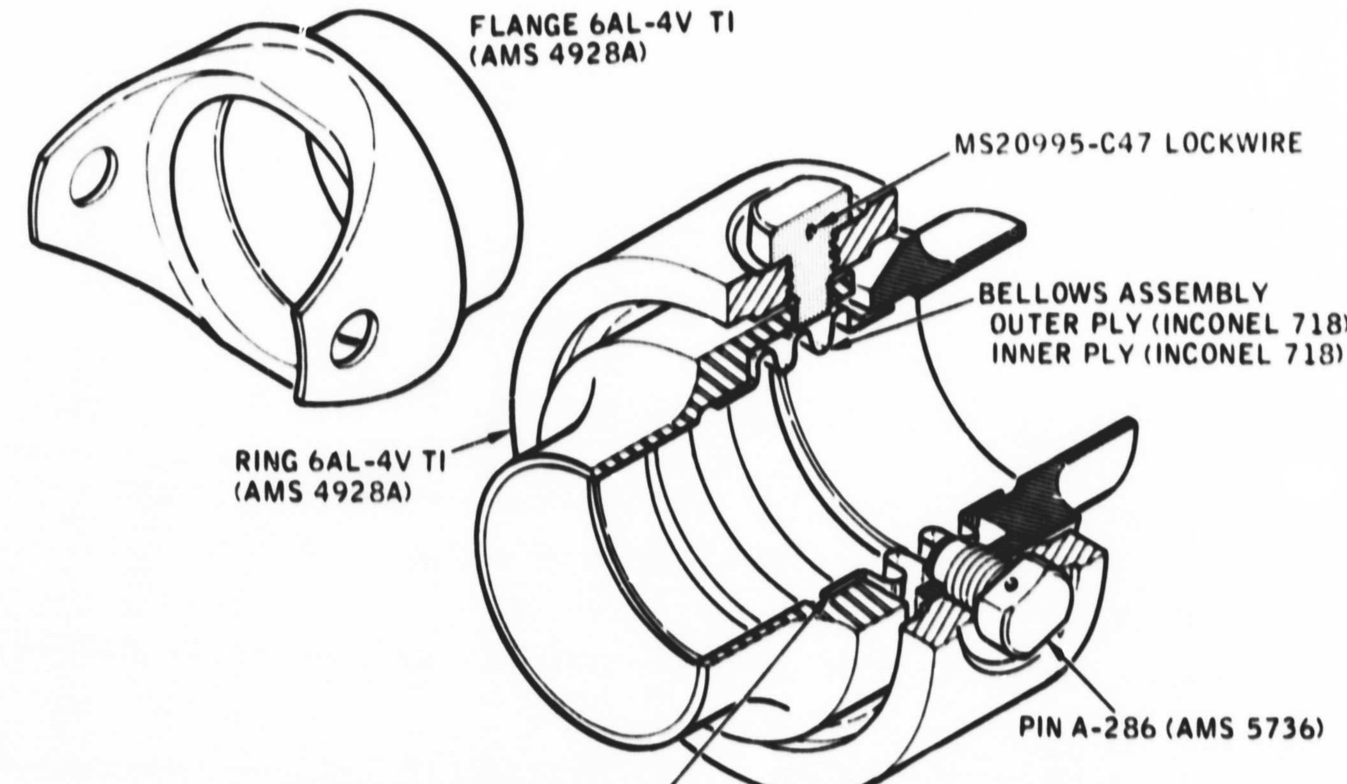

FIGURE 42. NEW HIGH FRICTION GIMBAL

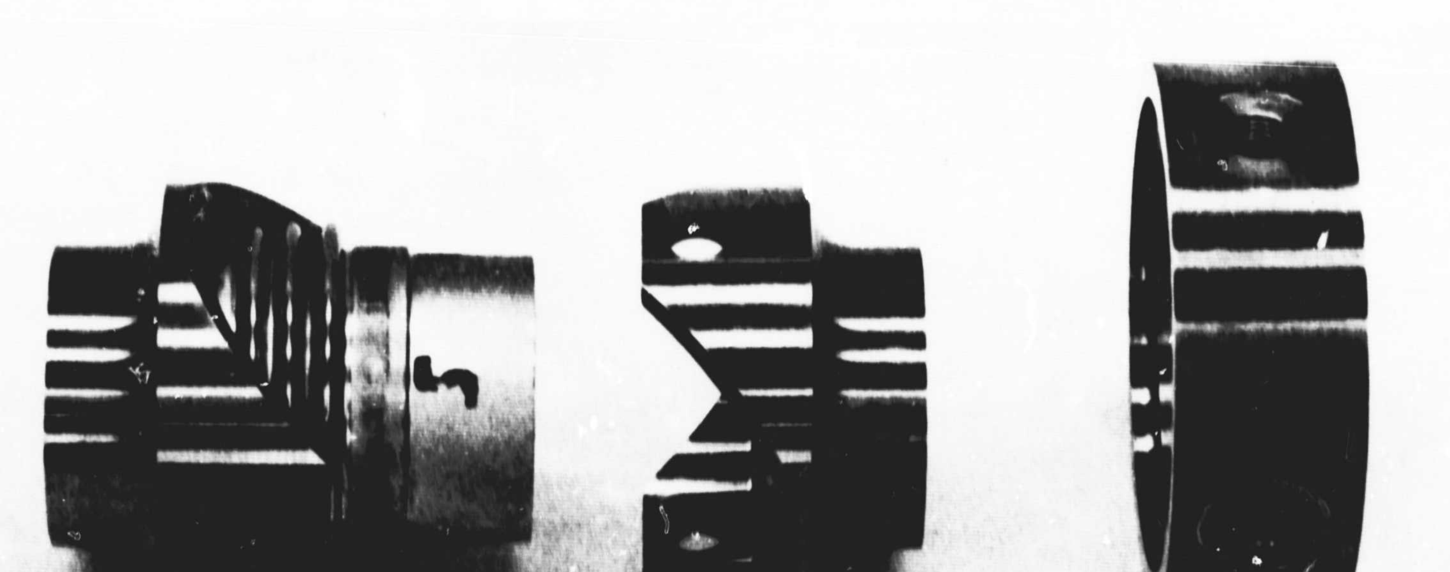

FIGURE 43. DETAIL COMPONENTS OF HIGH FRICTION GIMBAL FOR TITANIUM DUCT ASSEMBLY

FIGURE 44. ASSEMBLY OF TITANIUM HIGH FRICTION GIMBAL

Lug failures caused a number of assembly designs to be rejected. The curved flange lug extension inherently has more strength to resist the dynamic flexure. As a result, the reliability of the entire gimbal and of the duct assembly has been substantially improved.

By fitting the flanges entirely in the circular ring, turning operations dominate the manufacturing effect. These operations are much less expensive than the milling machine operations. The bottoming out mechanism for the gimbal is preserved more effectively as a result of this new concept. The flanges and the bellows are fully protected. A circular ring with no slots is obviously the more economical element to manufacture.

Repeated pin failures of the conventional gimbals created another critical area. Large lock wire bolts are used with the new high friction gimbal. They eliminate the danger of pin failures and greatly improve reliability; furthermore, these bolts permit substantial ease of assembly and disassembly. The new gimbal design provides for relaxed tolerances and the easing of tolerances provides an additional basis for reducing manufacturing costs.

In the case of the conventional gimbals, disassembly proved to be a difficult task. Many gimbal parts had to be scrapped which contributed to higher costs. In addition, tighter tolerances continually caused problems in assembly of the components which make up the entire gimbal. The new high friction, lightweight gimbal design avoids the extensive problems of tight tolerances.

Another very serious source of rejection involved the welding of the bellows to the flange. The bellows plies are generally roll welded at the ends and sealed. Then the bellows are subjected to a forming operation which produces the convolutions. The next operation consists of trimming the weld nugget. Depending upon the design there may be more than one weld. In some cases the weld nuggets overlap. The succeeding operation consists of trimming through the center of the nugget. The bellows is slipped into the flange and fusion welded. The purpose of the heavy nugget on the bellows is to provide the necessary weld material during the fusion welding process; however, despite the automatic setup of the process, the fusion welding torch did not slip back and off the heavy nugget and move onto the plies. The plies of the bellows are apparently damaged when this happens, producing a leak or other imperfection which is revealed by a subsequent X-ray examination. The rejection rate has been excessively high for this type of conventional fabrication.

The new design provides for the brazing of the bellows plies to the flange and is expected to eliminate totally the high rate of rejection and accompanying excessive costs. Furthermore, brazing solves the dissimilar metal problem and allows full optimization of gimbal design. Crack prone welds are eliminated with their accompanying problem of porosity and notch-sensitive heat-affected zones.

It has been common practice to plate the pins or lugs with silver or some other alloy to eliminate the possibility of galling; however, this expensive process of pin or lug plating is not justified because combinations of pin and lug material can be effectively selected which do not gall. Furthermore, the vibratory phases of the pre-flight certification tests do not have a duration which would make galling a problem. Therefore, plating, in general, should be eliminated and is not included in the new high friction gimbal design.

In addition to the unnecessary expense, plating has another very harmful result. It reduces frictional effects which result from rotation of the pin in the lug hole. These frictional effects can help to suppress the dynamic response of critical duct assemblies during the vibration tests of pre-flight certification programs. A new gimbal design is characterized by a very large diameter bolt. The proportioning of the bolt greatly exceeds strength requirements. Diameter is selected to accommodate the fact that frictional resisting moment is a function of the diameter of the bolt. Within limits, the larger the diameter of the bolt, the greater the frictional dissipation of the energy.

The A286 alloy has been selected for the bolt material. This bolt material acting in a flange of 6Al-4V-Ti eliminates the danger of galling and produces a high kinetic coefficient of friction. Close tolerances between the bolt and flange holes produce improved frictional effects; however, to hold manufacturing costs at a minimum, it has been decided to maintain relaxed tolerances and to count upon the larger diameter of the bolt for increased frictional dissipation of energy. The extended length of the skirt, on the back side of the flange of the gimbal for welding to the duct itself, avoids excessive reheating of the brazed area between the bellows and flange.

Full evaluation of this gimbal concept has not been possible since it has not been incorporated into the testing program. The influence of a gimbal pre-stress force for increasing the damping contributions of the gimbal must await test evaluation.

A design specification drawing (Fig. 45) is included as a part of this appendix.

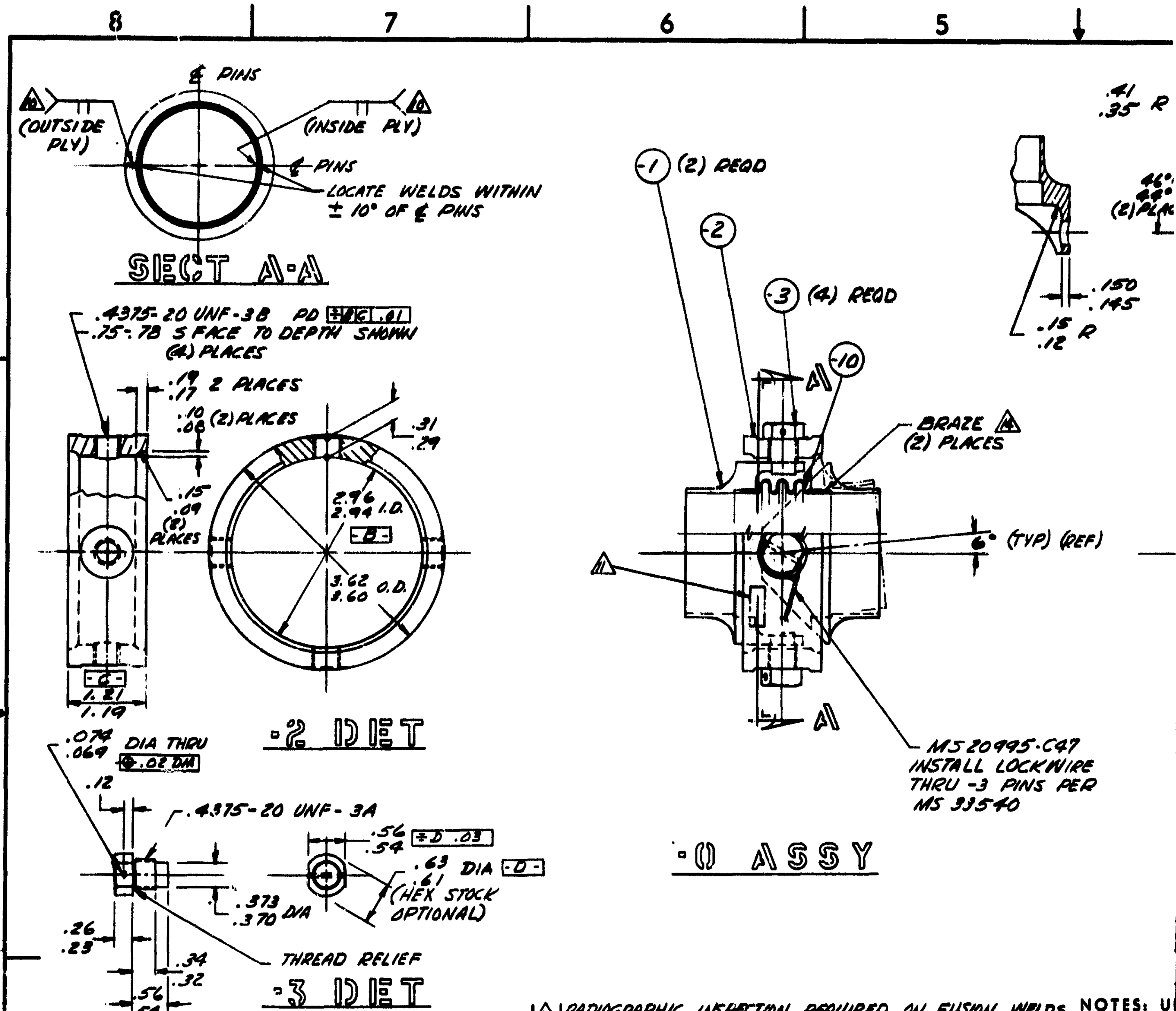

15 HEAT TREAT CRES A286 ITEMS TO 130,000 MIN ULTIMATE TENSILE STRENGTH, 85 000 MIN YIELD STRENGTH & 15% MIN ELONGATION

10 RADIOGRAPHIC INSPECTION REQUIRED ON FUSION WELDS. PROCEDURES & ACCEPTANCE STANDARDS TO BE IN ACCORDANCE WITH MSFC DWG 10509306

11 IDENTIFY SOLAR NUMBER BY ELECTRO CHEMICAL ETCH PER SOLAR SPEC 9-6 CLASS "C"

12 GIMBAL JOINT SHALL ANGULATE IN THE PLANE OF THE PINS THROUGH ± 6° MIN

13 OPERATING DATA FOR BELLOWS:

OPERATING PRESSURE	: 170 PSIG
SURGE PRESSURE	: 450 PSIG
PROOF PRESSURE	: 450 PSIG
BURST PRESSURE	: 750 PSIG
TEMP RANGE CAPABILITY	: −360°F TO +400°F

14 BRAZE ALLOY – FOR BRAZING INCONEL 718 BELLOWS TO 6AL-4V TITANIUM FLANGES USE ONE OF THE FOLLOWING BRAZE ALLOYS. BRAZE BETWEEN 1400F & 1450 F FOR EITHER ALLOY

(a) COPPER-SILVER-TIN BRAZE ALLOY: C 85%, Ag 7%, Sn 8%

(b) PALLADIUM-SILVER-SILICON ALLOY: Pd 81.8%, Ag 14.3%, Si 4.6%

NOTES: U

1 DIMEN ARE B

2 DO N GIVEN

3 DRAW & SOL

4 PASSI

5 INCONI E S

6 HEAT T MATE

7 HEAT T ULTIM & 10%

8 FUSION CLAS

9 RESIST EXCE

Foldout Frame 1-A

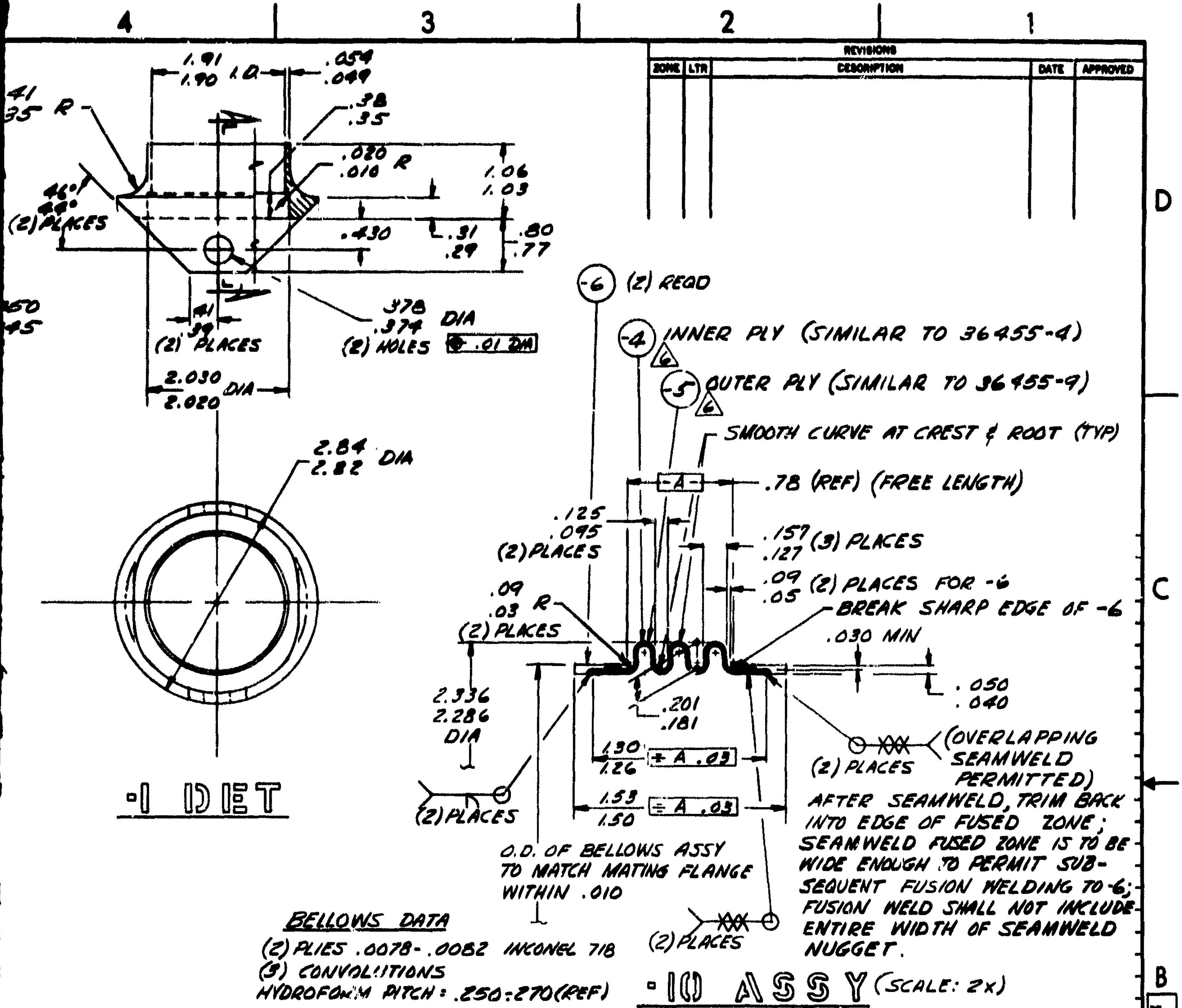

EXPERIMENTAL

NOTES: UNLESS OTHERWISE SPECIFIED

- DIMENSIONS LOCATING THE TRUE POSITION ARE BASIC
- DO NOT SCALE DRAWING. WORK TO DIMENSIONS GIVEN
- DRAWING INTERPRETATION PER MIL-D-1000 & SOLAR SPEC 9-4 SECT 5.0 & 6.0
- PASSIVATE DETAIL PARTS ONLY PER MIL-S-5002
- INCONEL 718 SHEET & STRIP TO BE PER SOLAR ES 9-221
- HEAT TREAT INCONEL 718 ITEMS TO 170 000 PSI MIN ULTIMATE TENSILE STRENGTH & 15% MIN ELONGATION
- HEAT TREAT & AGE 6AL-4V TITANIUM TO 140,000 PSI MIN ULTIMATE TENSILE STRENGTH, 130 000 PSI MIN YIELD & 10% MIN ELONGATION.
- FUSION WELD TO CONFORM TO MSFC DWG 10509308 CLASS I
- RESISTANCE WELDING TO COMPLY WITH MIL-W-6858 EXCEPT THAT PARA 9.2 (b) SHALL NOT APPLY

QTY REQD -0	QTY REQD -10	PART NUMBER	DESCRIPTION	MATERIAL	SPECIFICATION	UNIT WT
NR		MS20995-C47	LOCKWIRE			
1		-10	BELLOWS	ASSY		
	2	-6	WELDBAND	INCONEL	MIL-N-6840	.022
	1	-5	OUTER PLY	.0078-.0082	SHT INCONEL 718	.03
	1	-4	INNER PLY	.0078-.0082	SHT INCONEL 718	.03
4		-3	PIN	BAR	A286 AMS 5736	.044
1		-2	RING	BAR	6AL-4V Ti AMS 4928A	.581
2		-1	FLANGE	BAR	6AL-4V Ti AMS 4928A	.253

-0 | -10 ← ASSY NO. LIST OF MATERIAL (PARTS LIST) ASSY WT: 1.395#

APPROVED BY

GOVT CONTRACT NO.

PROJECT ENGR: O. W. Lautenbach

DESIGN: R.K. [illegible]

CHECK: O.W. Lautenbach

DRAFT: [illegible] 10-9-67

DESIGN ACTIVITY

CUSTOMER

SOLAR
A Division of International Harvester Company

DRAWING TITLE: GIMBAL ASSY, 2.00 O.D., HIGH FRICTION - LIGHT WEIGHT

SIZE: D | CODE IDENT NO.: 55820 | DRAWING NO.: 51346

SCALE: FULL | TOTAL WT. | SHEET 1 OF 1

FIGURE 45. LIGHTWEIGHT HIGH FRICTION GIMBAL ASSEMBLY

Foldout Frame 1-B